Master Thesis, Department of Geosciences

Diagenesis and reservoir quality of deeply buried Upper Jurassic sandstones in the Central Graben

A mineralogical, petrophysical and petrographical approach

Muhammad Adnan Younis

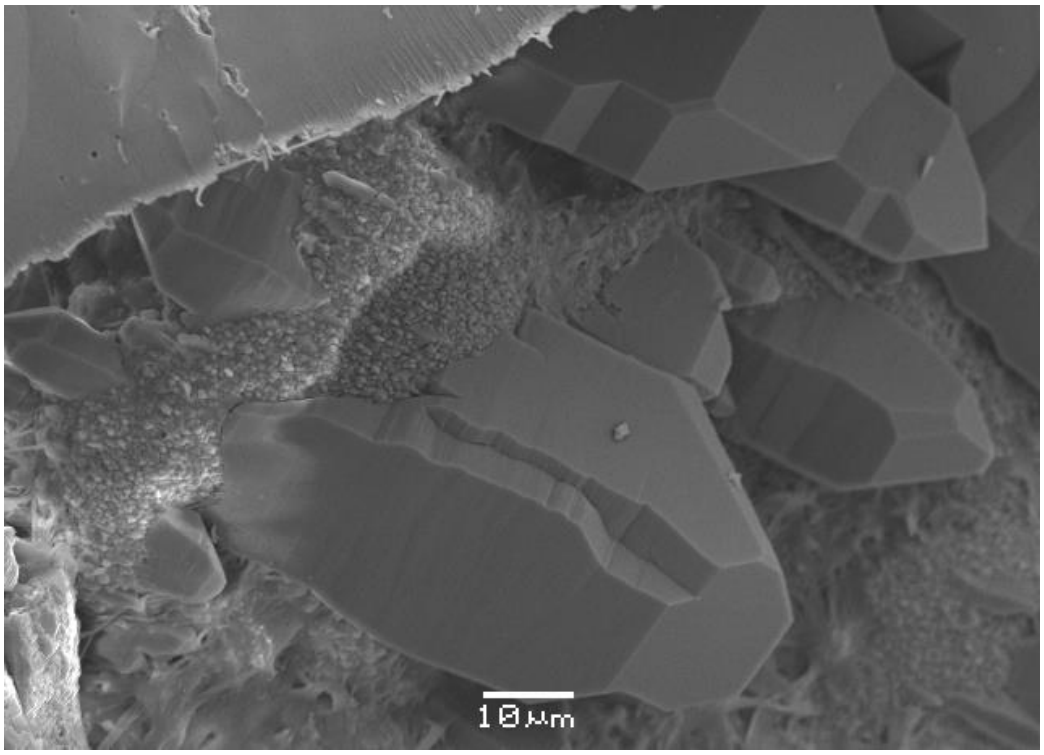

UNIVERSITY OF OSLO

FACULTY OF MATHEMATICS AND NATURAL SCIENCES

Diagenesis and reservoir quality of deeply buried Upper Jurassic sandstones in the Central Graben

A mineralogical, petrophysical and petrographical approach

Muhammad Adnan Younis

Master Thesis in Geosciences

Discipline:Petroleum Geology and Petroleum Geophysics

Department of Geosciences

Faculty of Mathematics and Natural Sciences

University of Oslo

03.06.2013

Tutor: Jens Jahren (UiO)

This work is published digitally through DUO – Digitale Utgivelser ved UiO
http://www.duo.uio.no
It is also catalogued in BIBSYS (http://www.bibsys.no/english)

DEDICATION

To my brother Waqas Younis with love

ACKNOWLEDGEMENTS

I feel great honor in expressing my avid gratifications to my supervisor Jens Jahren, under whose dynamic supervision, auspicious and considerate guidance, encouragement and altruistic attitude, I was able to accomplish work presented in this dissertation.

I also extend my special thanks to Phd Student Tom Erik Maast for his esteemed guidance, during thin section study. I also thank to Berit Løken Berg for always being supportive and helpful in my SEM studies. Without her help I believe my project was incomplete.

Thanks to all of my friends and study mates for all fruitful discussions through the entire length of this thesis.

Finally, and most importantly, I would like to thank my wife Hina. Her support, encouragement, quiet patience and unwavering love were undeniably the bedrock upon which the past two years of my life have been built.

Muhammad Adnan Younis

03.06.2013

ABSTRACT

This study deals with the diagenesis and reservoir quality of deeply buried (>4 km) Upper Jurassic sandstones from the Central Graben, North Sea. Petrophysical and petrographical analysis has been done on the cored interval from well 1/3-9S.

Quartz cementation is mostly considered as the most important porosity-destroying process in deeply buried quartz rich sandstones. Hence it is important to recognize the factors that may hinder the quartz precipitation and preserve the reservoir quality (porosity and permeability) to below the depths, usually recognized as economic basement. Micro-quartz and illite coating has been observed in the study area. Grain-coats are believed to be the important porosity preserving mechanisms for deeply buried (>4 km) sandstones in North-Sea.

High porosity (>10%) and low porosity (<10%) zones have been marked in deeply buried Upper Jurassic sediments. It has been observed that micro-quartz and illite coatings are present in all of the samples. Presence of illite coating around the detrital grains is sparse, while micro-quartz coats are extensively observed around the grains. These observations indicate that the presence of micro-quartz coating is significantly important in preserving the porosity. Moreover SEM analysis shows that in high porosity zones higher amount of micro-quartz coating has been observed as compare to the low porosity zones. Micro-quartz grain coating is common in the Upper Jurassic sediments of North Sea and is generated by the transformation of siliceous sponge spicules (Rhaxella Perforata).

Overall high IGVs (30 – 38%) have been observed in this study. High IGVs and well preserved porosity indicates that mechanical compaction is not very significant in the cored interval. It has been observed that samples with higher carbonate cement (≥ 6%) exhibits comparatively higher IGVs as compare to the samples without or lower carbonate cementation. This early carbonate cement, well sorting and fine grain size of the particles helped to reduce the effect of mechanical compaction and preserve the high IGVs and porosity.

.

Table of Contents

1. INTRODUCTION

1.1 Introduction

This study is a part of collaboration project with Det Norske Oljeselskap ASA and Institute of Geosciences at University of Oslo. The aim of the study is to understand the processes which preserve the reservoir quality of the deeply buried reservoirs of Central Graben, North Sea.

A reservoir is defined as a subsurface rock that has permeability and effective porosity and has ability to contain commercially exploitable quantities of hydrocarbon. Mechanical compaction and chemical compaction are considered as the porosity destroying processes. Quartz cementation is considered as the most common porosity-reducing mechanism at depth greater than 2.5 km (Bjørlykke et al. 1992).Significant amount of quartz cementation occurs at depths 3.5 - 4.5 km, corresponding to 120 – 160 ºC temperature range and strongly reduced the reservoir quality of the sandstone (Bjørlykke and Jahren 2010). Grain coating is consider as an important factor to preserver the reservoir quality of the deeply buried reservoirs (> 4 Km) and has ability to inhibit the quartz cementation.

1.2 Aim and objectives of the study

The main aim of the study is to integrate the petrographic and petrophysical log data for well 1/3-9S to qualify and quantify the reservoir quality with respect to quartz cementation and porosity preserving process in Upper Jurassic sandstones in the Central Graben, buried to more than 4 Km depth. For this purpose two levels of investigations have been used:

1) Well correlation and interpretation of petrophysical logs.
2) Petrographic analysis with the help of optical microscopy and scanning electron microscopy.

Mineral identification and point counting has been performed with the help of optical microscope. Scanning electron microscopy has performed with focus on the identification and quantification of the grain coating, if present.

1.3 Study Area

The study area is located at the Cod Terrace within the Central Graben in blocks 1/3, 2/1 and 7/12 belonging to Tambar, Gyda and Ula field respectively (Figure 1.1). The key well 1/3-9S is located on Tambar field in block 1/3.

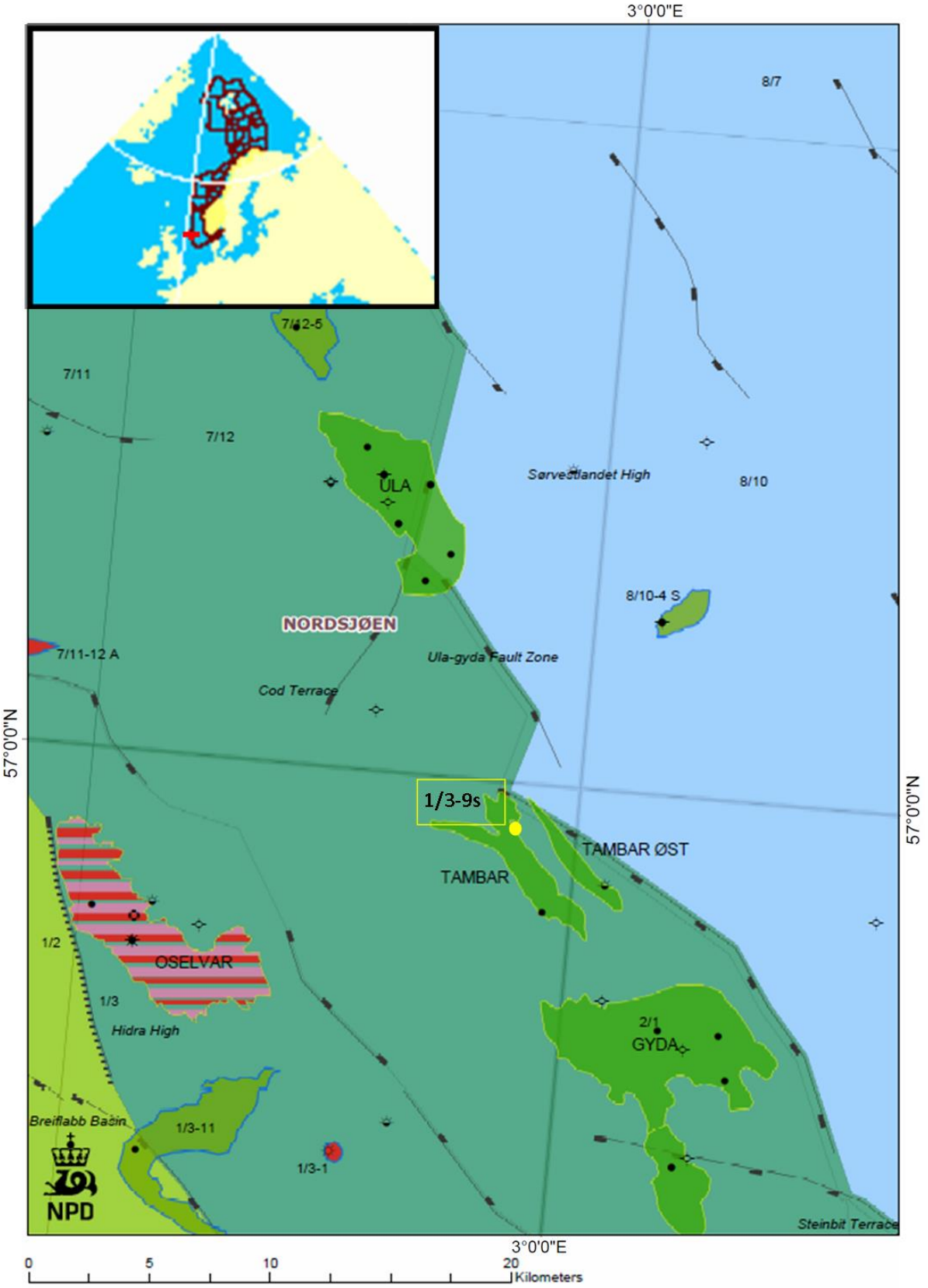

Figure 1: Structural element map of the study area. Yellow dot shows the location of the well 1/3-9S located in Tambar field (Modified from NPD 2013).

2. GEOLOGICAL FRAMEWORK

2.1 Introduction

This chapter emphasis on the geology including structural setting, evolution, stratigraphy and depositional environment of Upper Jurassic rocks in the Central Graben located in the middle and south of the North Sea (Figure 2.1).

The North Sea rift is a post Caledonian rift system. It has a prolonged extensional history starting from Devonian (Badley et al.1988; Bartholomew et al.1993). The North Sea basin has a very complex structure possibly due to two extensional phases:

1) Permo-Triassic extensional phase and Jurassic extensional regime and related subsidence.

2) Due to varied basin substrata upon which extensional events took place.

The variation is both in terms of composition and grain across the basin (Færseth 1996). The tectonic events like thermal cooling and subsidence are responsible for present North Sea sedimentary basin (Ravnås et al. 2000).

2.2 Structural elements

North Sea is termed as a hybrid basin i.e. a basin system that has not reached the thermal equilibrium due to previous extension and next phase of extension has started (Gabrielsen et al. 1990; Roberts et al. 1995).

The North Sea rift is a triple rift system with three arms: Moray Firth basin, the Central Graben and the Viking Graben (Figure 2.2). The Viking Graben and Moray Firth basins have asymmetrical character while Central Graben has symmetrical character (Zanella and Coward.2003).

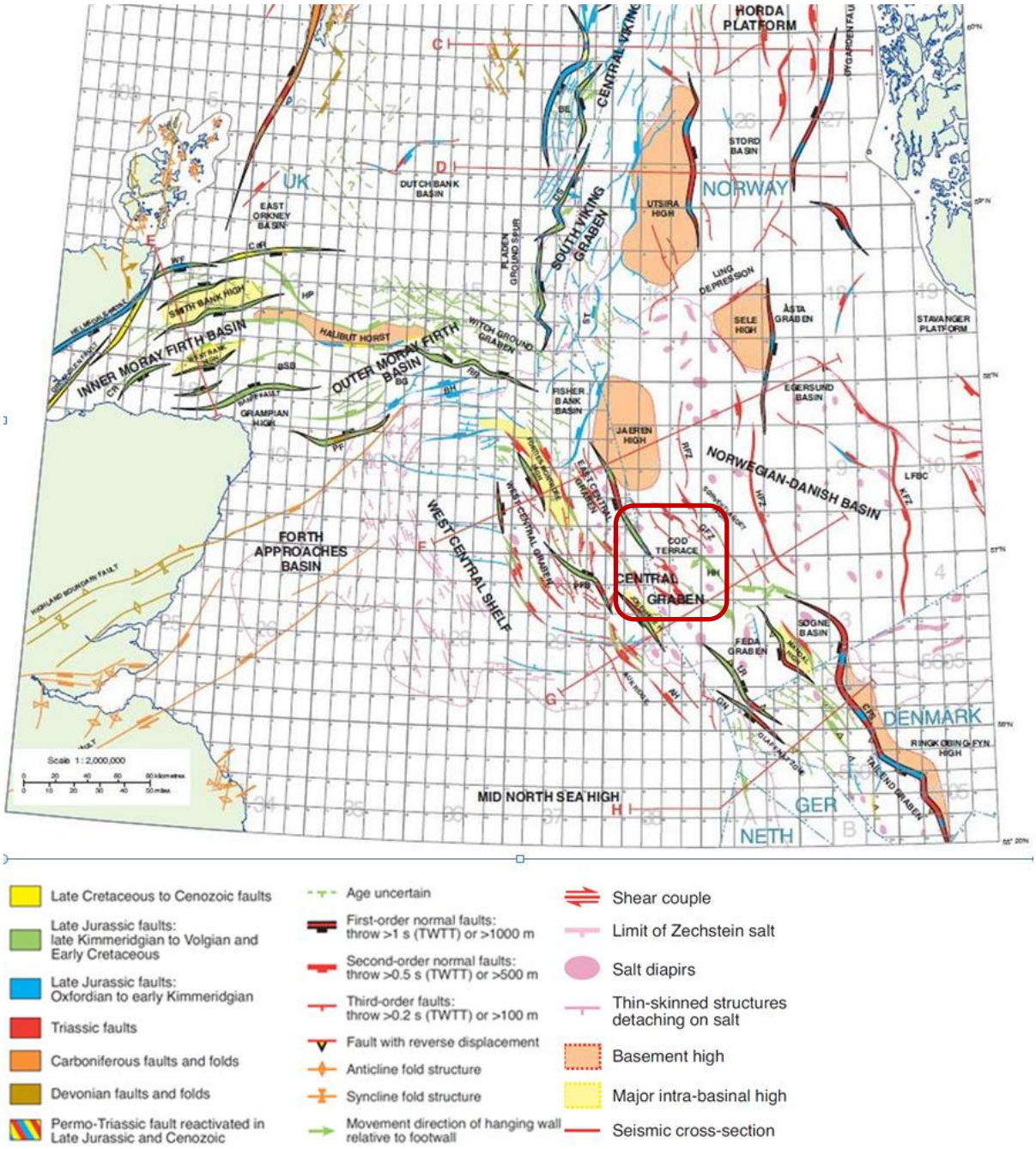

Figure 2.1: Regional structural map of North Sea. The study area is marked in red box (Modified after Zanella and Coward 2003).

Two major rift phases have contributed in the development of the North Sea:

1) Permo-Triassic Rifting

2) Jurassic Rifting

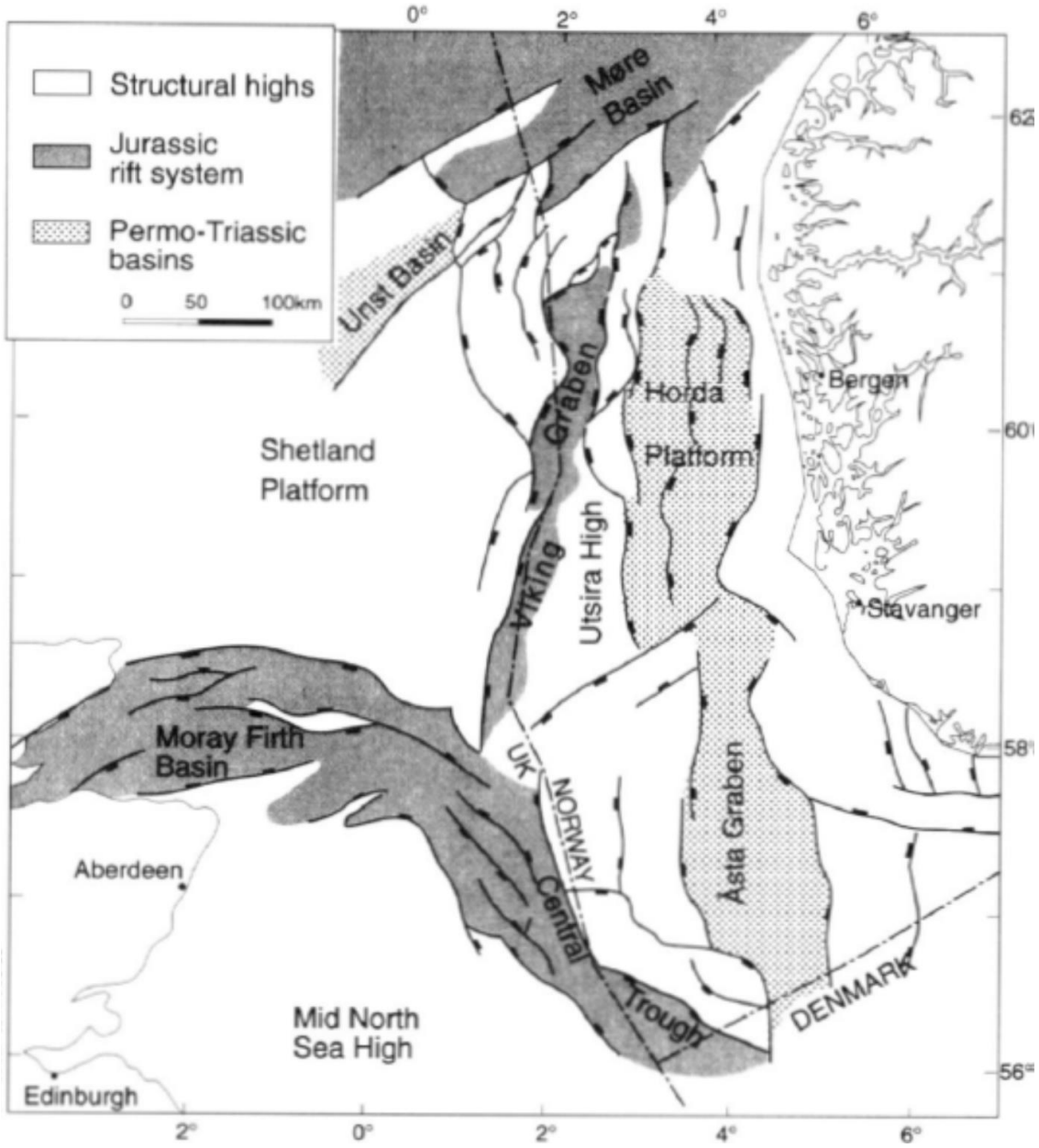

Figure 2.2: Different Structural elements formed in two extensional phases (Roberts et al. 1995).

2.2.1 Permo-Triassic rifting

It has been suggested from various modeling studies that the axis of Permo-Triassic stretching was lying beneath Viking Graben and was equally important in stretching and subduction of the basin as the Jurassic rifting phase (Kusznir et al. 1991; Roberts et al. 1995).
Rapid differential subsidence has been observed during the Triassic in Viking-Central graben of North Sea. But the dominant features resulting from rifting were not developed in Triassic time. However in Jurassic, structural features were more dominant and well developed. The

basins that underwent rapid subsidence in North Sea during Triassic are the Horn Graben (on the Danish continental shelf) and Gluckstad graben in northern Germany (Ziegler 1975).

2.2.2 Late Jurassic rifting

In the Central and northern North Sea there was very little rifting in early Jurassic. The main rifting phase occurred in late Jurassic in North Sea which developed the Central Graben, Viking Graben and Moray Firth basin triple-rift system. While In northern North Sea rifting may have started in mid-Jurassic times during Aalenian to early Bathonian deposition of the Brent group (Roberts et al., 1999) or during latest Bajocian to mid-Callovian (Rattey and Hayward 1993).

Roberts et al. (1990) proposed a vector-triangle model which showed that extension took place in Moray Firth, Viking Graben and Central Graben simultaneously (Figure 2.3). Multiple phases of faulting were distinguished by intermittent phases of relative tectonic inactivity which affected the architecture and nature of sediments in the basin (Ravnas et al. 2000).

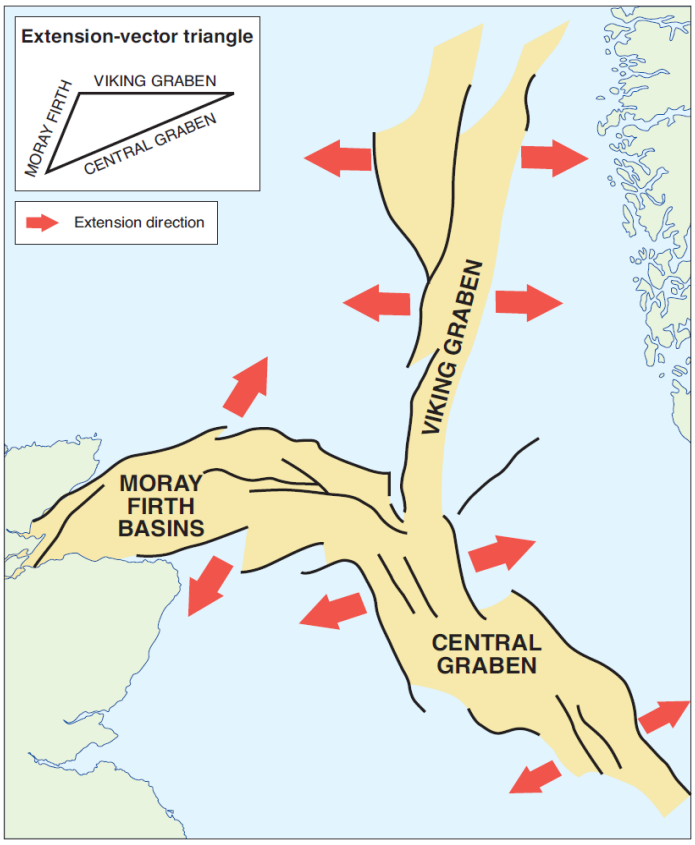

Figure2.3: Illustrating the extension vector triangle model of the North Sea rift. The model states that three arms of rift system spread in a single phase of extension simultaneously (After Roberts et al. 1990)..

Erratt et al. (1999) proposed a same kind of victor-triangle-model, which states that extension took place in two phases (Figure 2.4).He divided the extensional phases to Callovian to early Kimmeridian extensional phase and Early Kimmeridgian to Volgian extensional phase (Zanella and Coward 2003).

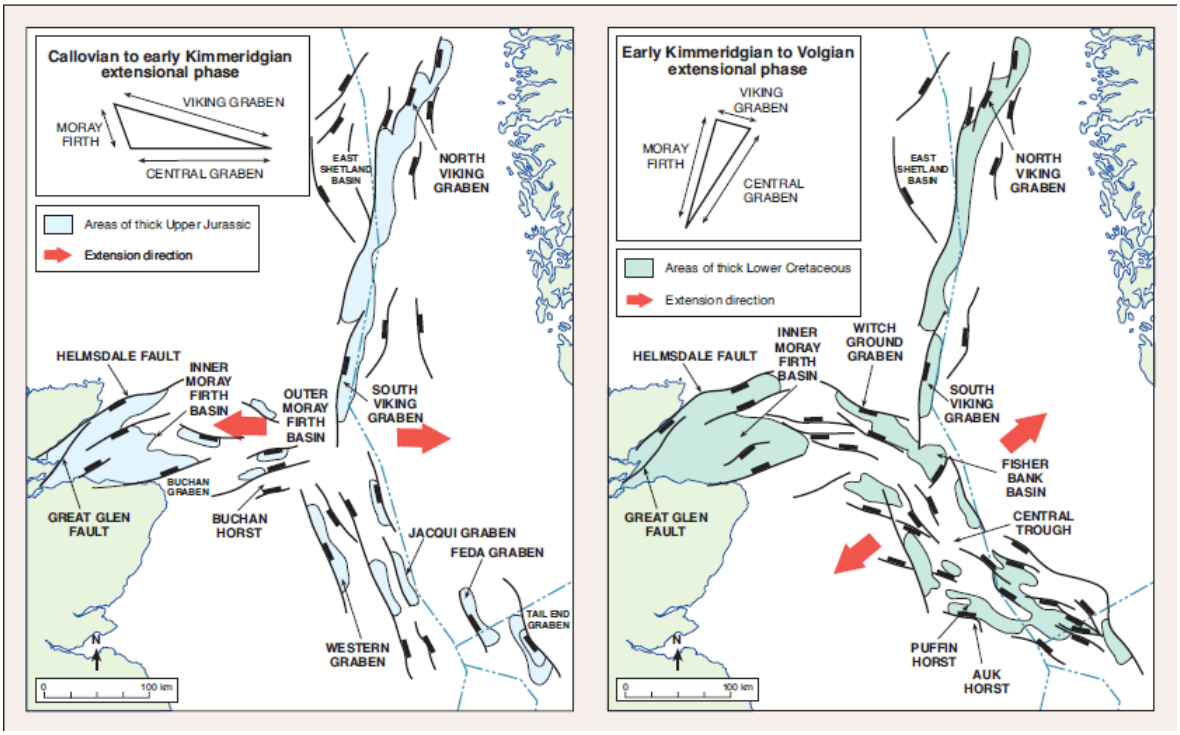

Figure 2.4: Orthogonal opening of the North Sea illustrated by two phase model (After Errat et al. 1999).

2.3 Structural Style and Structural elements

There is prominent difference in structural style between Central North Sea and northern North Sea-Moray Firth rift system. The difference is because of the Zechstein salt which is present in central North Sea and form a detachment surface. Most prominent structures present in the Central North Sea are formed by halokinetic deformation whereas the northern North Sea-Moray Firth system is characterized by rigid, faulted-block rotation. Because of these marked differences in structural style the formation of hydrocarbon traps and structural traps can be divided into two main categories.

1) Syn-rift traps consist of pre-rift reservoir rocks.
2) Post-rift traps, initiated by the tectonic inversion and diapirism and contains post-rift reservoir rocks (Zanella and Coward 2003).

The Central Graben has a South-East trend and consists of two troughs towards east and west of intrabasinal Forties-Montrose and Josphine highs. These two highs make a spike between two sub-basins. Central Graben can be regarded as a series of north-south trending sub-basins, which offsets along Tornquist basement lineaments to W-N-W direction (Erratt et al. 1999). The presence of thick Zechstein salt further complicates the central Graben structure (Frasser et al. 2003).

2.4 Stratigraphic framework

There are three main reasons which make Late Jurassic the most critical time in the evolution of the North Sea petroleum system.

1) Widespread Kimmeridge Clay Formation and its lateral equivalents were deposited at the time of Late Jurrasic, which are very good source rock for oil that has charged the major oil fields of the North Sea (Cornford 1998).
2) Complicated tectonic history is the major cause for the majority of structural traps, not only for hydrocarbon reserves in upper Jurassic and lower Cretaceous syn-rift reservoir, but also for the pre-rift hydrocarbon rocks of Devonian to Middle Jurassic age. About 80% of the discovered reserves along the North Atlantic margin, including the North Sea are from syn-rift and pre-rift deposition. (Knott et al. 1993).
3) Majority of the future prospects are most likely to be in upper Jurassic (Johnson and Fisher 1998; Boldy and Fraser 1999).

Hydrocarbon play of the Upper Jurassic has been largely organized by the progressive evolution and decay of Late Jurassic to Early Cretaceous rifting. Related structural and depositional processes applied a fundamental control on the distribution of seal, reservoir and source rock facies, and also on the development of hydrocarbon trapping configurations, mainly structural and partially stratigraphic traps. The play can be classified as two types of reservoirs: Coastal-shelf sandstones, and deep-sea submarine-fan sandstones in the form of basin floor and slope aprons fans (Fraser et al., 2003). These good quality reservoirs are present entirely in Moray Firth, Central and Viking Graben systems. These reservoirs also show a close relation between structural evolution and depositional setting (Erratt et al. 1999). Much thinner and lower reservoir quality coastal-plain facies are also present but they are quite thin as compared to the coastal-shelf equivalents. Mostly nature of reservoir sandstone is determined by the combination of sediment supply, subsidence and depositional process. But

in Central Graben pre-existing topography and salt movement are also very important which make Central Graben depositional system a complex system (Fraser et al. 2003)

As this study is based on Upper Jurassic sediments which were deposited in shallow marine/coastal shelf environment. Stratigraphic chart of the Norwegian Central Graben is show in (Figure 2.5).

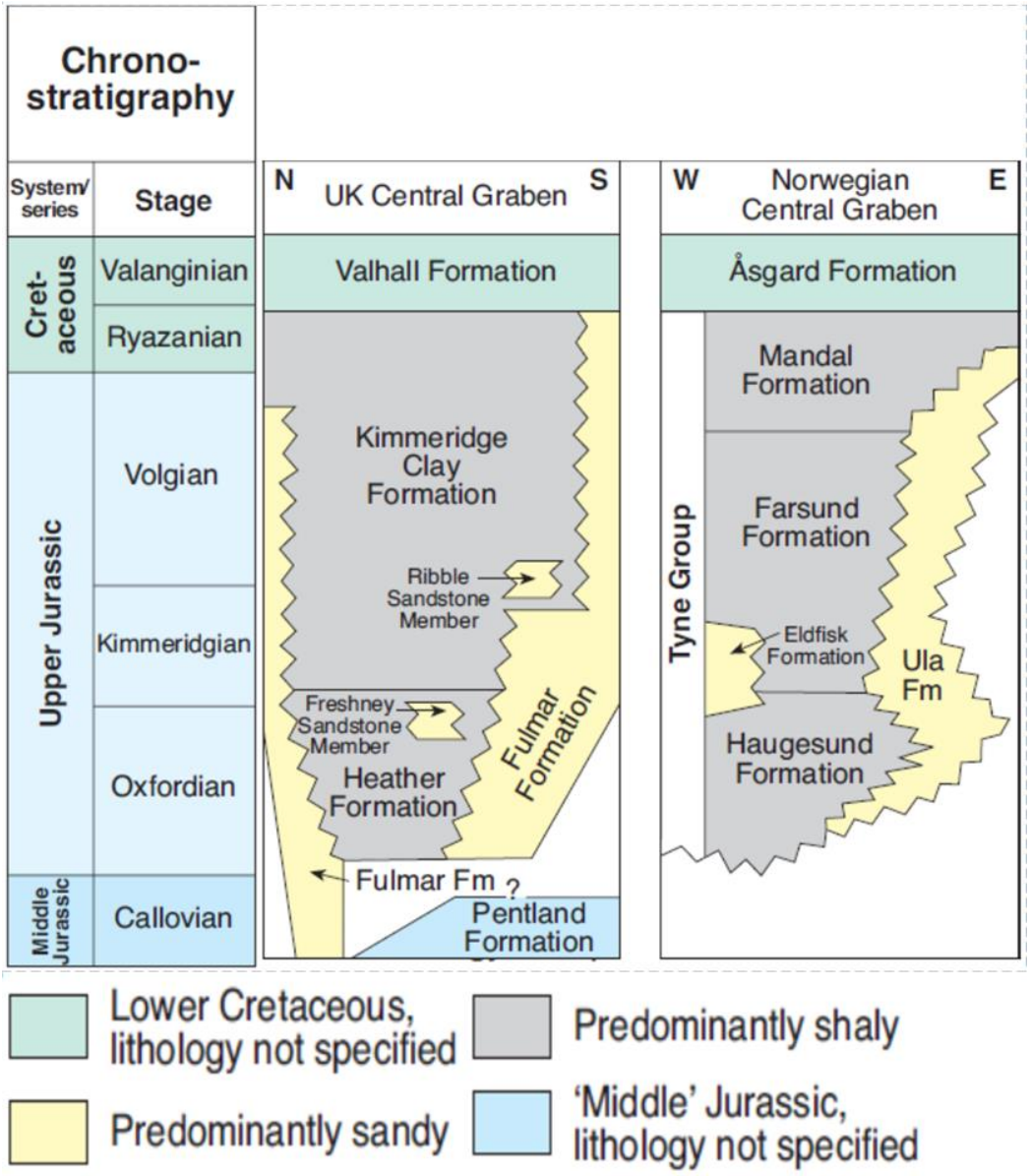

Figure 2.5: Stratigraphic overview of the Norwegian and UK Central Graben (Modified after Fraser et al. 2003).

2.4.1 Upper Jurassic deposits

In the Central Graben Upper Jurassic sediments were deposited as an open shelf environment subsequently an Oxfordian Sea level rise (Home 1987; Forsberg et al. 1993; Oxtoby et al. 1995). Before the Oxfordian transgression the Cod Terrace area was subarieally exposed during Early and Middle Jurassic and the Upper Jurassic sediments are frequently overlying the Triassic strata (Ramm et al. 1997). Good quality sandstones deposited in upper part of progradational cycles dominated by high energy environment under the effect of storm waves. High overpressures along with secondary porosity results in the preservation of the porosity in deeper parts (Fraser et al. 2003).

The reservoir rocks in the Cod Terrace are deposited after the Late Oxfordian relative sea level rise, especially on the downfaulted flank of the main Ula-Gyda fault zone (Home 1987). This downfaulted block separates the Cod Terrace from Sørvestlandet High (Figure 2.6) (Ramm et al. 1997).

The Upper Jurassic sediments consist of mudstones and fine to medium grained sandstones, deposited in offshore marine shelf environment. Most of the sandstones have fine grained clays and due to intense bioturbation primary sedimentary structures are not common. The grain size is ranging between 100µm to 300 µm. In response to relative sea level changes distinct cleaning upward trends are evident (Ramm et al. 1997).

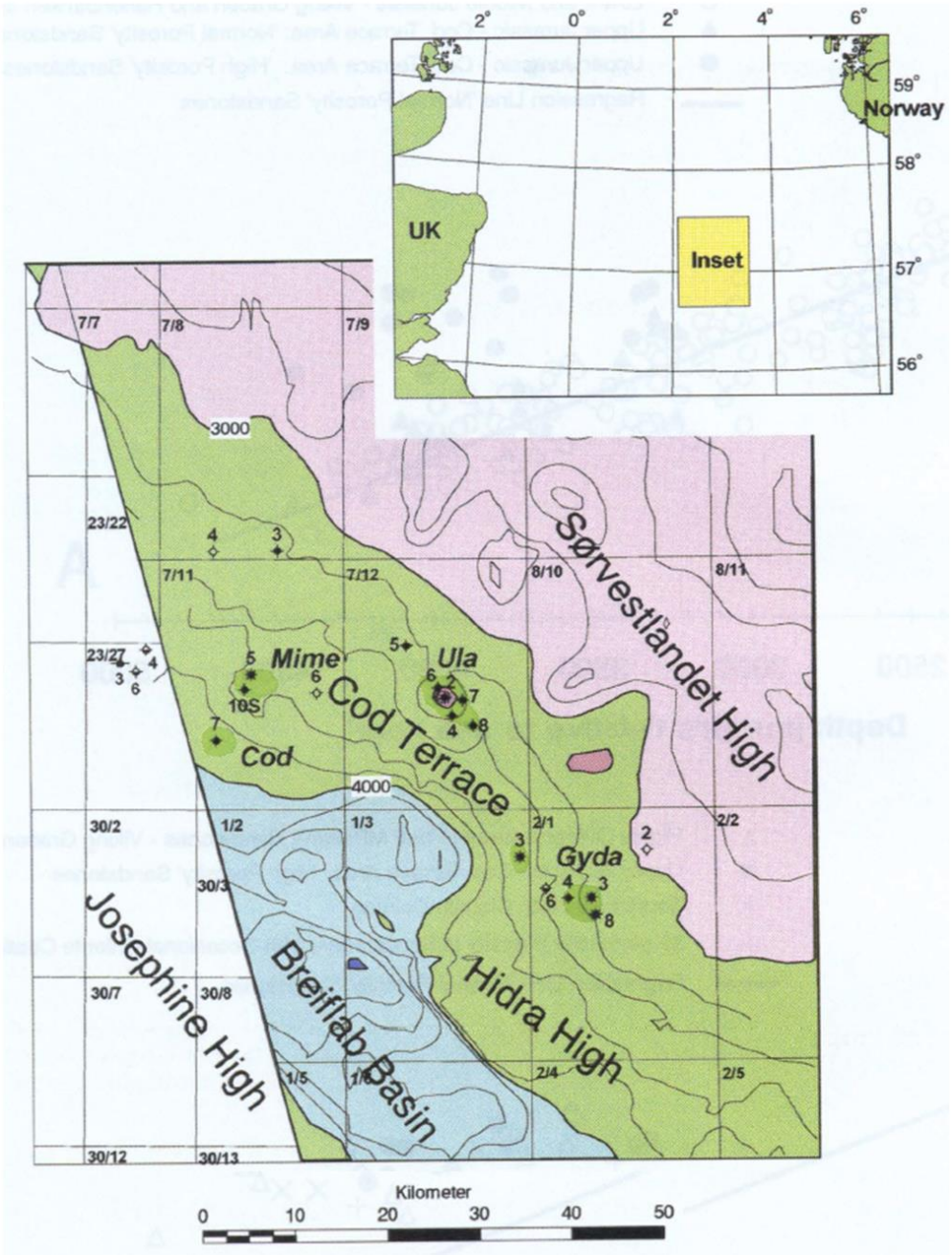

Figure2.6: Location map of the Cod Terrace area, Norwegian Central Graben (Ramm et al. 1997).

3. THEORATICAL BACKGROUND

3.1 Introduction

The primary composition of sandstone reservoir depends on parent rock composition, which is function of texture, depositional environment and processes related to the diagenesis. Diagenetic processes occur, near the surface and during deep burial. The properties of reservoir rock are subjected to change throughout their burial and subsequent uplift by the combined effect of mechanical and chemical compaction, which involves the precipitation and dissolution of minerals (Bjørlykke and Jahren 2010). In sedimentary basins compaction is responsible for the decrease in overall bulk sediment volume and reservoir quality (porosity and permeability) of the sandstone reservoirs (Fawad et al. 2011).

Bjørlykke and Jahren (2010) mentioned the following diagenetic processes:

(1) Near surface diagenesis.

(2) Mechanical compaction

(3) Chemical compaction

(4) Cementation

3.2 Near surface diagenesis

Near surface diagenesis includes the processes which are influenced by sea-water and meteoric water. Composition of sediments starts to alter immediately, after their deposition by various near surface diagenetic processes. Fluid flow and diffusion are the processes by which sediment react with water or air or both at depth (less than 1 to 10 m). Transportation of solids which are dissolved by fluid flow and diffusion is more effective near the surface. Sediments are more prone to change their bulk composition at shallow depth as compare to the greater burial (Bjørlykke and Jahren 2010).

Shallow marine diagenesis is strongly influenced by the deposition of biogenic silica and carbonate on the sea bed (Bjørlykke 1998). Meteoric water which is under saturated with respect to minerals, when seeps down in soil, it starts to react and dissolve unstable minerals like mica and feldspar and precipitate kaolinite (Figure 3.1). This process can be expressed by the following reactions:

$$\underset{\text{Feldspar}}{2K\,(Na)\,AlSi3O_8} + 2H^+ + 9H_2O \longrightarrow \underset{\text{Kaolinite}}{Al_2Si_20_5\,(OH)_4} + \underset{\text{dissolved silica}}{4H_4SiO_4} + \underset{\text{cations}}{2K^+\,(2Na^+)}$$

$$2KAl_3Si_3O_{10}(OH)_2 + 2H^+ + 3H_2O \longrightarrow 3Al_2Si_2O_5(OH)_4 + 2K^+$$

Muscovite — Kaolinite

The reaction above cannot take place in closed system because removal of cations, silica and availability of protons are necessary to complete the reaction (Bjørlykke 1998).
Meteoric water has tendency to flow along the most permeable beds in the basin (Bjørlykke and Jahren 2010). Meteoric water has ability to flow deep into the sedimentary basins. Many of the North Sea reservoirs exhibit lower salinities (<50%) as compare to the normal Sea water, represents influx of meteoric water (Bjørlykke 1998).

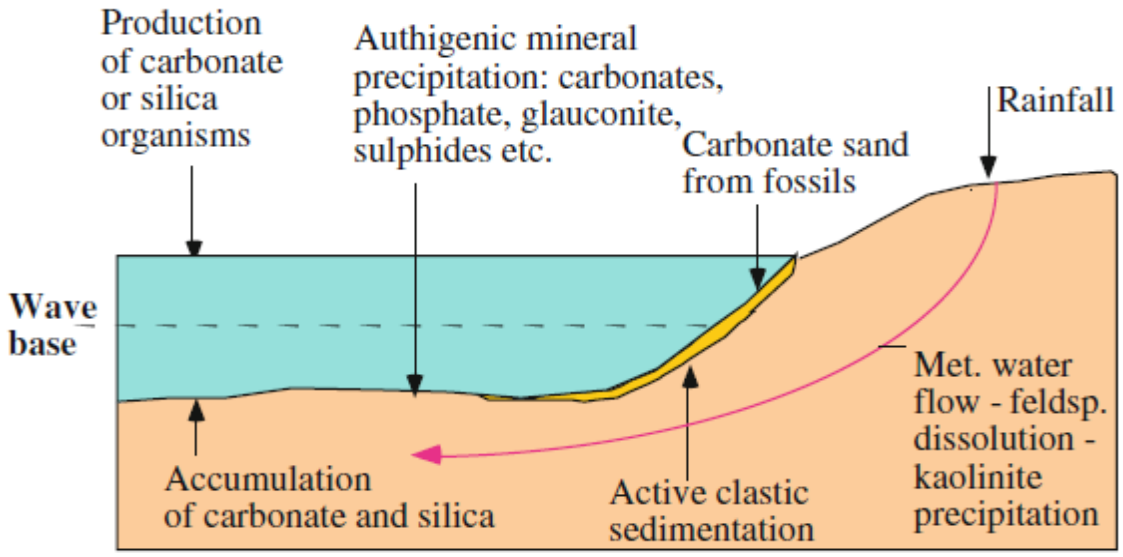

Figure3.1 Diagenetic processes in shallow marine environment (Bjørlykke and Jahren 2010).

3.3 Mechanical compaction

During burial, sandstones experienced compressive forces due to increase in overburden. It induced compaction in sandstones because of expulsion of pore water which results in the reduction of rock volume. Mechanical compaction which include reorientation, rotation and fracturing of brittle grains and deformation of ductile grains, participate for most of the early porosity loss (Berner 1980). Sandstones consist of more ductile components are severely affected by mechanical compaction and show porosity loss (Rittenhouse 1971).

In the absence of carbonate cement in well sorted sand, mechanical compaction is very significant for (0-2 Km) depths. Quartz cementation starts at 2 Km depth (80 - 100°C) in sedimentary basins with normal geothermal gradient. This quartz cementation stabilizes the grain framework and stops the further mechanical compaction. The measure of porosity loss by mechanical compaction determines the intergranular volume prior to the chemical compaction (Bjørlykke and Jahren 2010).

3.4 Chemical compaction

In basins like North Sea at 2-3 Km burial depth (80° - 100°C) quartz cementation starts to precipitate and increased the rock strength. Poorly sorted and lithic sand lose most of the porosity rather at shallow depths (1- 2 Km). In most cases only (2 – 4%) quartz cement has ability to stop further mechanical compaction by strengthen the rock frame work faster than increase in effective stress (Bjørlykke and Jahren 2010).

When quartz cementation start it does not stop until it destroy all the porosity or temperature decreases below 70-80°C (figure 3.2). In general, well sorted feldspathic sandstones and quartz arenites, quartz cementation is the main porosity destroying process (Bjørlykke and Jahren 2010). Quartz cementation is mainly controlled by area of grain surfaces available for precipitation and the time-temperature integral (Walderhauge 1994).

Various petrographic studies have been done to analyise the quartz cementation in the quartzose sandstones (McBride 1989). Fuchtbauer (1983) mentioned the five possible sources of silica cement as (1) quartz dissolution associated to the siltstones, (2) feldspar to clay minerals replacement, (3) pressure solution and stylolites, (4) smectite to illite alteration, (5) dissolution of the volcanic glass. Among these sources, stylolitization and quartz pressure solution (have received dominate attention) (Oelkers et al. 1996)

Slow subsidence rates and high geothermal gradients increases the amount of quartz cement at particular depth. At 100 to 120°C temperature some of the Kaolinite may recrystallize to dickite with same chemical composition. In sandstone buried to 3 Km or more K-feldspar is often replaced by albite and this phenomenon is called albitisation (Bjørlykke and Jahren 2010).

In general porosity is strongly reduced in sandstone reservoirs at 3-3.5 Km to 4-4.5 Km burial depth between 120 – 160°C because of precipitations of quartz cement (Bjørlykke and Jahren 2010). The quartz cementation rate increases as an exponential function of temperature and it is estimated that for every 10°C the rate of quartz cementation increases by a factor of 1.7 (Walderhaug 1996).

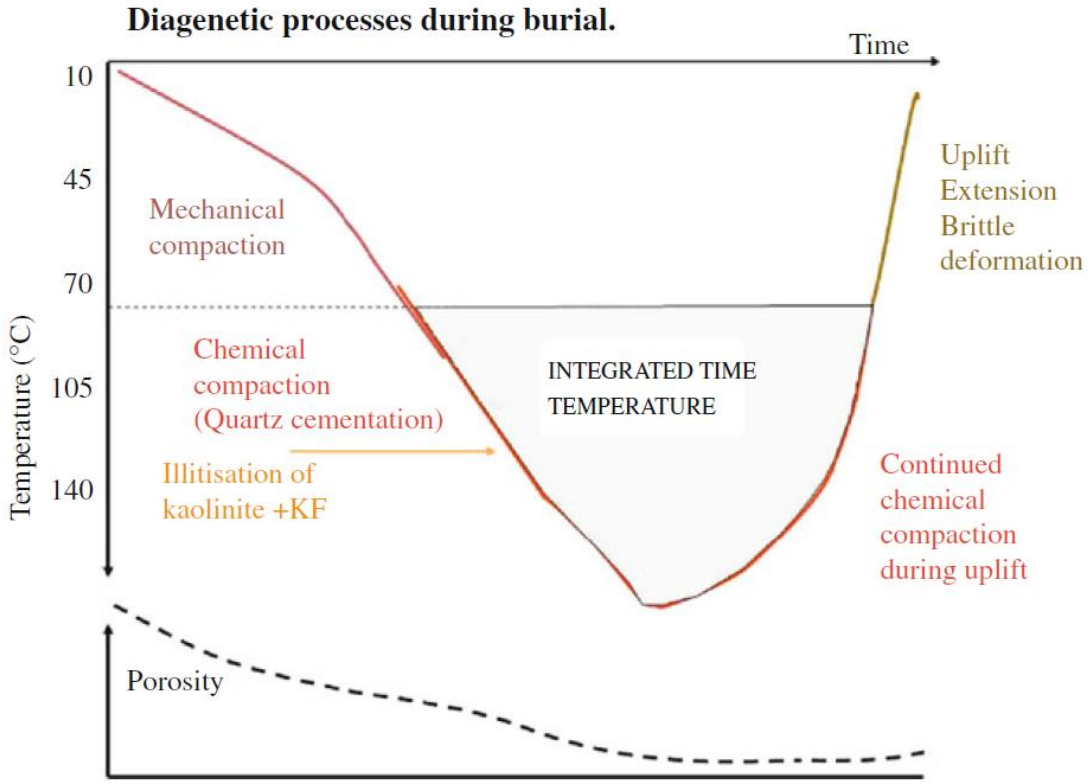

Figure 3.2: An overview of diagenetic process, mainly quartz cementation. It is notable that quartz cementation does not stop during uplift until temperature until (70-80°C) temperature (Bjørlykke and Jahren 2010).

It has been observed that rate of quartz cementation depend on the surface area available for cementation, temperature and the degree of supersaturation. When the quartz cementation fills the porosity it decreases the free surface area available for quartz overgrowth and subsequently reduced the rate of cementation (Bjørlykke and Jahren 2010).

3.5 Porosity preserving mechanisms

The diagenetic processes described in this chapter affect the reservoir quality of the sandstones. However Quartz cementation and mechanical compaction are the main porosity-destroying process in quartz rich sandstones during their progressive burial.

Clay coating and micro-quartz coating have been accepted by many workers as a porosity preserving agents in deeply buried sandstones reservoirs (Aase et al. 1996). Bloch et al. (2002) suggested three mechanisms which help to preserve the anomalously high porosity: (1) grain coating, (2) fluid over pressure, (3) early hydrocarbon emplacement. The focus of this study is deeply buried reservoir, having good reservoir properties because of the presence of porosity preserving mechanisms.

3.5.1 Early hydrocarbon emplacement

Previously it has been believed that anomalously high porosity and permeability in deeply buried sandstones reservoirs have been explained by the early hydrocarbon emplacement (Selley 1978; Gluyas et al. 1990; Rothwell et al. 1993). However Giles et al (1992) and Walder haug (1994a) proved that presence of hydrocarbon and high porosity does not have any relationship with each other.

Currently it is difficult to quantify the influences of hydrocarbon emplacement on porosity preservation and cementation in sandstones. It seems that some cement (e.g., illite, quartz) probably continue to precipitate subsequent of hydrocarbon trapping into the reservoirs (Bloch et al. 2002). Worden and Morad 2000 suggested that in water wet sandstone reservoir hydrocarbon emplacement will have no effect on the quartz cementation because the grains surface will be coated by water. However in oil wet systems, where surface of quartz grain will be coated with hydrocarbon the oil emplacement will hinder or retard the quartz cementation.

Generally no clear relationships have been observed between hydrocarbon fill and reservoir quality of the sandstones in North Sea (Aase et al. 1996). Ramm and Bjørlykke (1994) suggested that porosity is not considerably higher in hydrocarbon saturated sandstones as compare to the water saturated reservoirs.

3.5.2 Fluid overpressure

Fluid overpressure is expressed as the amount of pore-fluid pressure greater than the hydrostatic pressure (Dickinson 1953). Fluid over pressure has the ability to reduce the effective stress by bearing some of the mass of the overlying sediments; the fluid reduces the pressure on the grains and help to preserve the porosity Mechanical compaction in sandstones

are the result of effective stress. In some cases fluid over-pressure helps to reduce the effective stress and consequently preserve the porosity (Bloch et al.2002).

Fluid overpressure can develop (1) where porosity reduction rate is higher than the rate of fluid release, (2) where pore fluid expansion rate is higher than the rate of fluid escape, and (3) where large scale movement occur (Swarbrick 1997).

3.5.3 Clay-coating

Mineralogically, clay coats could be illite, chlorite or mixed layer smectite/illite. Clay coating could be authigenic or allogeneic in origin. Authigenic-clay coats are regenerated or newly formed minerals and have a radial morphology. Allogeneic clay coating refers to the clay minerals having laminar morphology and form from infiltration of clay in sand or as cutans in soils (Pittman et al. 1992).

The role of clay coating in preservation of porosity has been mentioned by a number of authors in their studies (Heald and Larse 1974; Thomson 1979; Smith 1985). Chlorite and illite coating is common in deeply buried sandstones of North Sea. It has been observed that chlorite is more effective in preserving porosity as compare to the illite (Heal and Larese 1974). Illite coating also has ability to retard the quartz over-growth but in other hand illite also participate to catalyze pressure solution along grain contacts (Thomson 1959).
Thick and continuous clays coats preserve the porosity by the blockage of the nucleation sites on already present detrital quartz grains. Thin and sparse clay coats are mostly ineffective regarding the precipitation of quartz cement (Pittman et al. 1992).

3.5.4 Micro-quartz coating

Anomalously high permeability and porosity (>20%) values have been recorded at depths greater than 4 Km, in Upper Jurassic sandstones of the North Sea. It has been proposed that these high porosity values are the result of continuous micro-quartz coating on the detrital grains (Aase et al. 1996).

Micro-quartz, like chlorite coats, forms on the surface of the detrital quartz grains and retard or inhibit the pore-filling quartz overgrowths (Bloch et al. 2002). The random orientation of minute micro-quartz crystals, covering the detrial grains interfere with the formation of macro-quartz overgrowth (Heald and Larese 1974).

Experimental data (Heald and Renton 1966) and morphology of micro-quartz crystals (Williams et al. 1985) indicate quick crystallization of micro-quartz phase from pore fluids with high saturation of silica. The silica is probably originated by dissolution of volcanic glass shards and sponge spicules, as a result of increase in temperature and burial (Aase et al. 1996; Ramm et al. 1997).

Precipitation of micro-quartz occurs at low temperature (60 - 65 ºC). At this time pore water is highly supersatured with respect to quartz because of the dissolution of Opal A and Opal CT (Bjørlykke and Jahren 2010). At higher temperatures when unstable silicates have already been dissolved and pore water became slightly supersaturated with respect to silica. This slightly supersaturated solution is unable to precipitate macro-quartz growth on micro-quartz coated grains which needs higher supersaturation (Aase et al. 1996).

4. METHODOLOGY

4.1 Introduction

The study has been done by using two types of investigations.

1) Well correlation and petrophysical analysis with the help of geophysical logs.
2) Petrographic analysis has been done with the help of optical microscopy and scanning electron microscopy.

4.2 Well information and dataset

For petrophysical study four wells 2/1-6, 1/3-3, 1/3-9S, 7/12-9 have been used in this project. All of the wells are located in the Cod Terrace area. Well 1/3-9S is the key well for this study as most of the petrophysical and petrographic analysis are based on this well. Rests of the wells (i.e. wells 2/1-6, 1/3-3, 7/12-9) are used only for well correlation purpose. The well information has been downloaded from Norwegian Petroleum Directorate (NPD 2013) website and illustrated in a table form.

Table 4.1Well Information abstracted from Norwegian Petroleum Directorate (NPD 2013)

Wellbore name	2/1-6	1/3-3	1/3-9S	7/12-9
UTM Zone	31	31	31	31
Structural element	Cod Terrace	Cod Terrace	Cod Terrace	Cod Terrace
Field	Gyda	Tambar	Tambar	Ula
Content	Dry	Oil	Oil	Oil
KB elevation (m)	25	25	23	23.5
Water depth	66	68	68	70
TD (m RKB)	4588	4876	4516	3820
Oldest penetrated age	Late Triassic	Late Permian	Late Jurassic	Triassic

4.3 Well correlation and petrophysical evaluation

For well correlation wells from Gyda, Ula and Tambar fields have been selected. The main purpose for well correlation is to identify high porosity and low porosity units of Upper Jurassic sequence through Gyda, Ula and Tambar fields. Two of the wells (i.e., 2/1-6, 1/3-3)

were already correlated by Ramm et al. (1997) on the basis of Gamma Ray and He-Porosity logs while wells 7/12-9 and 1/3-9S were not included in their study (Figure 4.1).

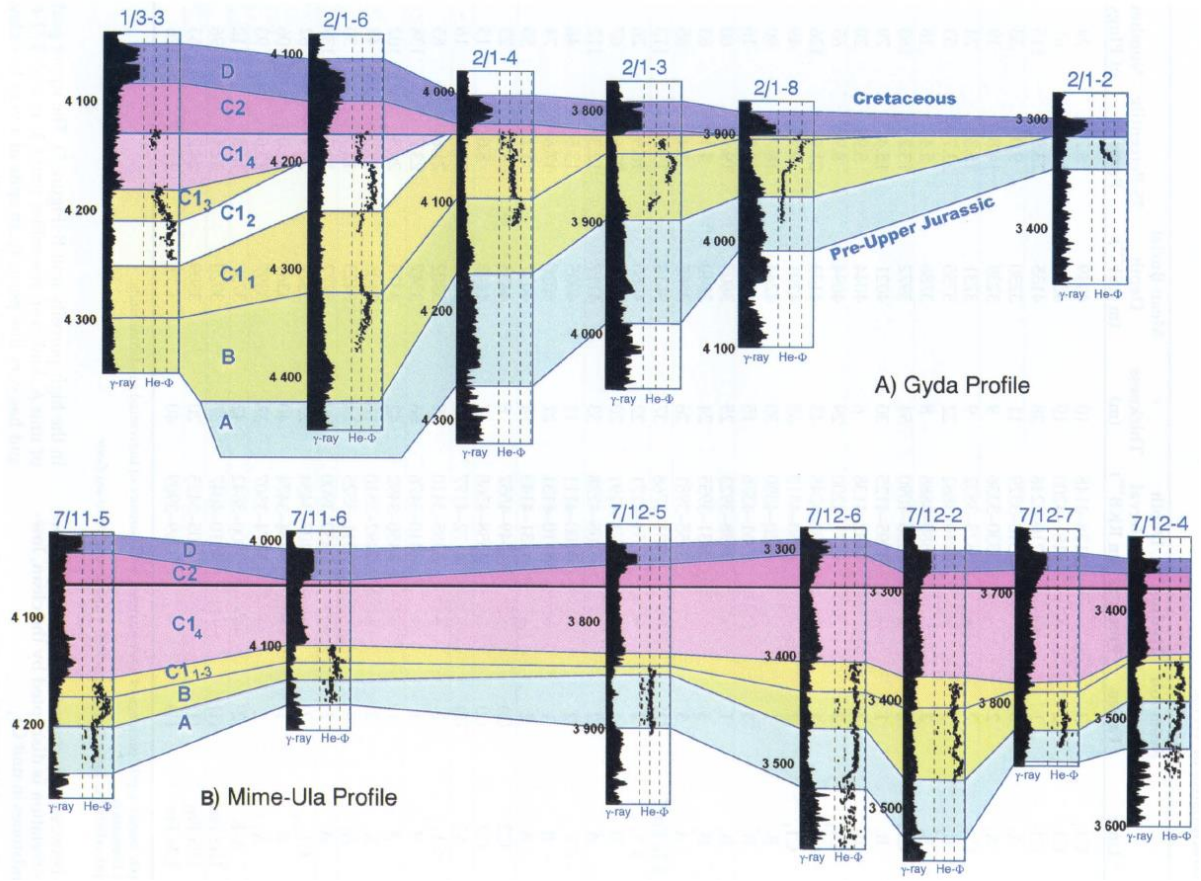

Figure 4.1: Well correlations between wells from Gyda (A) and Mime-Ulla area with the help of core porosity panels and Gamma ray log (Ramm et al. 1997).

In this study Gamma ray, Sonic, Bulk density, Neutron porosity and Density porosity logs are used in combination to mark the lithology and to identify the low porosity and high porosity units of upper Jurassic sequence. For correlation purpose Petrel 2012 has been used. For further petrophysical evaluation different cross plots have been generated in combinations particularly for well 1/3-9S which is the key well for this project.

For porosity calculation Density log has been used and density porosity was derived by using following equations.

$$\textbf{Bulk density } (\rho_b) = \phi \times \rho_f + (1- \phi) \times \rho_{ma} \quad \textbf{(equation 4.1)}$$

When equation 4.1 solved for porosity it becomes:

$$\textbf{Porosity } \phi = \frac{\rho ma - \rho b}{\rho ma - \rho f} \qquad \textbf{(equation 4.2)}$$

For porosity of sandstone $\rho_{ma=}\ \rho_{qz}$ and equation 4.2 will become:

$$\textbf{Porosity } \phi = \frac{\rho qz - \rho b}{\rho qz - \rho f} \qquad \textbf{(equation 4.3)}$$

He-porosity is the measurements taken from the well core and gives more reliable measurements for porosity. He-Porosity for upper Jurassic interval (4277 – 4353m) was available for well 1/3-9S and cross plotted (Figure 4.2) with Density porosity. The comparison shows that density porosity is acceptable and shows almost same trend. The scope of this study is to mark the high porosity and low porosity zone so density porosity log is quite acceptable.

Figure 4.2: He-porosity and Density porosity comparison for well 1/3-9S.

4.4 Petrographic analysis

For petrographic analysis core samples are taken from well 1/3-9S and studied under optical microscope and Scanning electron microscope (SEM).

4.4.1 Optical microscopy

For thin section study 20 thin sections were available (Table 4.2). Thin section study has been done with Nikon Optiphot-Pol petrographic microscope. During study enough time spent to identify and classify the minerals in order to minimize the error. This practice includes the mineral identification, grain size measurement, grain shape and sorting pattern. Other observations like quartz over growth, sponge spicules, cementation and grain coating were also examined to classify the sandstone.

Point counting has been done on all 20 thin sections from well 1/3-9S. For this purpose 300 points, calculated on each thin section. Objective of the point counting was to determine the percentages of rock composition (quartz, feldspar, and rock fragment), clays, cement (calcite and quartz), and porosity (primary and secondary). From the point counting results intergranular volume (IGV) has been measured. Paxton et al. (2002) defined the intergranular volume as the sum of depositional matrix, intergranular cement and pore spaces between the grains where, matrix is termed as clay and silt size particles between the grains (Figure 4.3).

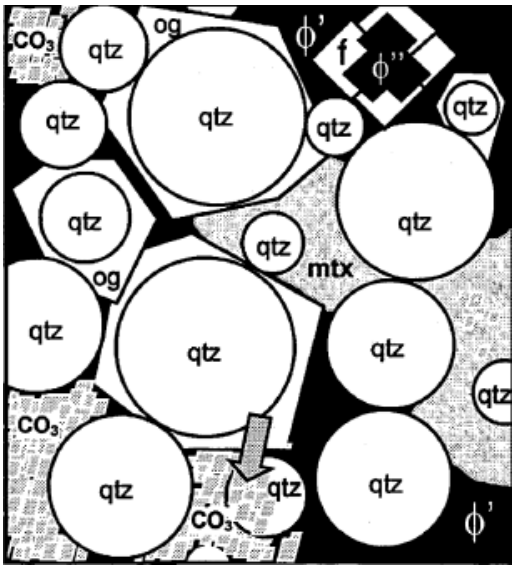

Figure 4.3: Sum of cement, matrix and porosity are termed as inter granular volume (Paxton et al. 2002).

Table 4.2 Thin sections with their depths for well 1/3-9S.

Sample no.	Well name	Measured depth (m)
1	1/3-9S	4295.66
2		4298.00
3		4299.00
4		4300.33
5		4302.33
6		4305.66
7		4307.33
8		4333.33
9		4336.33
10		4337.33
11		4338.33
12		4339.00
13		4339.69
14		4340.33
15		4341.33
6		4342.33
17		4343.33
18		4344.00
19		4347.33
20		4349.33

4.4.2 Scanning electron microscopy (SEM)

SEM study was completed by using JEOL JSM-6460LV Scanning electron microscope with a LINK INCA Energy 300 Energy Dispersive X-ray (EDX) system. For this study carbon coated thin sections and gold coated stubs have been analyzed under secondary electron microscope. SEM has ability to achieve very high resolution micrographs of the sample. Backscattered electron imagery (BEI) and Cathode-ray luminesces (CL) have been used in combination to identify the quartz overgrowth.

The SEM study Area measurements were also taken with the help of SEM to estimate the porosity and mineral composition. The data collected from SEM analysis in the end integrated with the optical microscope observation to minimize the errors. An attempt has been made to quantify the grain coating present on the grains by visualizing the coating in SEM.

5. WELL CORRELATION AND PETROPHYSICAL EVALUATION

5.1 Introduction

The main objective of the well correlation was to correlate the upper Jurassic sequence in four selected wells. Only data from well 1/3-9S has been petrographically and petrophyscially analyzed because this is the key well for this study. The rest of wells (Table 5.1) have been used only for well correlation purpose.

Table 5.1 the data is extracted from Norwegian Petroleum Directorate website (NPD 2013).

Wellbore name	2/1-6	1/3-3	1/3-9S	7/12-9
UTM Zone	31	31	31	31
Structural element	Cod Terrace	Cod Terrace	Cod Terrace	Cod Terrace
Field	Gyda	Tambar	Tambar	Ula
Content	Dry	Oil	Oil	Oil
KB elevation (m)	25	25	23	23.5
Water depth	66	68	68	70
TD (m RKB)	4588	4876	4516	3820
Oldest penetrated age	Late Triassic	Late Permian	Late Jurassic	Triassic

5.2 Well Correlation

Well correlation has been done among four selected wells to correlate the high porosity and low porosity zones for upper Jurassic sequence. Ramm et al. (1997) have already interpreted (Figure 4.1) the wells 2/1-6 and 1/3-3 on the basis of Gamma ray log and core-porosity but did not include the wells 1/3-3S and 7/12-9 in their correlation.

Gamma ray, sonic, neutron porosity, density, density porosity and He-porosity logs have been used in combination for well correlation (Figure 5.1). Interpretations of these wire line logs helped to mark the high porosity and low porosity zones (Table 5.2). Interpretation is mostly based on density porosity logs as density log show a small deviation from He-porosity in well 1/3-9S, which is considered acceptable. The study identifies five upper Jurassic sequences; P4, P2, P1, S2 and S1. P2 and S2 are high porosity zones while P4, P1 and S1 show relatively low porosities. In well 7/12-9 P4, S2 and S1 are not recognized.

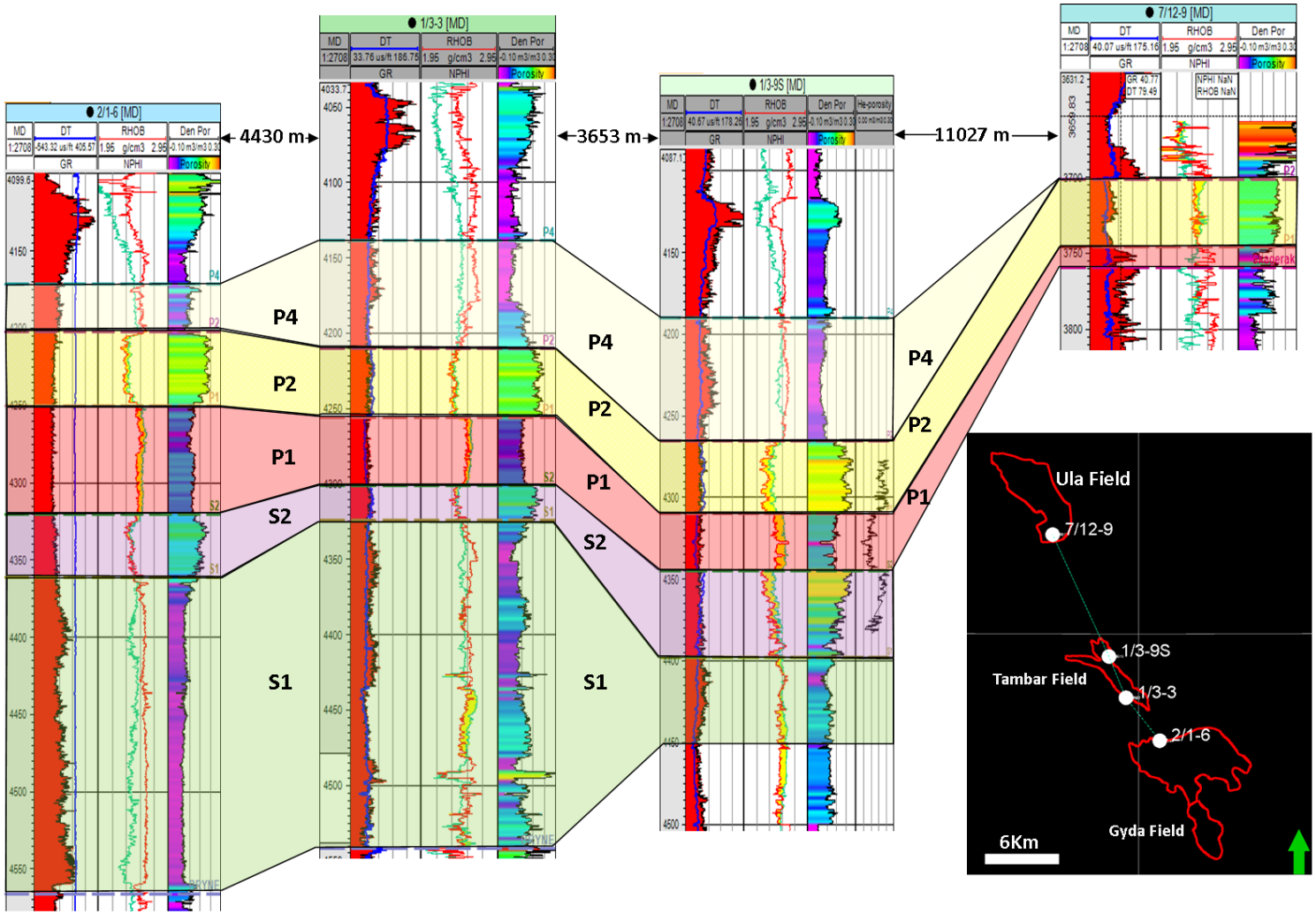

Figure 5.1 Well correlations between Gyda, Tambar and Ula field wells; map view shows the location of the wells.

High porosity units P2 and S2 have low gamma ray characterization and high porosity value i.e. >15% while P4, P1 and S1 shows relatively high gamma ray signature and porosities less than 15%. Where porosities are very low less than 10% are because of muddy intervals and show clay content (e.g. in well 1/3-9S depth interval (4403 – 4430 m RKB) and high gamma ray values.

5.3 Cross Plots

Different cross plots have been generated to evaluate the petrophysical logs. In Figure 5.2 porosities are cross plotted against measured depth for all four wells. It is notable that P2 and S2 units fall in relatively high porosity zone as compared to the P4, P1 and S1 units.

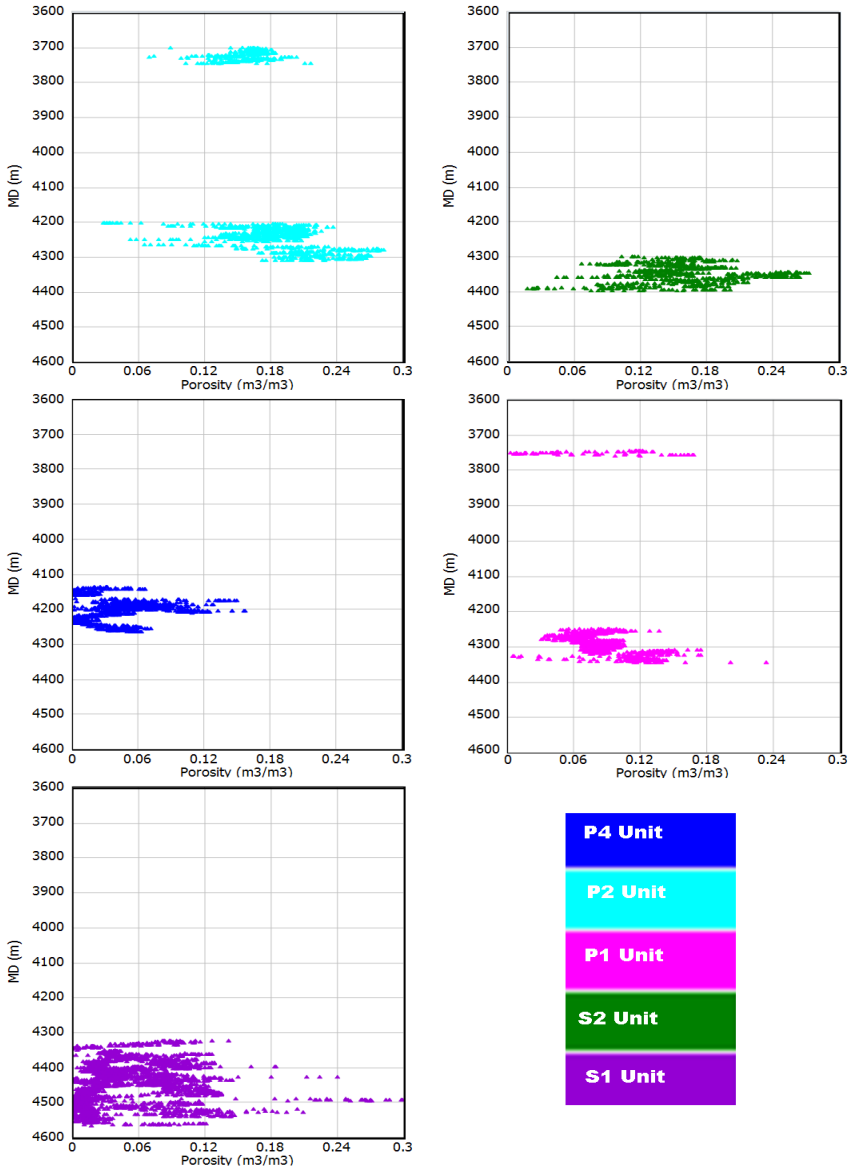

Figure 5.2 Porosity and measured depth cross plotted to show the porosity range in all wells.

As well 1/3-9S is the key well for this study further data analysis has been done on this well. In Figure 5.3 gamma ray histograms have been generated. A cutoff value of 60 API has been applied to distinguish between sand and shale. The histogram shows that P2 and S2 units have very high sand population as compared to the P4, P1 and S1 units. This higher clay values resulted in low porosity for these units in 1/3-9S well.

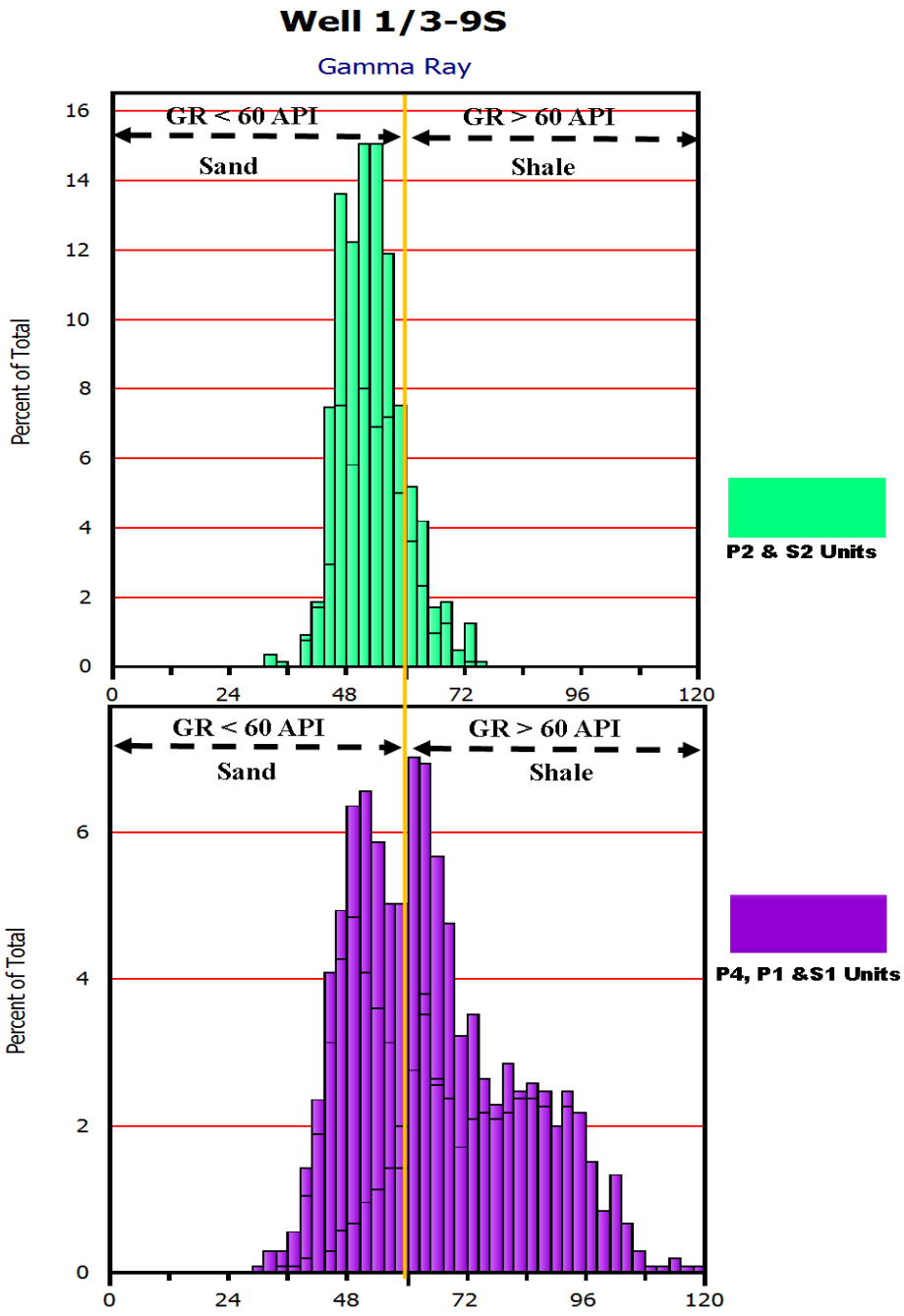

Figure 5.3 Gamma ray distributions plotted for 1/3-9S well (4190 m to 4450 m interval). A cutoff value of 60 API is selected to mark the boundary between sand and shale.

A cross plot between Density and Vp, color coded with Gamma Ray for 1/3-9S well has been generated (figure 5.4). High porosity sand has Vp (m/s) ranges between 3500 to 4400 m/s and shows low density. Low porosity sands have higher Vp (m/s) values (4400 – 5200 m/s) and density range between 2.30 to 2.5 g/cc. Shaly sand and shale both have higher density values while shale has very low P-wave velocity. In Figure 5.5 Density versus P-wave plot, color coded with formation tops has been generated. High porosity zones P2 and S2 shows the low p-wave velocity and low density as compared to the low porosity zones P1, S1 and P4. This cross plot also shows a clear V-shape and validates the figure 5.4 interpretation.

The effect of increasing clay content in upper Jurassic interval (4190 – 4450 m RKB) for well 1/3-9S has been depicted by a velocity-porosity relation color coded with gamma ray in Figure 5.6. Cross plot shows that velocity increases and porosity decreases by increasing clay content until it reached the transition point. After transition point the shaly sand has been converted to sandy shale and show high gamma ray values in the plot.

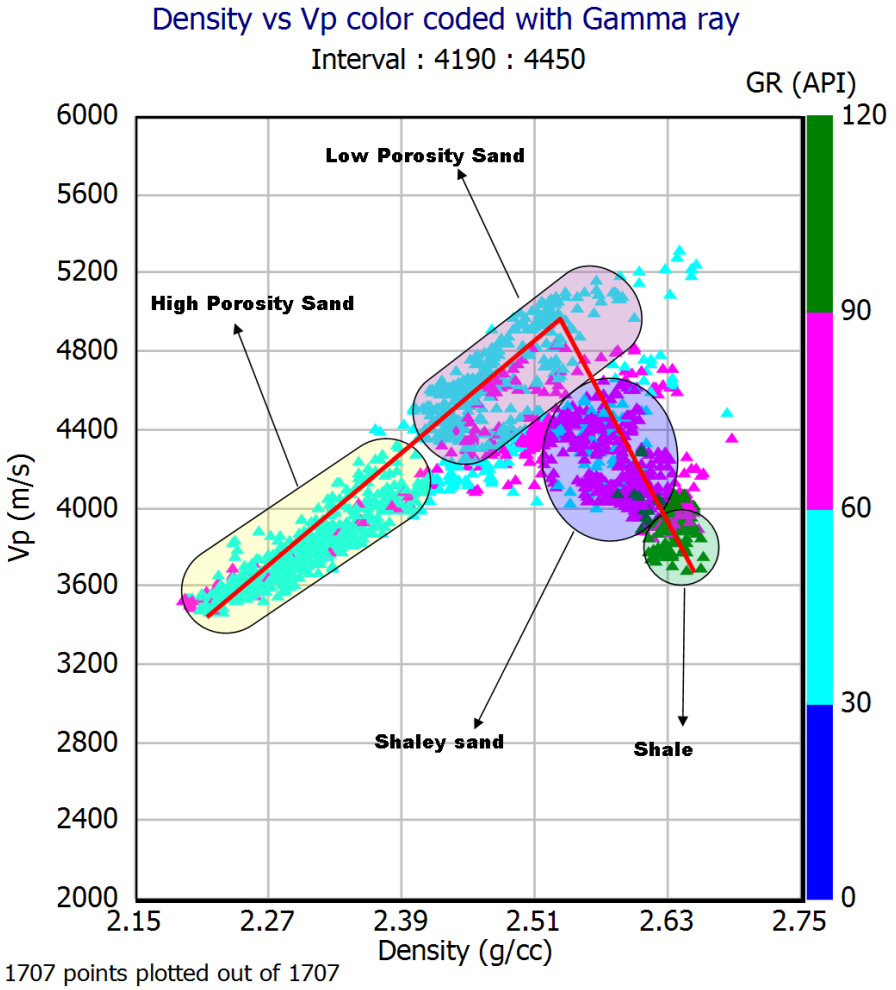

Figure 5.4 shows cross plot between P-wave and Density color coded with Gamma ray. A clear V-shape trend can be observed.

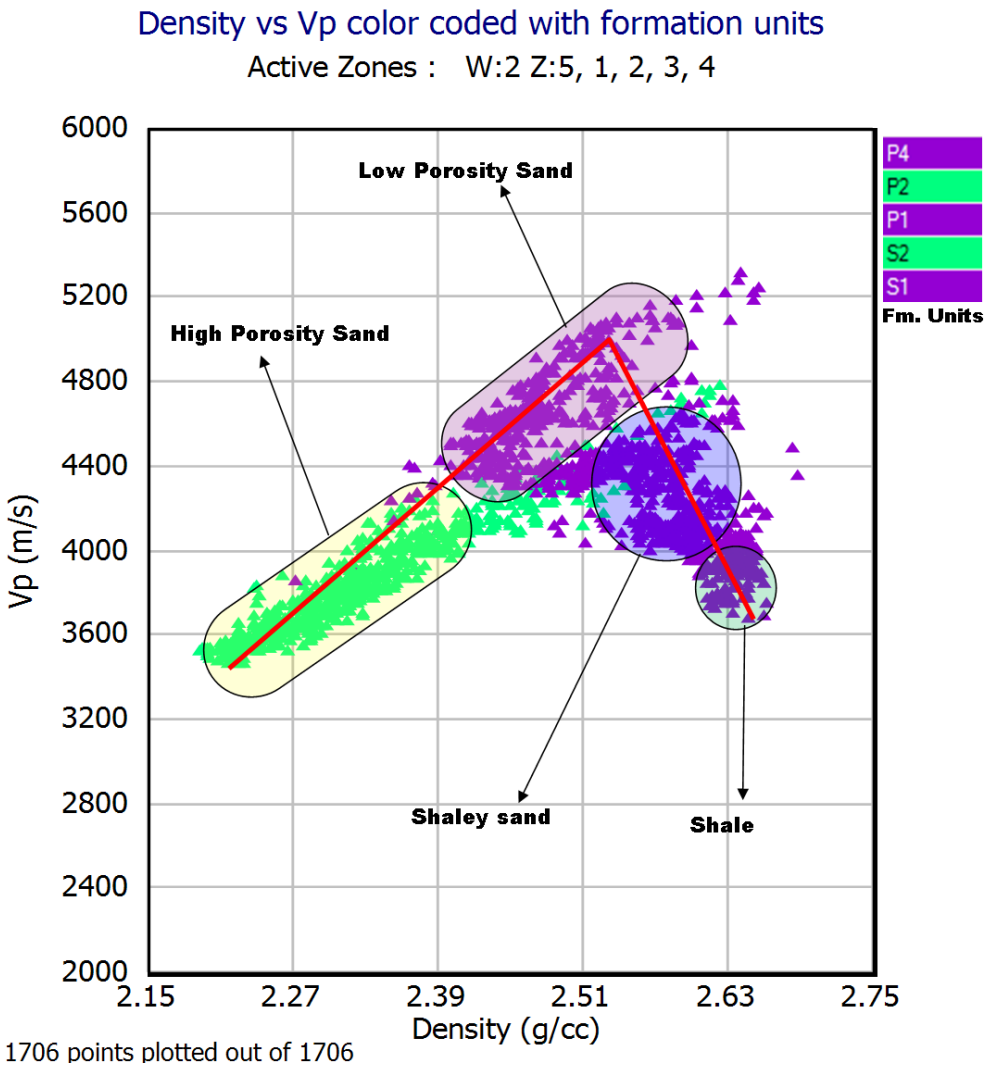

Figure 5.5 P-wave versus density color coded with lithostratigraphic units for 1/3-9S well.

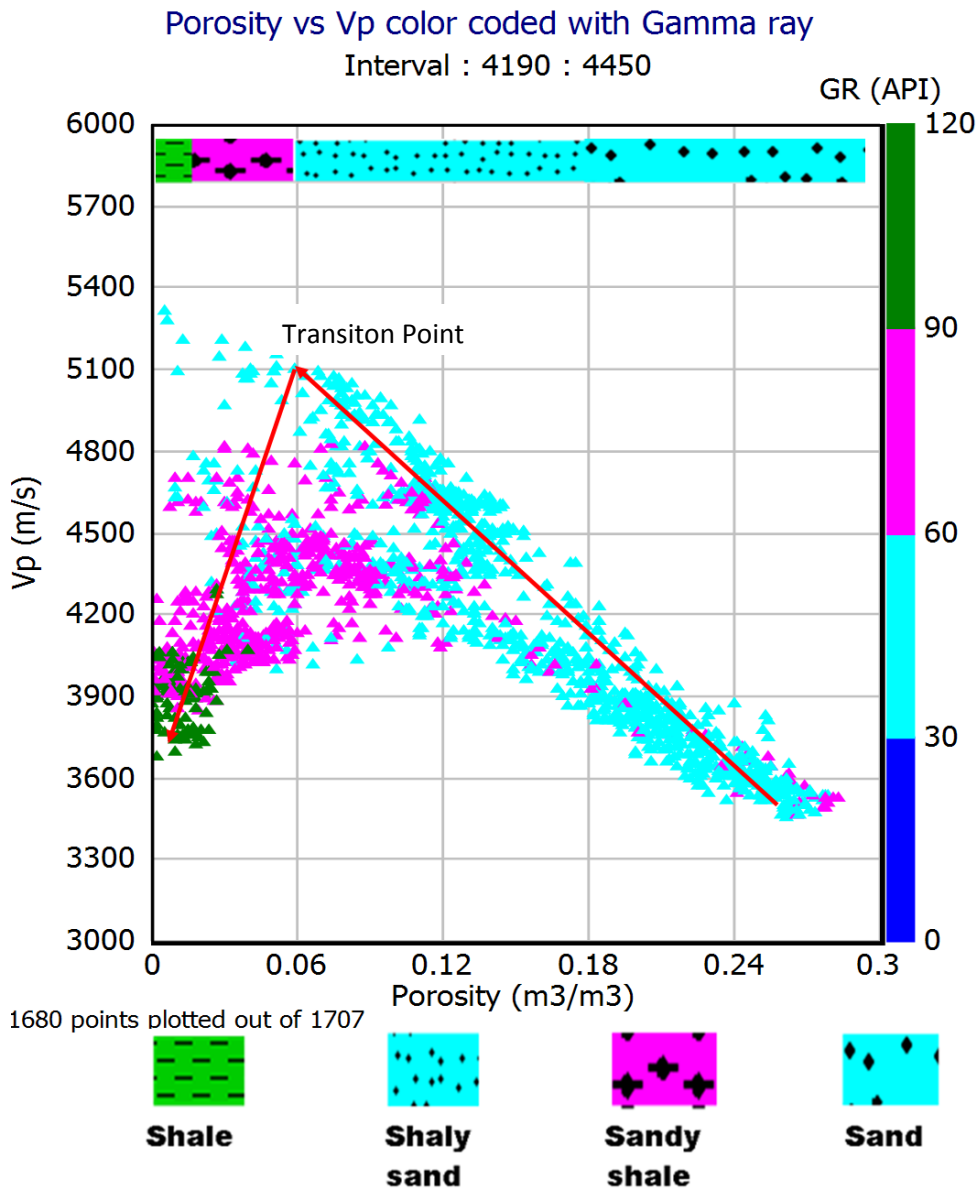

Figure 5.6: Vp vs Porosity (in fraction) color coded with gamma ray for 1/3-9S well

6. PETROGRAPHIC EVALUATION

6.1 Introduction

A Petrographic and mineralogical study was done on the samples taken from well 1/3-9S to determine the relationship between preserved porosity and composition of the upper Jurassic sandstone. From petrophysical analysis (Chapter 5) it is evident that porosities are well preserved in deeply buried upper Jurassic sandstones, so the purpose of the petrographic study is to determine the factors which preserved porosity at this depth. Sorting, grain size and grain composition have been analyzed with the help of optical microscopy. A scanning electron microscope (SEM) analysis was also performed on all 20 samples to estimate the presence of grain coats, type of grain-coats and to which extent the coating has covered the grains.

6.2 Results

6.2.1 Point count

A point counting was done on 20 thin sections taken from well 1/3-9S at 4295.66 m – 4349.33 meter depths. The main purpose of the point count was to quantify the grains, matrix, cement and porosities. Results of point count have been shown in table 6.1.

6.2.1.1 Point count results

The point counting results shown in figure 6.1 are subdivided into four main categories; grains (including secondary porosity), matrix, quartz cement, carbonate cement and primary porosity. All samples are plotted according to their measured depth (m). For further simplification data has been divided into four zones where A1and A2 depicts high porosity (more than 10%) units while B and C are low porosity units (less than 10%). Moreover unit C has very high carbonate cement as compared to other units.

Table 6.1 Results of the point count done on petrographic microscope for Well 1/3-9S.

Sample No.	Depth (m)	Frame work composition			Matrix	Cement		Porosity		IGV	Sequences
		Quartz	Felds.	lithic frag.		Qtz cem.	Cal Cem.	prim.	Sec.		
1	4295.66	55.30	4.60	1.30	11.30	2.30	6.60	17.60	1.00	37.80	A1
2	4298.00	57.30	5.60	2.00	12.30	4.60	1.60	15.00	1.60	33.50	A1
3	4299.00	62.60	3.30	2.30	2.90	4.00	2.30	21.00	1.60	30.20	A1
4	4300.33	60.30	5.60	1.60	11.60	4.60	0.30	15.00	1.00	31.50	A1
5	4302.33	62.60	4.00	0.60	15.30	5.30	2.00	9.60	0.60	32.20	B
6	4305.66	61.60	3.60	1.60	9.60	15.00	2.30	5.00	1.30	31.90	B
7	4307.33	60.10	5.60	0.30	15.30	15.30	0.30	3.10	0.00	34.00	B
8	4333.33	62.00	5.30	0.60	11.60	13.60	0.00	6.60	0.00	31.80	B
9	4336.33	57.60	7.00	0.00	21.00	9.30	1.00	3.10	1.00	34.40	B
10	4337.33	62.00	4.60	0.30	9.60	10.60	5.60	7.30	0.00	33.10	B
11	4338.33	59.30	5.60	0.60	6.00	14.30	4.60	9.00	0.60	33.90	B
12	4339.00	58.10	3.30	0.00	3.60	3.60	22.30	8.60	0.60	38.10	C
13	4339.69	59.30	3.60	0.60	8.90	6.60	11.60	8.10	1.30	35.20	C
14	4340.33	61.00	5.30	0.60	6.60	6.60	2.60	16.30	1.00	32.10	A2
15	4341.33	61.30	4.60	0.00	9.60	4.60	4.00	13.60	2.30	31.80	A2
16	4342.33	60.50	7.30	1.00	6.60	5.00	3.60	15.00	1.00	30.20	A2
17	4343.33	60.00	4.60	1.60	13.60	3.30	2.60	14.30	0.00	33.80	A2
18	4344.00	58.00	7.30	0.00	16.60	6.30	2.10	9.10	0.60	34.10	A2
19	4347.33	59.30	5.60	0.60	8.60	6.60	3.30	14.30	1.60	32.80	A2
20	4349.33	58.30	3.30	0.00	15.60	7.00	0.30	14.60	0.60	37.50	A2

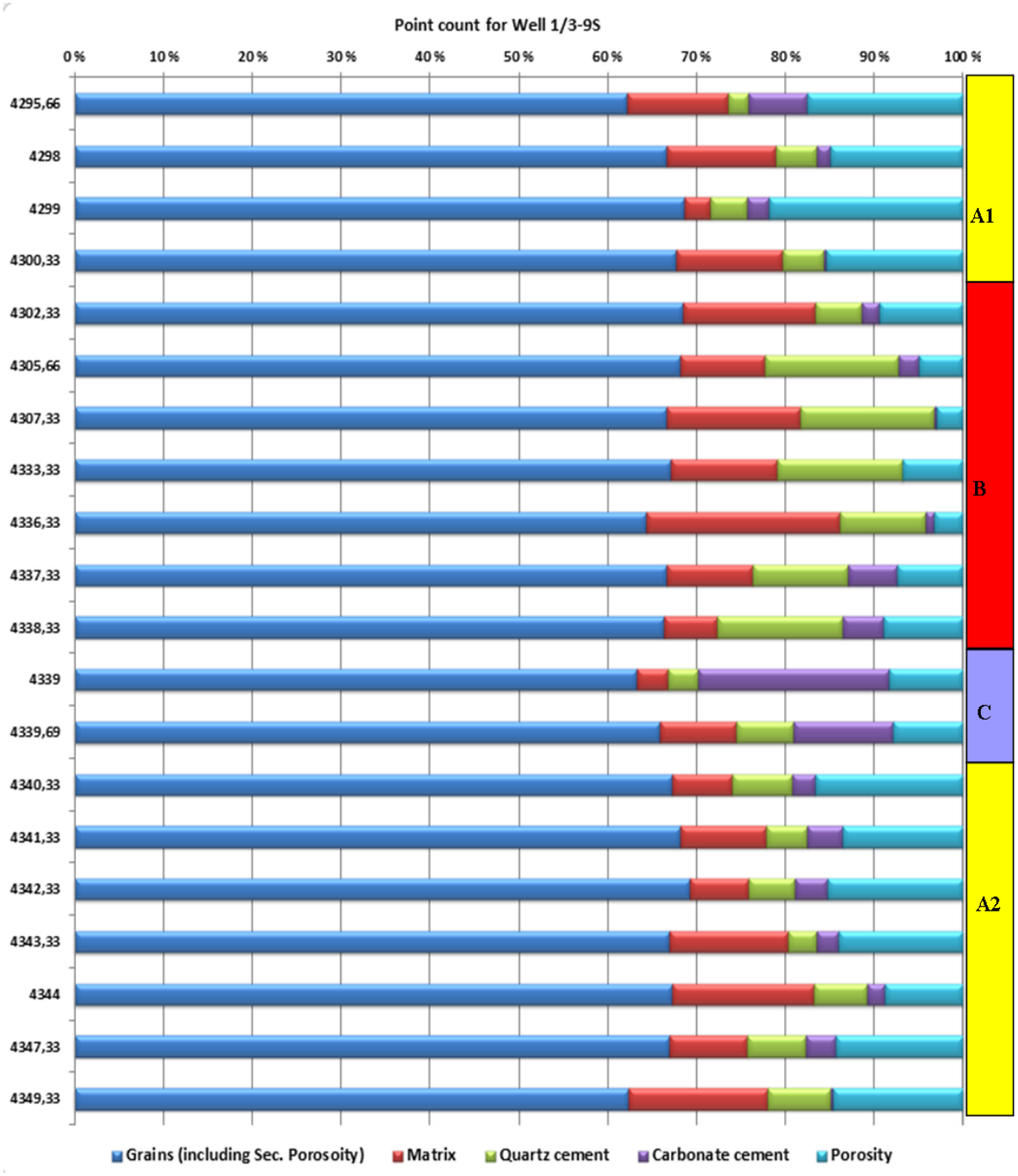

Figure 6.1 Point count results shown with respect to the sample depths. The right column shows the variation in porosity. A1 and A2 are high porosity units while B and C are low porosity units.

6.2.1.2 Petrographic classification

Frame work composition of the rock taken from point count results and divided into the three components; quartz, rock fragments and feldspar. These three components have been plotted on the ternary diagram of Dott (1964) to determine type of sandstone (Figure 6.2). As majority of the samples have less than 15% matrix and ample amount of quartz thus it lie within the definition of arenites. By using Dott (1964) arenites ternary diagram (Figure 6.2) it has been observed that all of the samples fall in the subarkose area. Sandstones with 5-25% feldspar are called subarkose. Only three of the samples overlap to the quartz arenites area with less than 5% feldspar.

According to Bjørlykke and Jahren (2010), in tectonically stable area with mature relief there is enough time for the weathering of transit sediments and in situ bedrock. In such conditions, sediments are eroded and deposited many times prior to their final deposition. As a result most of the feldspar grains break down during transportation phase and orthoquartzites or subarkose will be deposited.

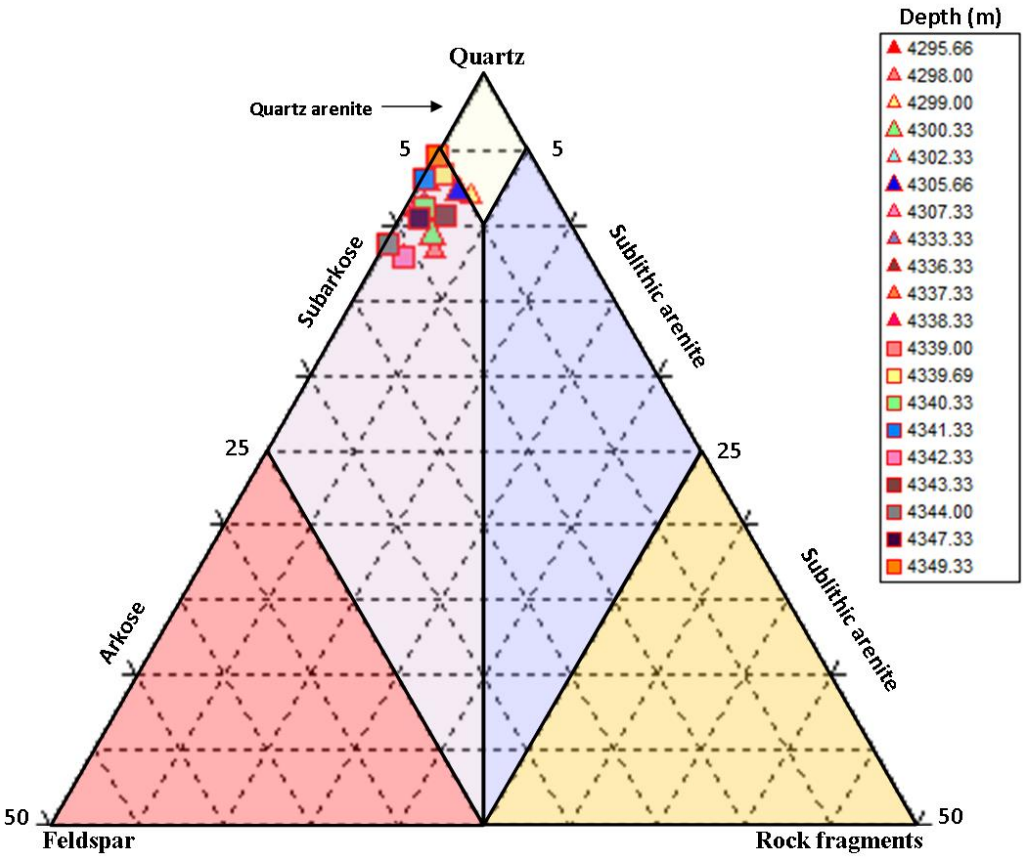

Figure: 6.2 Classification of sandstones (from Dott 1964). Samples with their depth have been shown with legend.

6.2.1.3 Primary porosity

Primary porosity was one of the important counts in point counting which shows the current porosity of the samples. The bar chart (Figure 6.3) represents the porosities of the samples with increasing depth and two types of sequence have been observed. A1 and A2 shows high porosity values ranging between 10 to 21% while B and C sequence represent low porosity values ranging between 3.1 to 9.6%. Mean porosity values (Table 6.2) for sequence A1 and A2 are 17.15 and 13.88% while B and C sequence has 6.24 and 8.35% mean values respectively.

Table 6.2: Mean percentage of primary porosity for A1, B, C and A2 sequences.

Mean Porosities %			
A1	B	C	A2
17,15	6,24	8,35	13,88

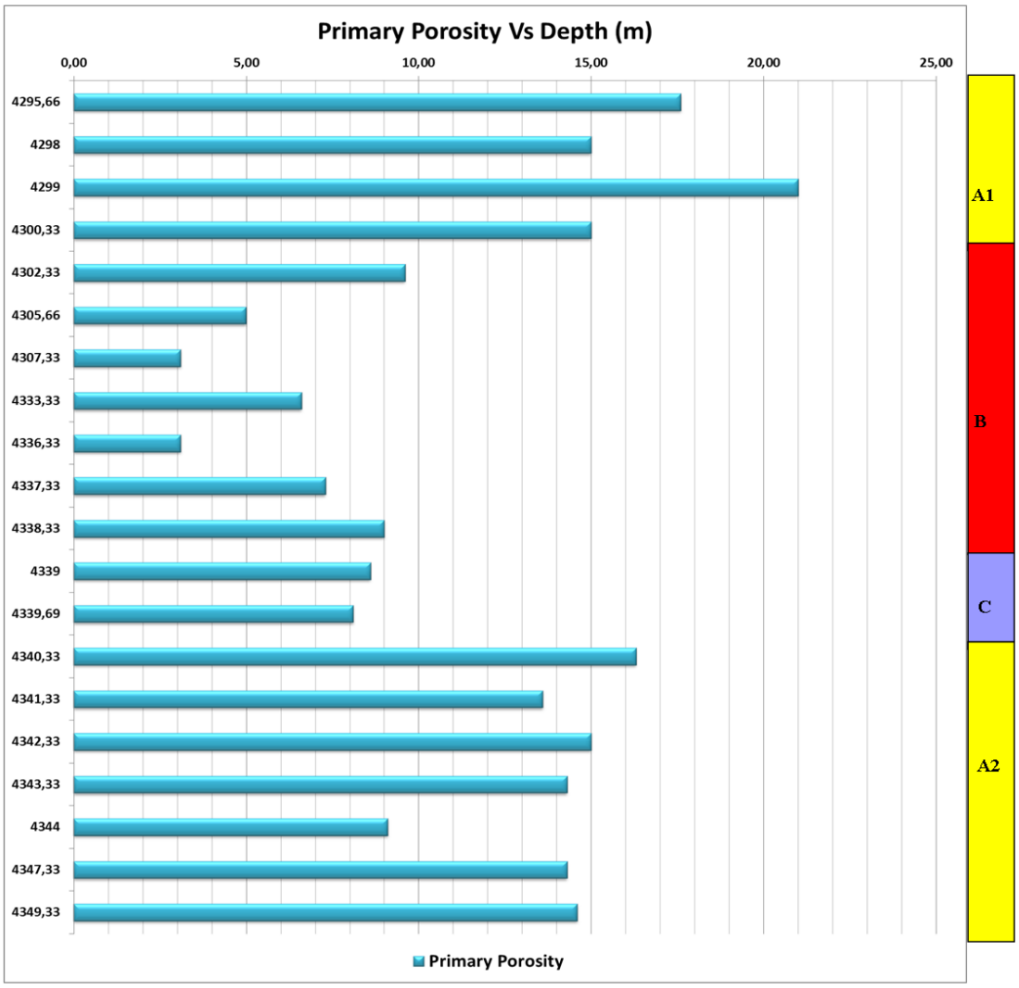

Figure 6.3: Bar chart diagram of the primary porosity vs. depth. In right column different sequences has also been identified on the basis of low and high porosity of the samples.

Precipitation of quartz cement is one of the reasons which reduced the primary porosity at greater depths. To analyze the relation of primary porosity with quartz cementation a bar chart has been generated (Figure 6.4) and sequences have also been marked. Overall we can say that there is a linear relation between quartz cement and primary porosity.

It has been observed that samples with high primary porosity (A1and A2) have less quartz precipitation as compared to the low porosity sequence B. The sample 4307.33 shows highest amount of quartz cement (15.3%) with a very low (3.1%) primary porosity while on the contrary sample 4299 shows high porosity (21%) and low quartz cement with value of 4%. Sequence C has both low porosity and low quartz cementation, which is possibly due to the emplacement of early carbonate cement.

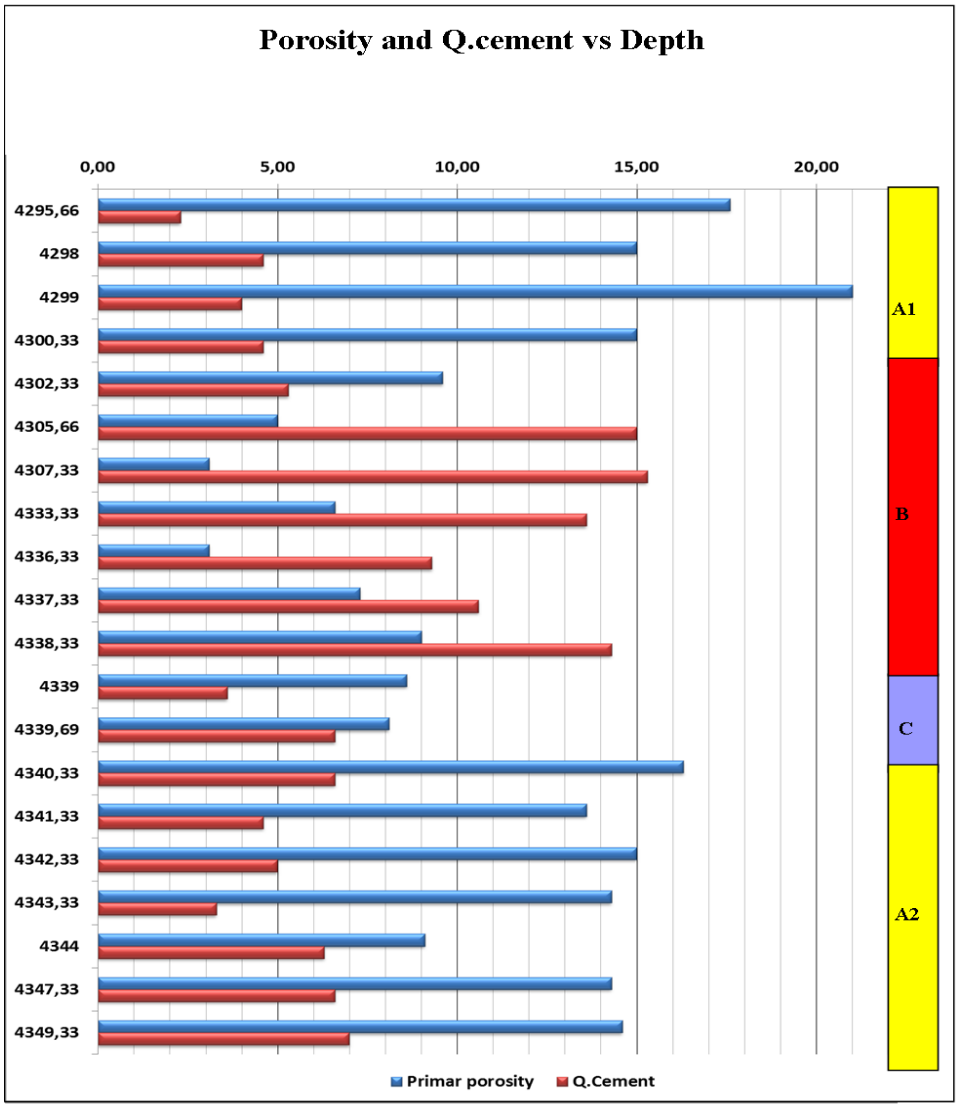

Figure 6.4: Bar chart showing the relation between primary porosity and quartz cementation vs depth. Primary porosity and quartz cementation was calculated during point counting.

6.2.1.4 Authigenic clays

A significant amount of authigenic clays have been observed during point counting and it was observed that most of the clay is illite and very few kaolinites which were later on confirmed by the SEM analysis.

After 3.7 to 3.8 Km burial depth a rapid increase in the digenetic illite has been observed (Thomas 1986; Scotchman et al. 1989). The strong increase in the abundance of illite below 3.5 to 4 Km is because of the illitization of kaolinite, which seems to require 130 to 140 ◦C temperature (Bjørlykke et al. 1986).

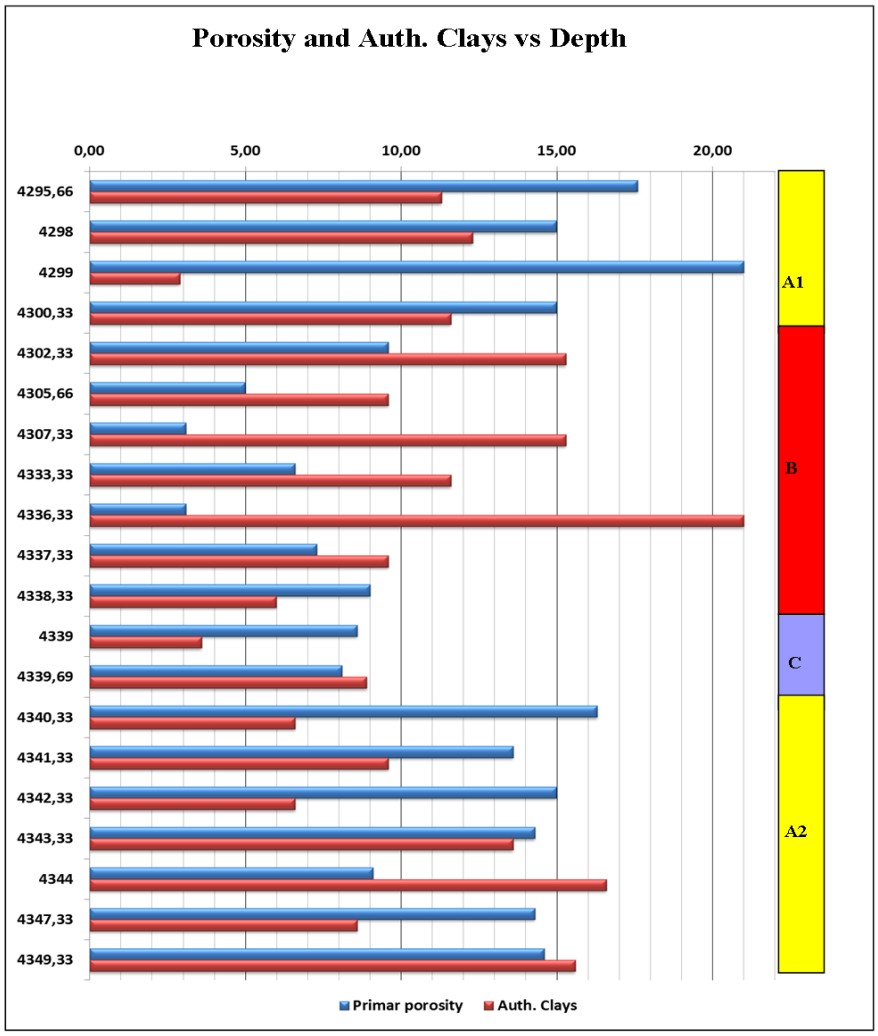

Figure 6.5: Bar chart shows the comparison of primary porosity and authigenic clays.

Scanning electron microscopy shows that illite is present as a grain coat and pores filling material. From (Figure 6.5) it is observed that authigenic clays are comparatively less in sequences A1, A2 and C while in sequence B amount of authigenic clays are more. This high amount of illite in sequence B is one of the reasons of its low porosity.

6.2.1.5 Carbonate cement

Carbonate cement has also been point counted during point counting and a bar chart (Figure 6.6) has been generated with porosity. It has been observed that the sequence C has very high amount of carbonate cement with 22% in sample 4339. While in rest of the samples carbonate cement is randomly distributed and has not very significant amount.

Figure 6.6 shows the cyclic increase in the carbonate cementation. This cyclic increase indicates that carbonate cement has increased with decreasing depth from 4349.33m until 4339 m. After that point (4339 m) carbonate content has again decreased and another cycle of increasing carbonate content is observable until 4295.66 m depth (Figure 6.6). It suggests that 4339 m depth may represent a Maximum flooding surface (MFS) because of the maximum carbonate content found at this level.

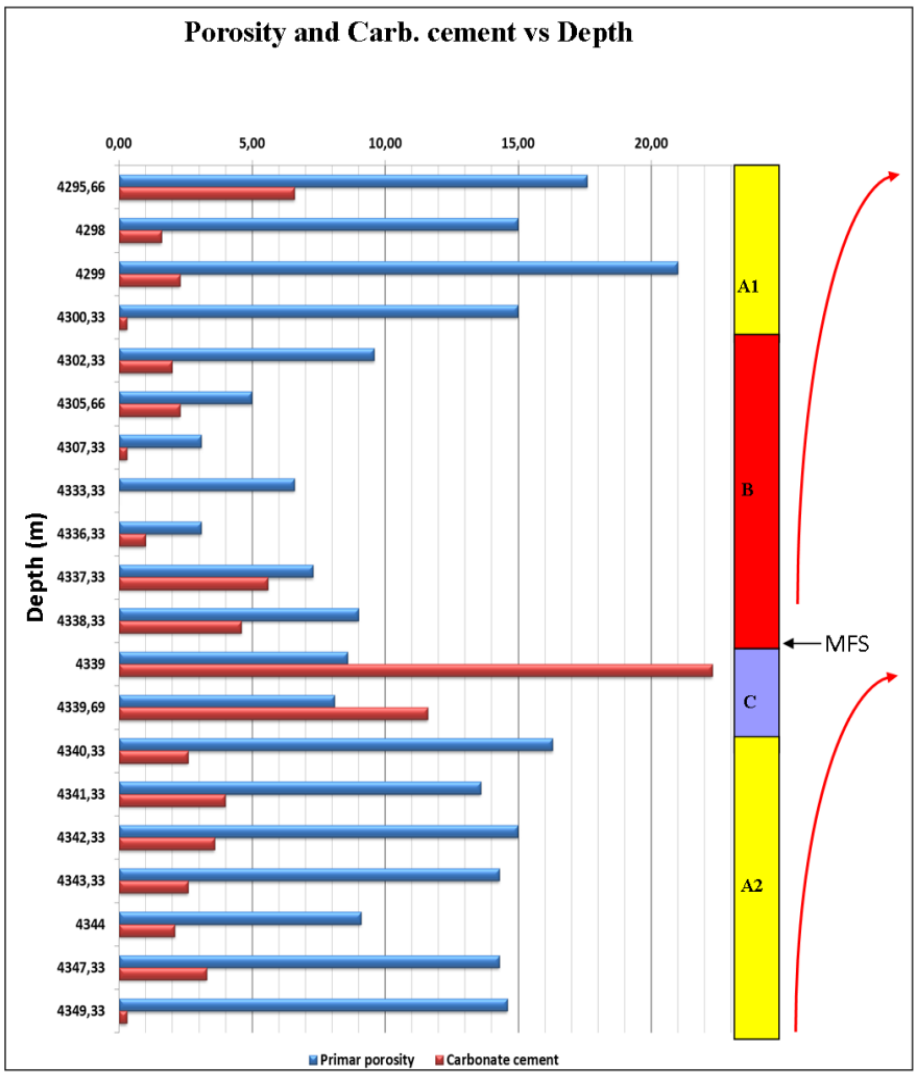

Figure 6.6: Bar chart showing the comparison of porosity and carbonate cement. Red arrows showing the increase in carbonate cementation and the suggested MFS is marked with respect to the carbonate cement.

6.2.1.6 Intergranular volume (IGV)

Intergranular volume (IGV) has been calculated from point counting to get the estimation of compaction and cementation. Calculated IGV is the sum of matrix, cement and porosity for each sample and shown in Figure 6.7.

The average IGV values for all sample is 33.50% while some of the samples show slightly higher values (up to 38.10%) than the average values. These higher values are because of the early carbonate cementation and higher content of antigenic clays. In some samples the values are little lower than the average values which shows the higher mechanical compaction and low quartz cement content. For example in sample 4299 the IGV is 30.20% and quartz precipitation is 4% calculated

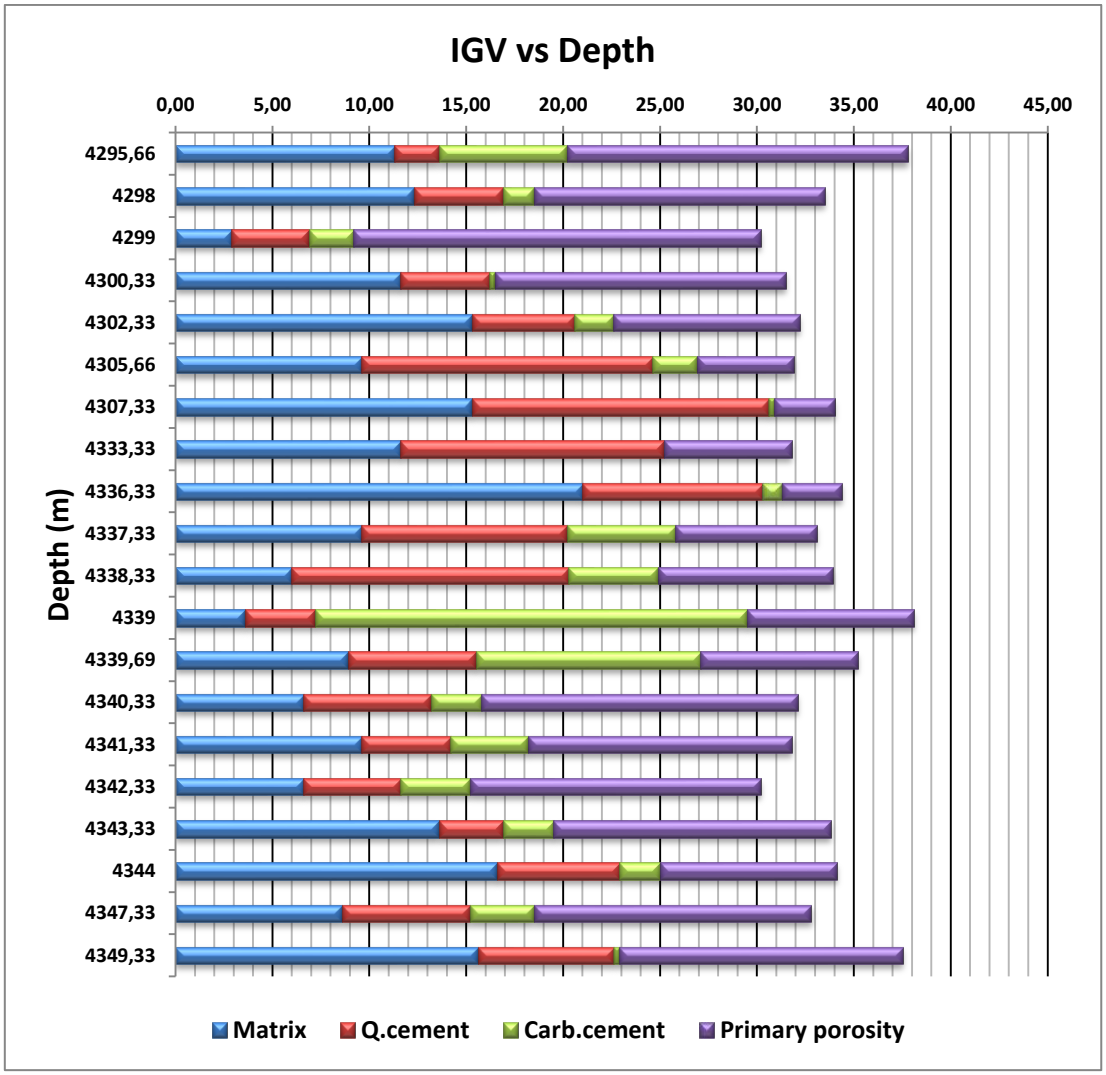

Figure 6.7: Calculated IGV values arranged by increasing depth.

6.2.1.7 Textural character

Grain size and sorting has been determined by measuring the long axis of the grains by measuring the 50 grains from each sample. Grain size measurements are presented as arithmetic mean average of the grains and sorting is measured as the standard deviation of the grain size measurements. A plot has been generated (Figure 6.8) to display the sorting and grain size of the samples. Almost all of the samples fall under fine grained and moderately well sorted parameters.

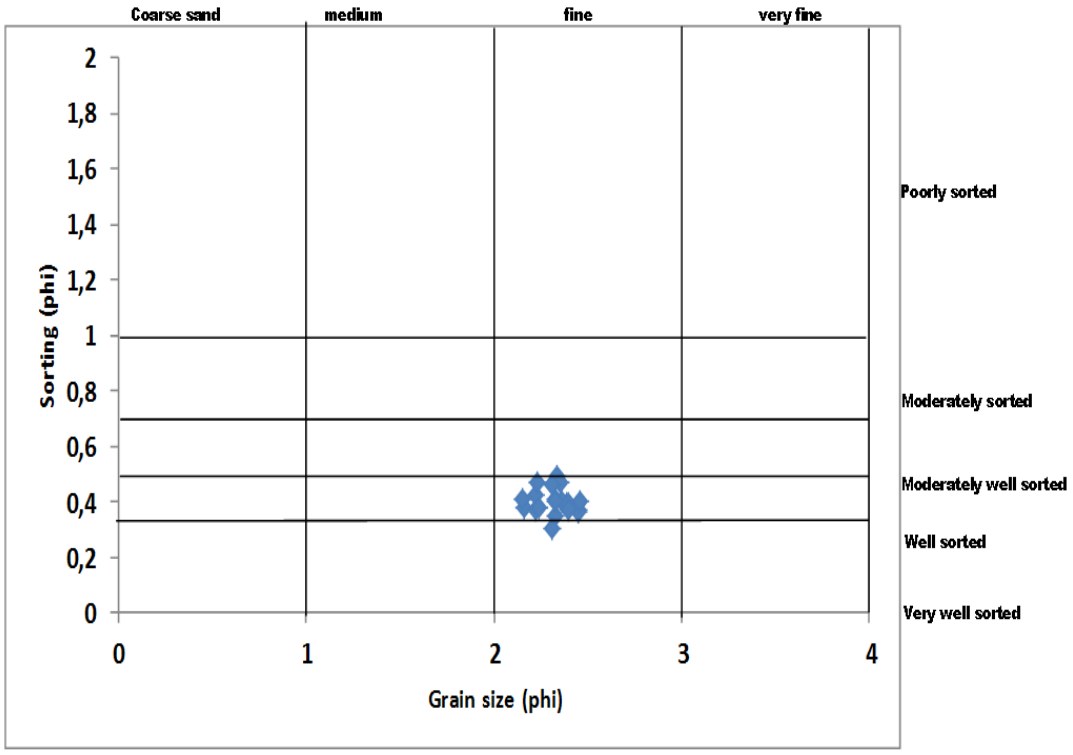

Figure 6.8: Textural characteristics of the all 20 samples from well 1/3-9S.

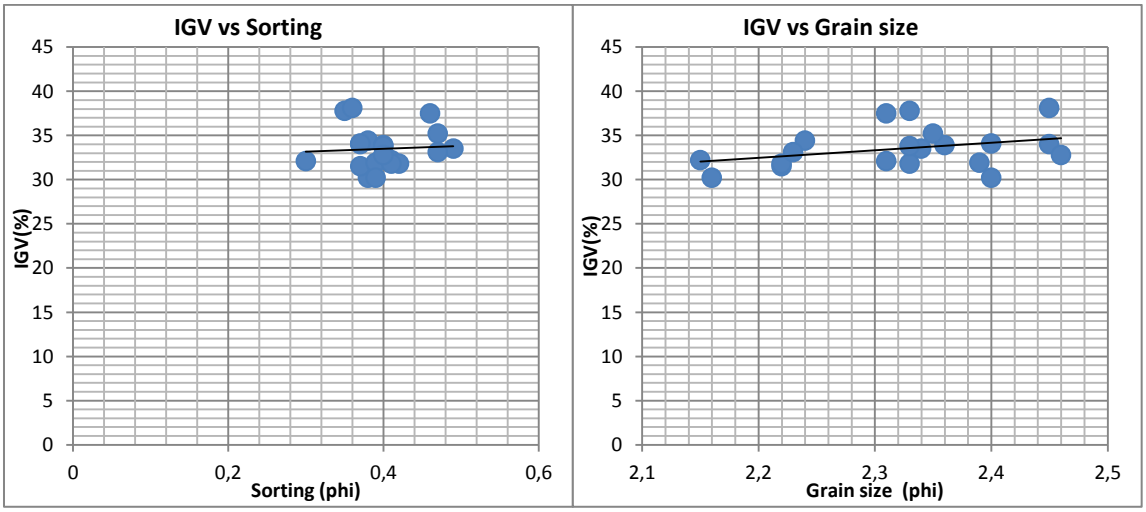

Figure 6.9: IGV is plotted against sorting and grain size.

IGV is plotted vs sorting and grain size (Figure 6.9). Overall no considerable variation has been observed in both plots as grain size and sorting is nearly uniform throughout the sample interval. Grain size is measured by measuring the longer axis of the 50 random grains from each sample.

Sediments can be classified by two basic properties; texture and mineral composition (Krynine 1948). Folk 1951 have described the four stages of textural maturity for sediment (Table 6.3).

Table 6.3: Stages of sediments maturity (Folk 1951).

1 Immature stage	2 Sub-mature stage	3 Mature stage	4 Super mature stage
Sediments have considerable clay and mica, the grains are poorly sorted and grains are angular.	Sediments have very little clay; grains are poorly sorted and angular.	Sediments don't have any clay; grains are well sorted and sub angular.	Sediments are without clay, grains are well sorted and rounded.

After complete study of the samples it has been observed that the sediments are without any detrital clay, grains are moderately well sorted and sub angular. Thus studied samples fall under mature stage.

6.2.1.8 Thin section observations

Optical microscope with an attached camera has been used to capture the images from thins section. Figure 6.10 (a and b) display the well preserved porosity and white arrow shows the secondary porosity, possibly because of the feldspar dissolution. Grain coating can also be observed in figure 6.10a which might be the reason of well preserve porosity in this sample. Figure 6.10 (b and c) display the comparatively less porosity and illite is present as pore filling clay.

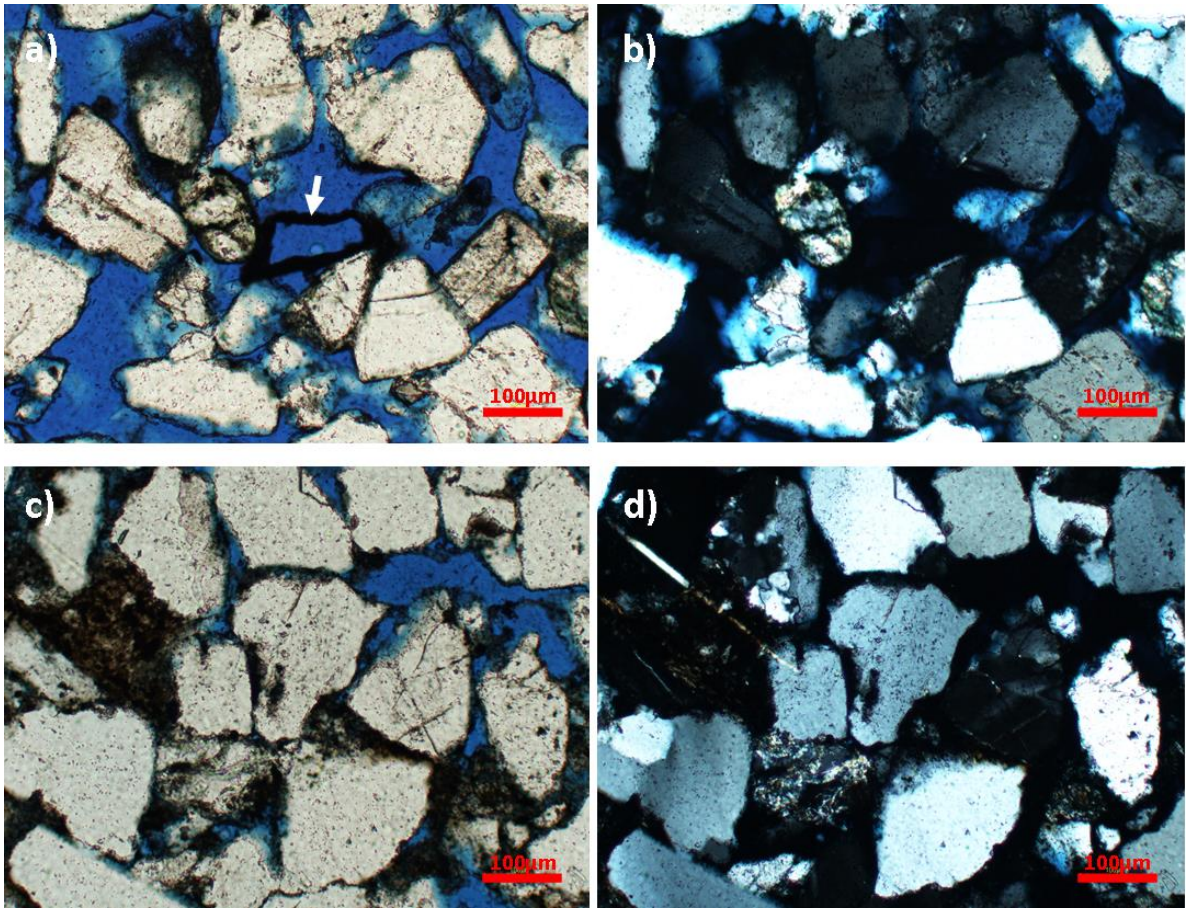

Figure 6.10: Images taken with optical microscope from sample 4299.00 (a, b) and 4339 (c,d). **a)** Secondary porosity is shown with whit arrow; overall image showing well preserved porosity because of the grain coating observed around the grains. **b)** Same image as in a) captured with cross polar. **c)** Illite as pore filling clays have destroyed the porosity, overall porosity showing less porosity as compare to the a. **d)** Same image as in c) with cross polar.

Sample 4339 shows high percentage of carbonate cement. Figure 6.11 showing the carbonate cement as calcite (a and b) and rhombohedral crystals of dolomite in figure 6.11 (c and d).

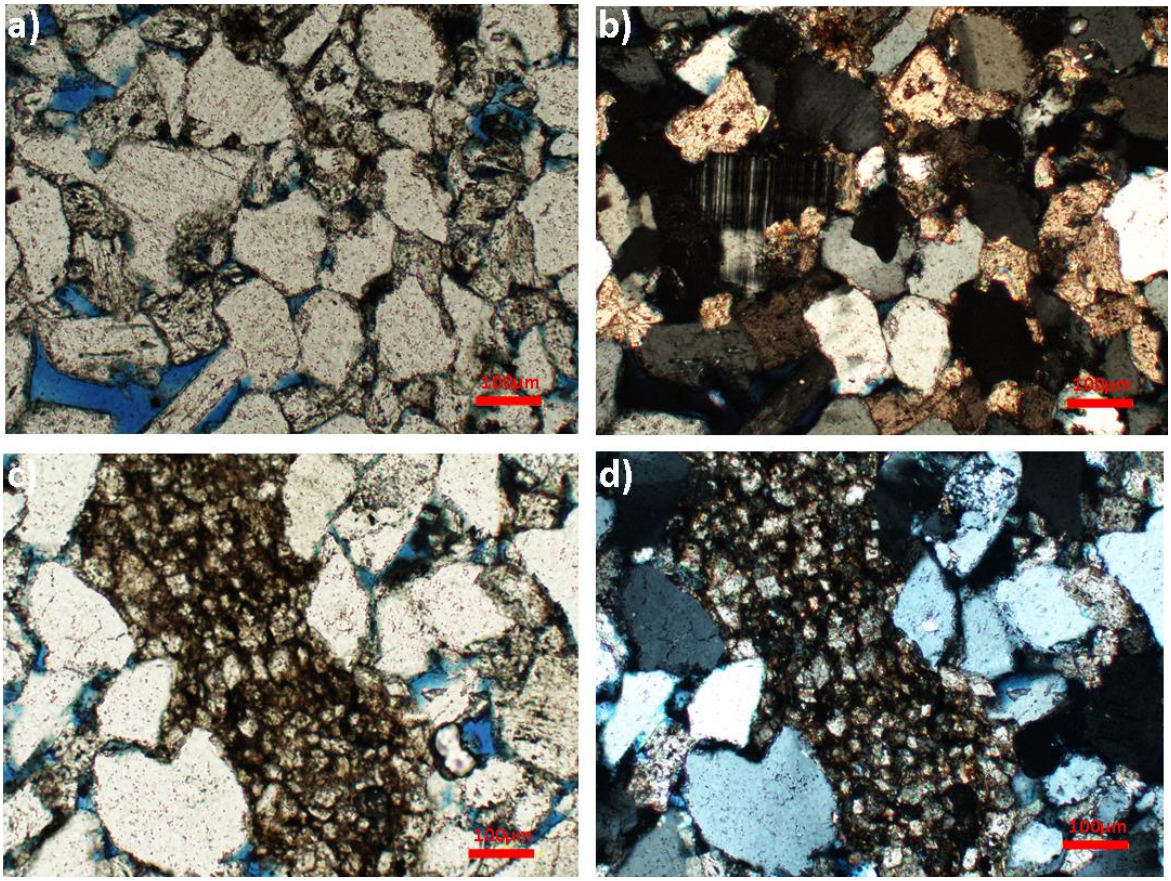

Figure 6.11: Images taken with optical microscope from sample 4339.00. **a and b)** shows the carbonate cement present in the pores and twinned feldspar crystal in cross polarized image. **c and d)** Displays rhombohedral crystals of dolomite in the pore spaces.

6.3 Scanning electron microscopy (SEM)

For further investigation, gold coated stubs and carbon coated thin sections from well 1/3-9S have been analyzed under scanning electron microscope. The main purpose was to examine the grain coating present on the grains, mineral identification and pores filling clays present between the pore spaces. Minerals have been identified with the help of Energy Dispersive Spectrometer (EDS). For quartz overgrowth Cathode ray luminescence (CL) and backscatter image used in combination.

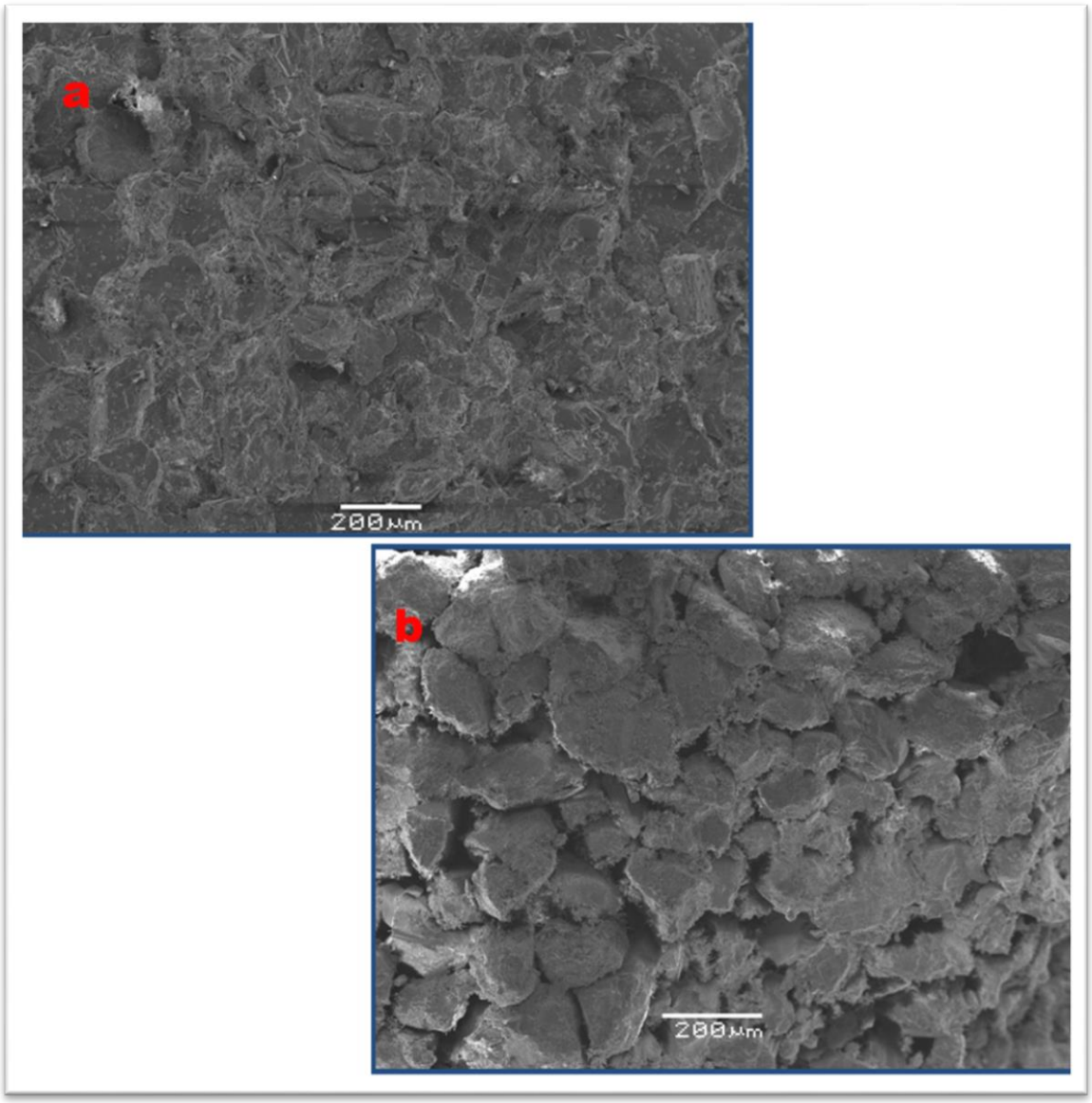

Figure 6.12: SEM image taken from 4336.33 m (**a**) and 4347 m (**b**), image **a** shows very low porosity with high cementation and belong to facie B, image **b** shows moderate porosity and less cementation and belongs to facie A2.

Two figures (6.12a, 6.12b) have been presented to show the difference of porosity observed between sample 4336.33 and 4347.33. Figure 6.12a has very low porosity and highly cemented while figure (6.12b) contains good porosity and low cementation. Porosity has been preserved due to the micro-quartz coating. Figure 6.13 is meant to display how much porosity the grain coats can preserve. Note the growth of quartz cement on detrital grain where grain coat is absent.

Figure 6.13: Backscattered images from 4347.33 m, grains are extensively coated with micro-quartz cement.

6.3.1 Results

6.3.1.1 Grain coatings

All 20 sub-mounted samples have been analyzed under SEM to investigate the type of coating and the extent the coating has covered the grains. It has been observed that micro quartz and illite coating is present to some extent in almost all the samples. Micro-quartz crystals range in size from diameter of 0.5 to 2 µm (Figure 6.14). Among micro quartz and illite coating, micro quartz is the most common grain coats which covers the detrital grains and preserve the porosity (Figure 6.15).

Illite coating has also been observed with the combination of micro-quartz coating in almost all of the samples (Figure 6.16, 6.17). Illite coating is less common as compared to the micro-quartz coating.

It has been observed that pre-described facie A1, A2 and C are more extensively coated as compare to the facie B. A scheme has been established to quantify the amount of micro-quartz and illite as a grain coat (Table 6.4). The quantities are estimated during SEM analysis.

Table 6.4: Amount of grain coating, estimated from sub-mounted samples of Well 1/3-9S.

Sample No.	Depth (m)	Micro qtz.	Illite	Sequence
1	4295,66	3	1	A1
2	4298	3	2	A1
3	4299	3	1	A1
4	4300,33	3	1	A1
5	4302,33	1	2	B
6	4305,66	1	1	B
7	4307,33	0	1	B
8	4333,33	1	2	B
9	4336,33	0	1	B
10	4337,33	1	2	B
11	4338,33	2	1	B
12	4339	2	1	C
13	4339,69	1	2	C
14	4340,33	3	1	A2
15	4341,33	3	1	A2
16	4342,33	3	1	A2
17	4343,33	3	2	A2
18	4344	2	1	A2
19	4347,33	3	2	A2
20	4349,33	3	2	A2
0: Not present 1:Little coverage 2:Moderate coverage 3: Good coverage				

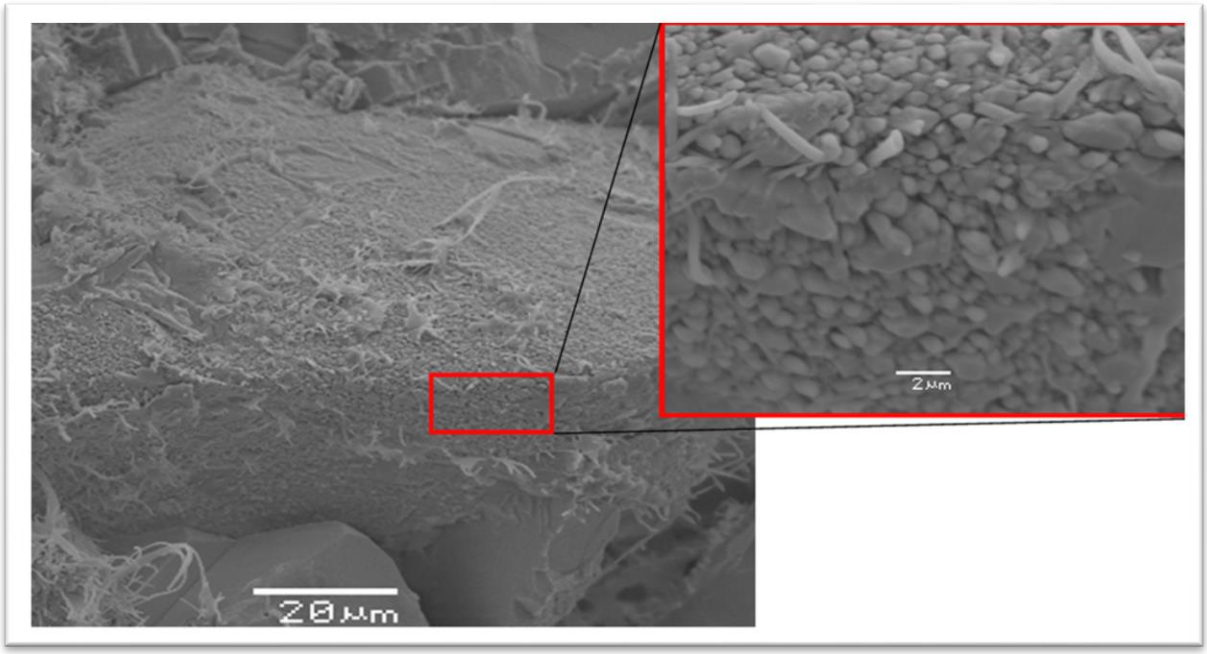

Figure 6.14: Showing coating of micro-quartz and illite. Variation in micro-quartz can observe in inset image.

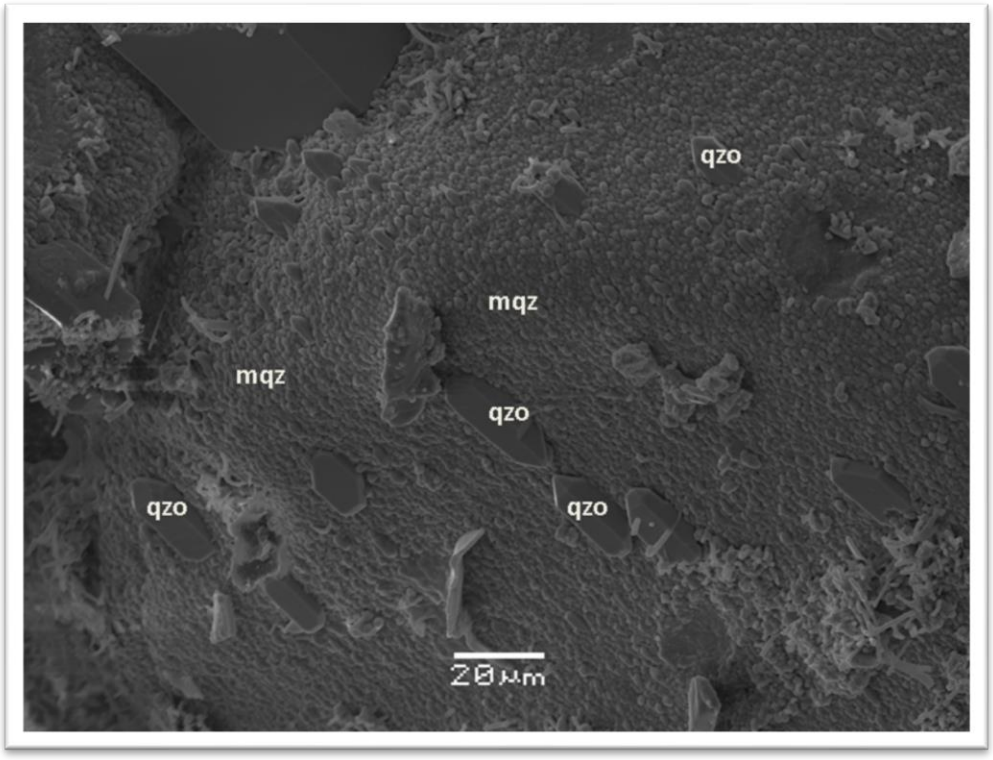

Figure 6.15: SEM image taken from 4298 m, euhedral overgrowth appear on the grain where micro-quartz coat is not present.

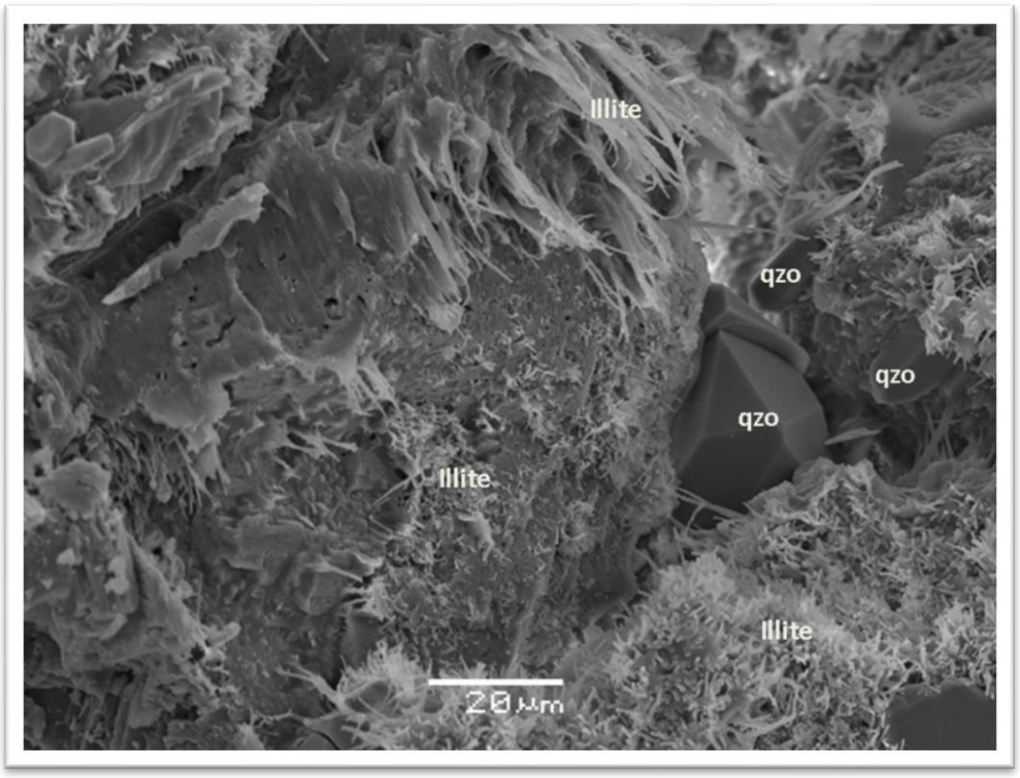

Figure 6.16: SEM image taken from 4302.33 m showing the illite coating. Quartz overgrowth is present where coating is absent.

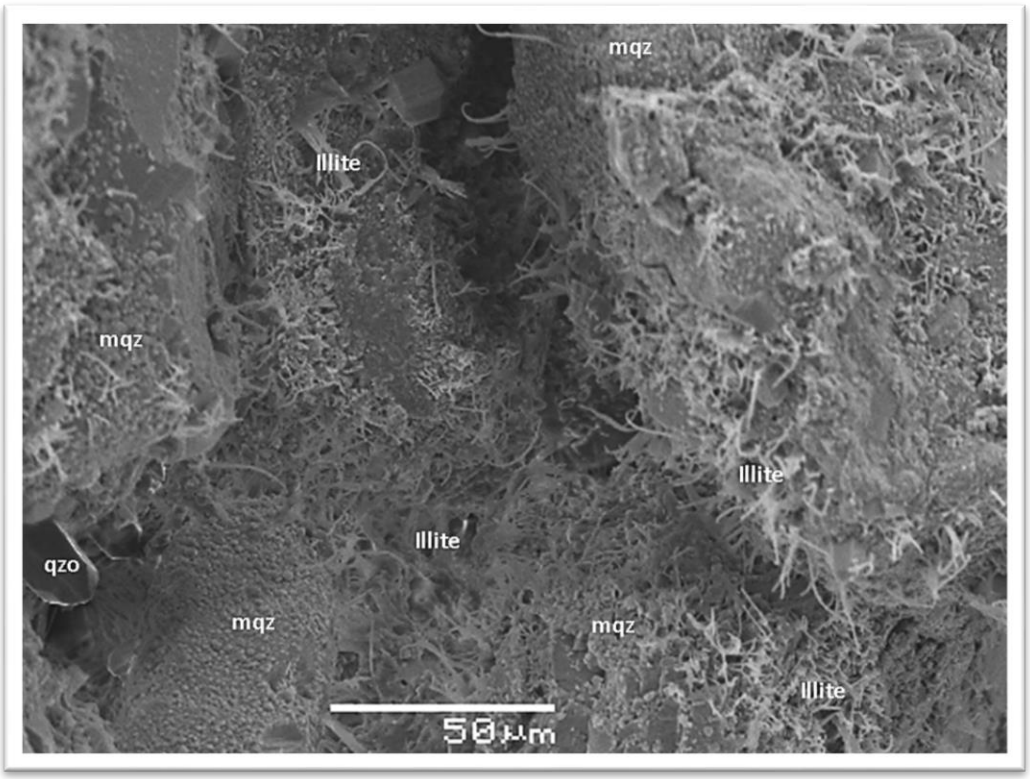

Figure 6.17: SEM image taken from 4349.33 m. Porosity has been preserved because of illite and micro-quartz coat.

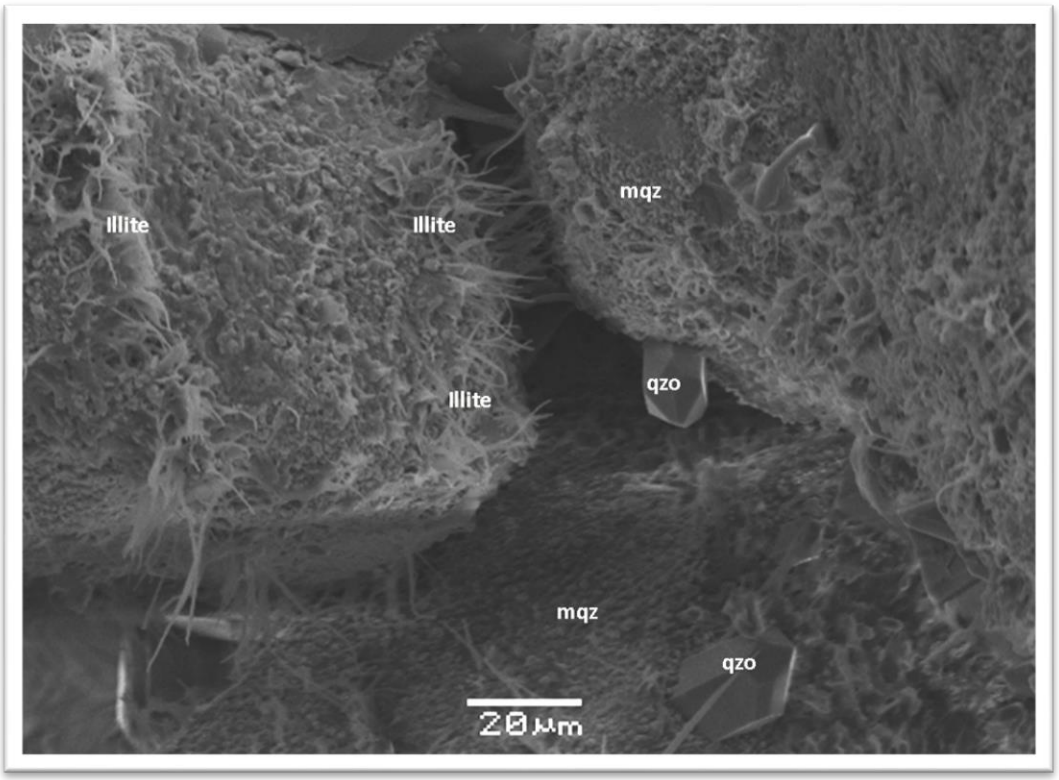

Figure 6.18: SEM image taken from 4299 m to show the illite and micro-quartz coating. Macro quartz overgrows in area where coating is absent.

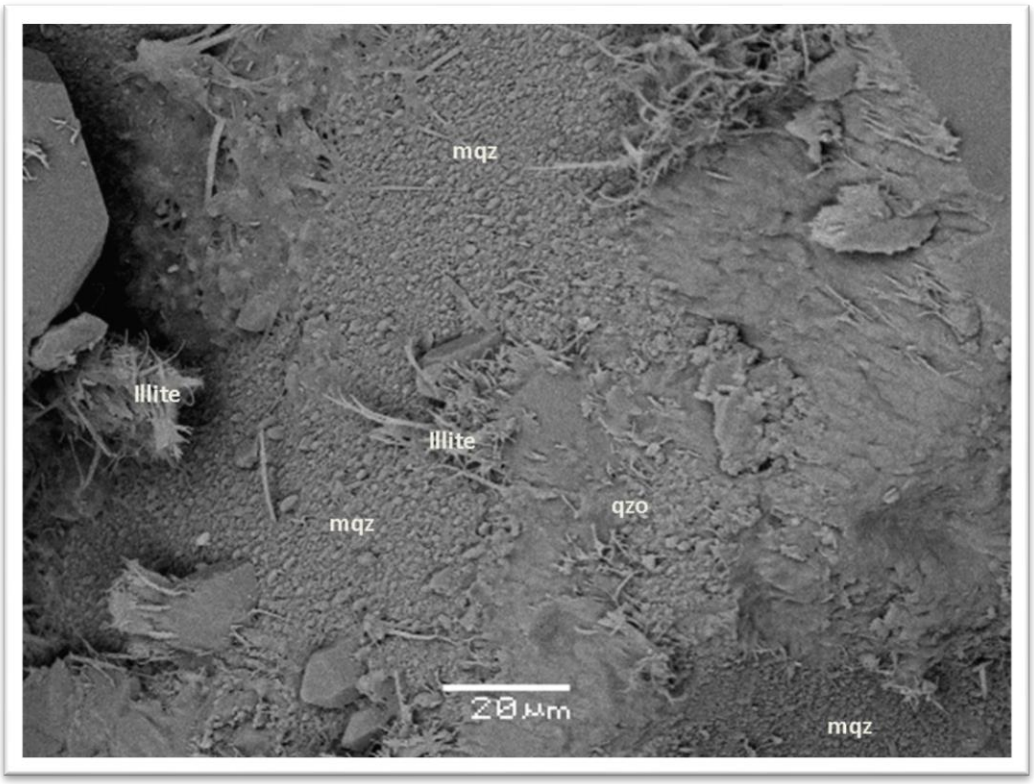

Figure 6.19: SEM image taken from 4344 m, grain is coated with illite and micro-quartz

6.3.1.2 Quartz overgrowth

Quartz cementation was one of the parameter counted during point counting (Table 6.1). It is notable that quartz cementation is more in facie B as compare to the other facies (figure 6.19). To get a visual estimation, all 20 samples have been scanned with secondary electron microscope (SEM) to confirm the results of optical microscope. Mostly same trend has been found throughout the samples. Figure 6.20 showing the euhedral quartz overgrowth where grain coat is not present.

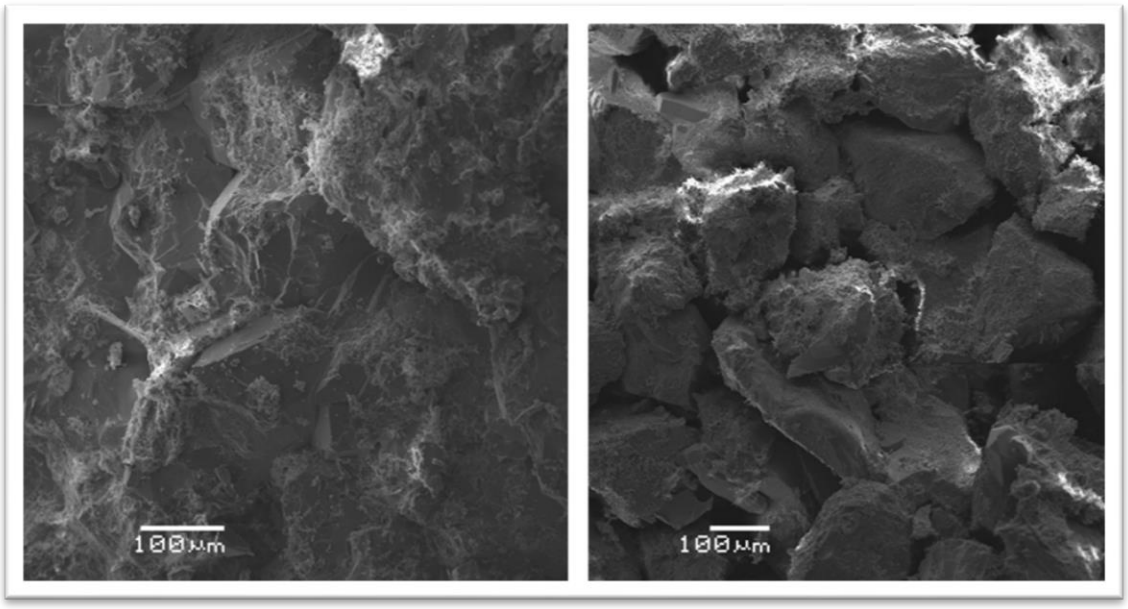

Figure 6.19: SEM image taken from 4307.33 m belongs to facie B (left) and 4300.33 m (right) belongs to facie A1. Note the difference in quartz cementation and porosity between the two samples.

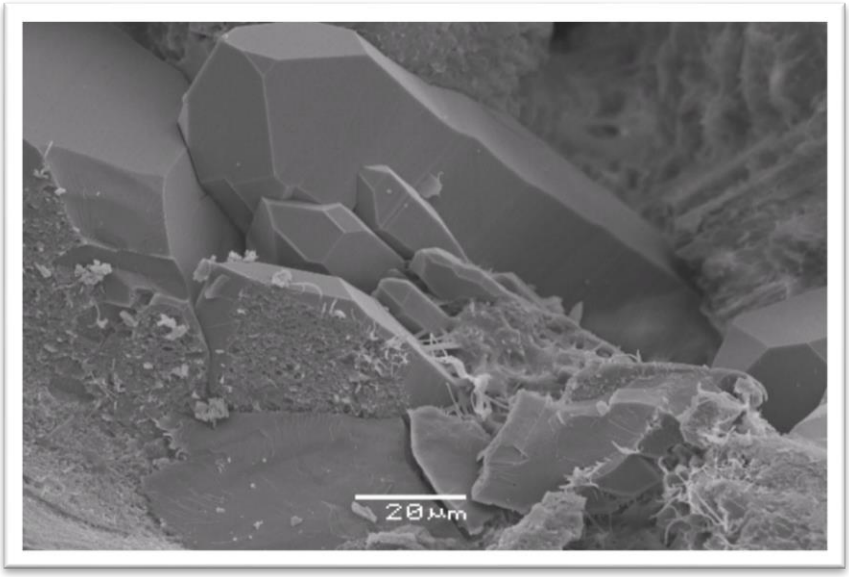

Figure 6.20: SEM image taken from 4338.33 m shows the population of the macro quartz cements where grain coat is not present.

Cathode luminescence (CL) and Backscatter image (BEI) have also been used on carbon coated thin sections in combination to confirm the presence of quartz overgrowth (figure 6.21 and 6.22). The detrital grain usually shows luminescence when exposed to the CL causing a contrast which help to mark the boundary of the detrital grain and cement.

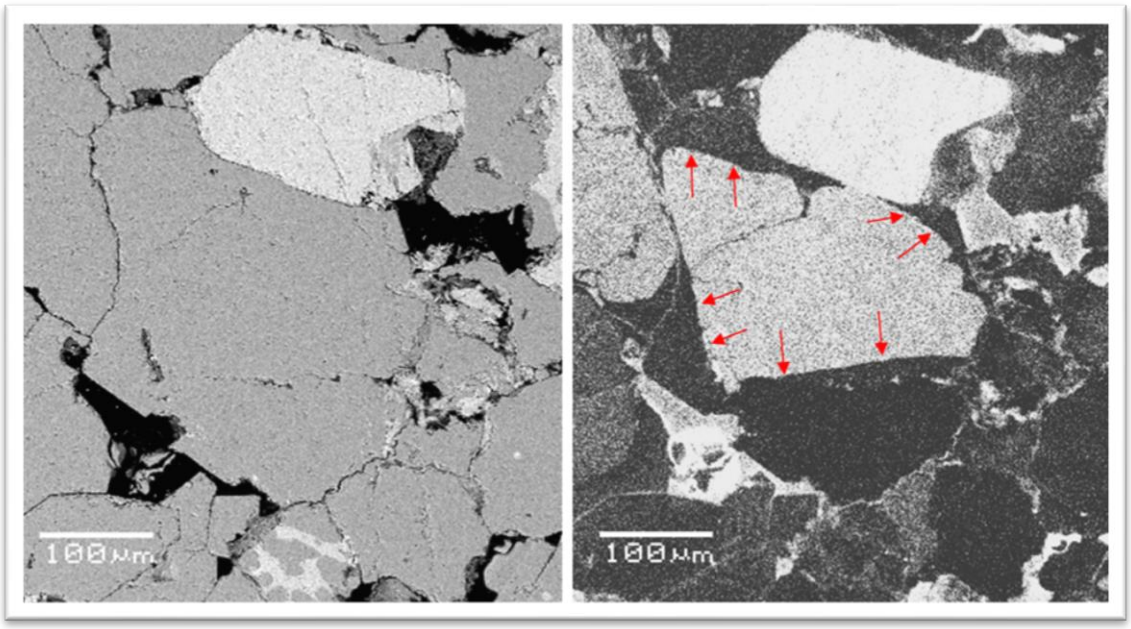

Figure 6.21: SEM image from 4307.33 m to the left and same image when exposed to cathode luminescence to the right. Note the quartz cementation (red arrows) around the illuminated detrital quartz grain.

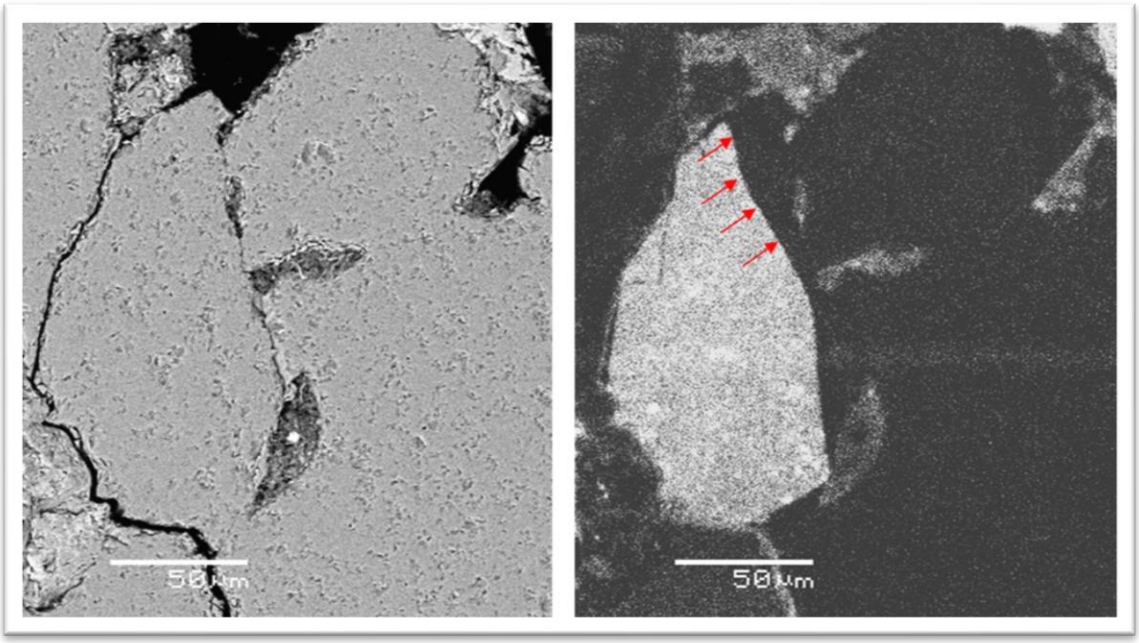

Figure 6.22: SEM image from 4307.33 m to the left and same image when exposed to cathode luminescence to the right. Note the quartz cementation (red arrows) around the illuminated detrital quartz grain which was not visible in secondary electron image.

6.3.1.3 Authigenic clays

Point counting results shows the significant amount of clays found in most of the samples. SEM results confirmed that only authigenic illite is present as clay in the samples. The amount of illite observed in point counted is closely matched with the SEM results. Figure 6.23 shows the area measurement taken by SEM from sample 4298.00 which shows close match to the point count result of the sample.

It has been observed that the illite is present as a pore filling clay and grain coat. Example of the pore filling illite is shown in figure 6.24, 6.25 and 6.26. The characteristic morphology of the clay confirms that the illite is authigenic.

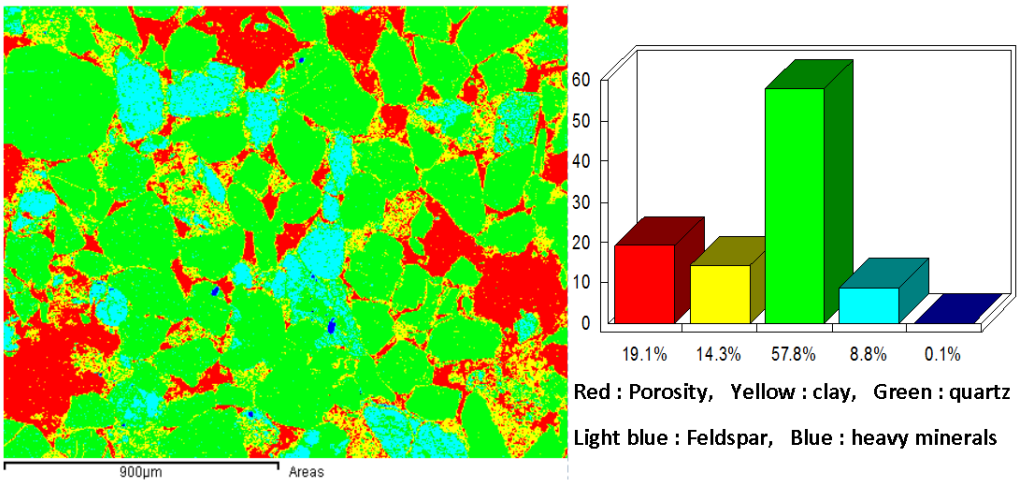

Figure 6.23: SEM area measurement from part of the sample 4298.00 m.

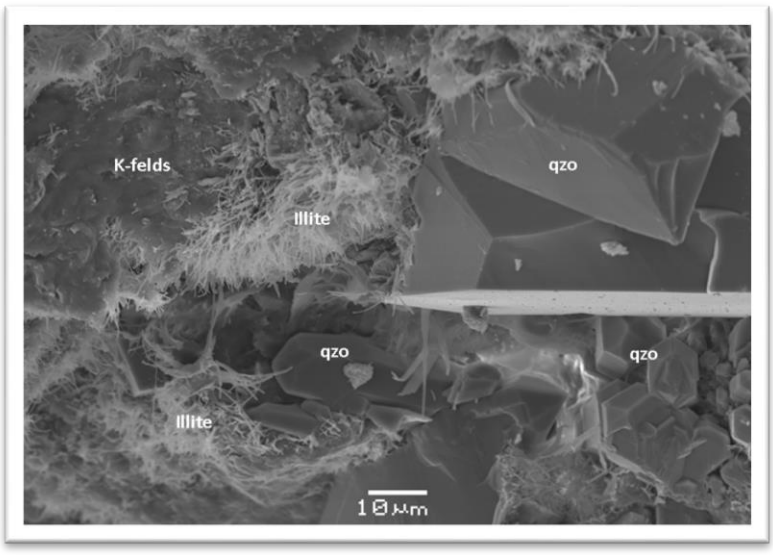

Figure 6.24: SEM image taken from 4305.66 m shows the authigenic illite destroying the porosity.

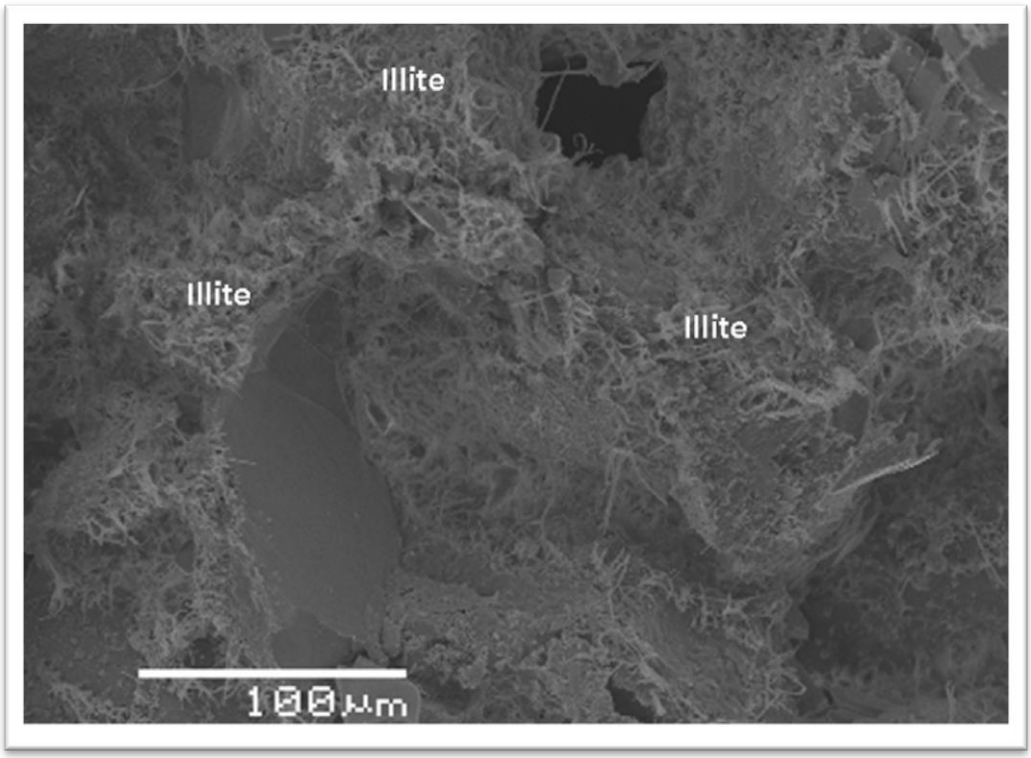

Figure 6.25: SEM image taken from 4349.33 m. Illite has inhibited the quartz overgrowth but it also destroyed the porosity of the sample.

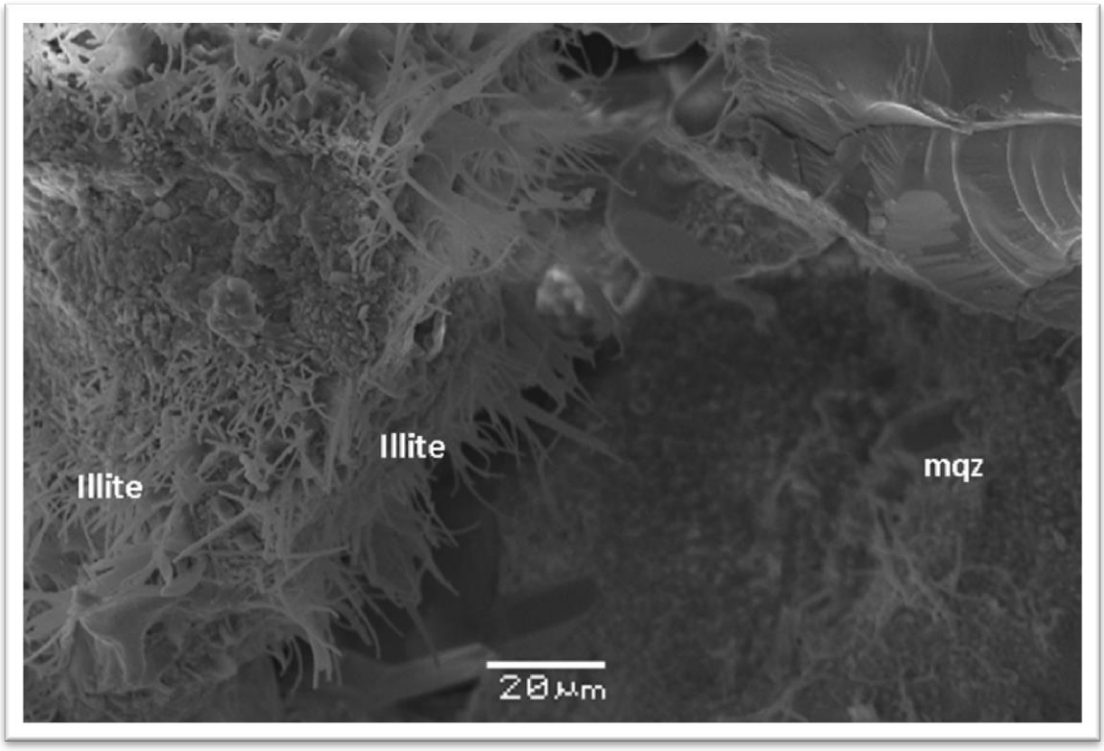

Figure 6.26: SEM image taken from 4340.33 m showing the pore filling illite and micro-quartz.

6.3.1.4 Carbonate cement

Point count results show considerable amount of carbonate cement in some of the samples. The samples from depth 4339.00 m and 4339.69 m shows 22.30 and 11.60 % carbonate cement when analyses with optical microscope. Same samples, when scanned with secondary electron microscope (SEM) confirm the high percentage of carbonate cement (figure 6.27). Carbonate cement is present as a dolomite (figure 6.28), calcite and ankerite.

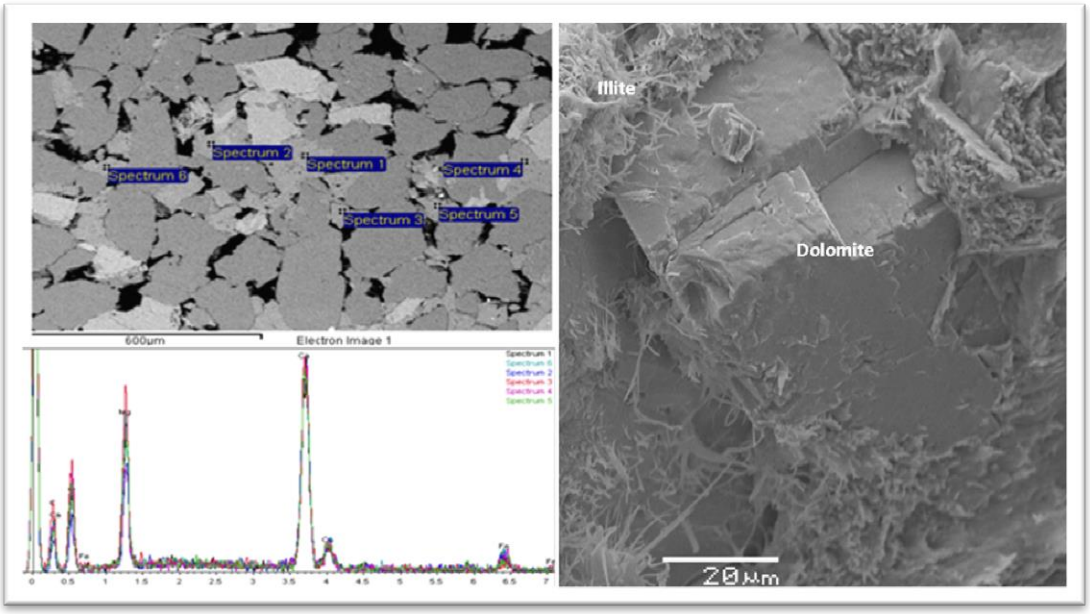

Figure 6.27: Backscattered electron image (left) from 4339.00 m shows the abundance of Ferroan Dolomite and secondary electron image (right) from same depth shows the dolomite crystal.

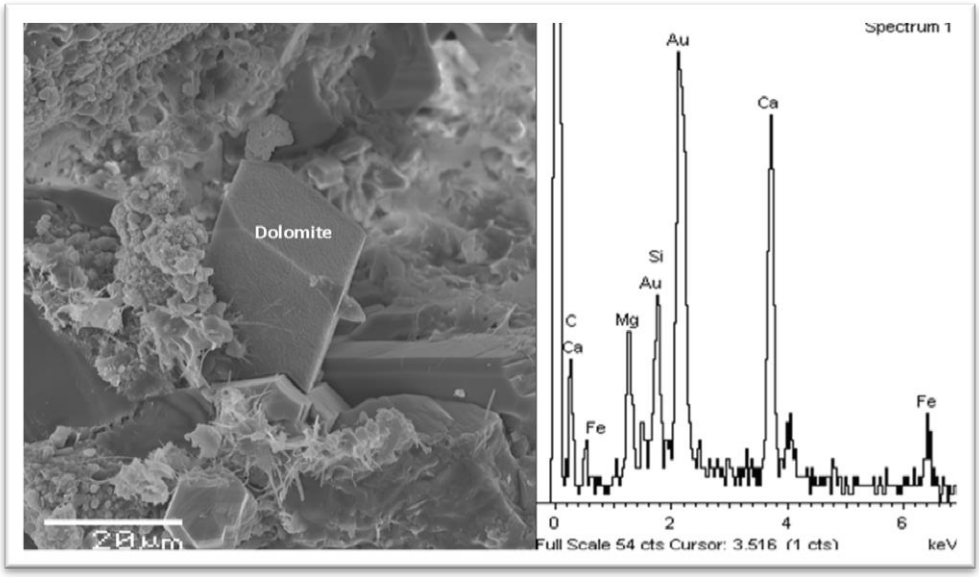

Figure 6.28: SEM image from 4295.66 m shows the presence of dolomite as carbonate cement.

6.3.1.5 Feldspar and other minerals.

Point counted data shows the 3 to 7% feldspars in the samples. Point counting results were compared with the scanning electron microscope (SEM) results shows that point count results underestimate the percentage of feldspars because it is difficult to discriminate the untwined albite and quartz grain. SEM results shows that most of the feldspar found in samples are k-feldspar (figure 6.29). Some other minerals like pyrite, rutile and apatite have also been found in very minor amount (0.1% in each sample).

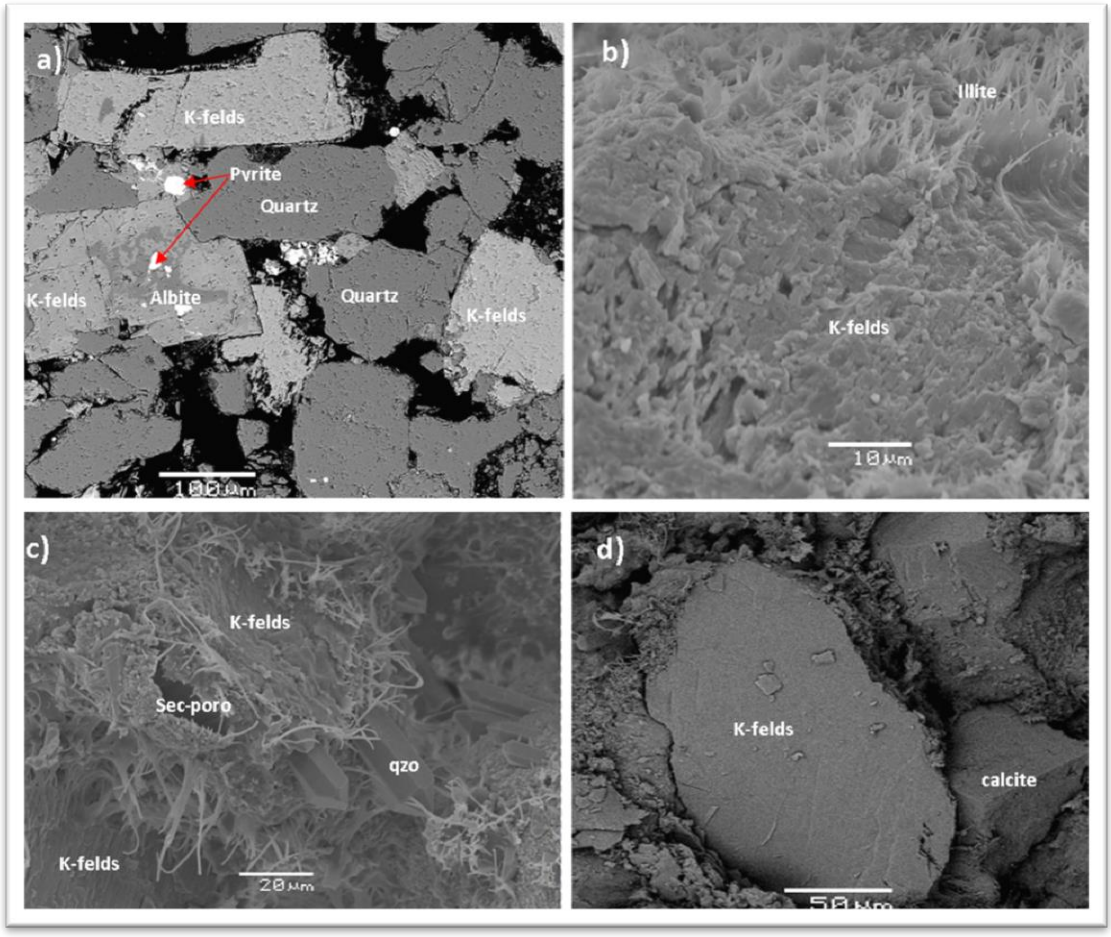

Figure 6.29: a) Backscattered image from 4298 m (thin section) shows the albite, k-feldspar and pyrite with different shades of gray color. b) SEM image from 4305 m (stub) shows the k-feldspar with illite coating. c) SEM image of 4349.33 m (stub) shows the secondary porosity because of the dissolution of k-feldspar. d) Backscattered image from 4340.00 m (stub) shows the large k-feldspar and calcite

7. DISCUSSION

7.1 Introduction

From chapter 6 it has been clear that the illite and micro-quartz coatings are the main porosity preserving processes in the area for deeply buried (>4km)Upper Jurassic sediments. The samples without or very little grain coats show very low porosities with minimum value of 3.1% porosity at 4307.33m depth. Grain size and sorting can also be taken as a secondary factor in preserving good porosity (Appendix A).

After studying the samples it seems possible to divide the studied interval (4295 – 4349.33 mRKB) into different zones. Four zones (A1, B, C, and A2) have been identified from the petrographic study. A1 and A2 are high porosity zones while B and C are low porosity zones.

Low and high porosity zones have also been marked with the help of petrophysical data for Upper Jurassic interval (4259 – 4349.33 m RKB). It has been observed that the P4, P1 and S1zones show lower porosity as compare to the P2 and S2 zones (Figure 5.1). An attempt has been made to integrate the petrophysical and petrographic data (Figure 7.1). A1 and A2 zones (high porosity) fall fairly within P2 and S2 zones (high porosity), B and C zones (low porosity) fall within P1 (low porosity) zone.

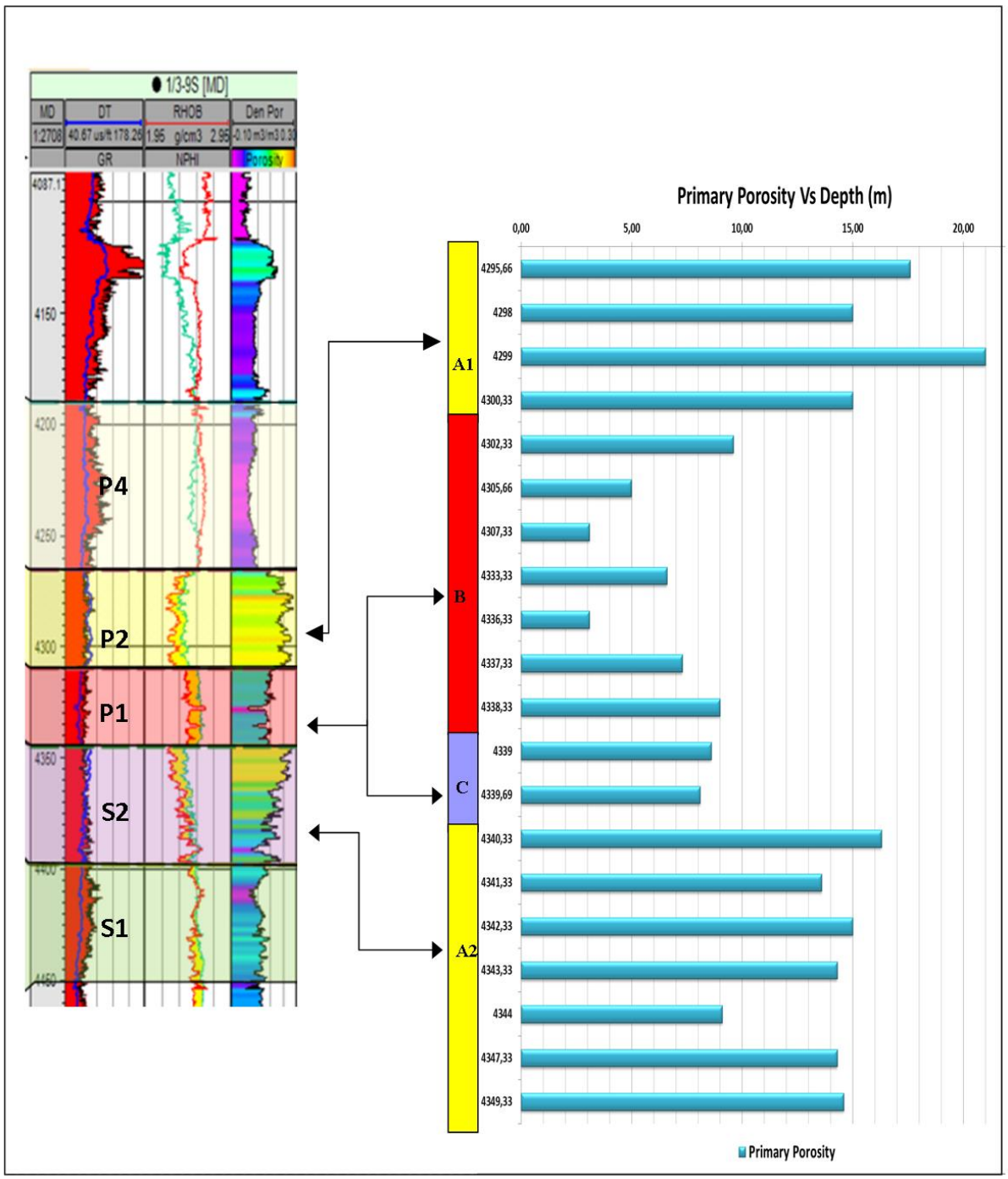

Figure 7.1: An integration of petro-physical data with petrographic data.

7.2 Mechanical compaction

The intergranular volume has been calculated from thin sections by using optical microscope. By definition intergranular volume (IGV) is equal to the intergranular porosity + depositional matrix + pore filling cement. All these parameters were calculated in point counting and IGV has been calculated for all samples.

The IGV values calculated for this study by point counting ranges between 30% to 38%, showing that some of the samples have undergone more mechanical compaction (with low IGV %) as compared to the samples having high IGV %(35 - 38%). By analyzing the point count table (Table 6.1) a relation between carbonate cement and intergranular volume (IGV) can be made. It has been observed that samples with significant amount of carbonate cement (6 - 22%) have preserved the IGV (35 – 38%). Maximum preserved IGV (38%) has been measured from sample at 4339 m, containing 22% carbonate cement. It seems that this early carbonate cement reduces the effect of mechanical compaction by stiffening the grain frame work. Although a high percentage of carbonate cement destroy the intergranular porosity in samples where carbonate cementation was less than 6%, preserve porosity and IGV.

The above results agree with earlier studies of mechanical compaction e which states that mechanical compaction determines the intergranular volume (IGV) before the chemical compaction starts. In the absence of carbonate cement, well sorted sediments are significantly affected by mechanical compaction during the first (0-2 Km) of its burial. Quartz cementation starts at 2 Km depth (80 - 100°C) in sedimentary basins with normal geothermal gradient. This quartz cementation stabilizes the grain framework and stops the further mechanical compaction (Bjørlykke and Jahren 2010).

Petrographic classification (Figure 6.2) shows that all of the samples are subarkosic with more than 5% feldspars. It has already been discussed that the amount of feldspars is underestimated in point counting results because of the untwined albite content. It is difficult to differentiate the untwined albite and quartz grains during rapid point counting in an optical microscope. Although no clear trend has been found between the feldspar content and IGV%, high feldspar content probably increases the mechanical compaction, resulted in comparatively lower IGV values in some of the samples.

7.2.1 Textural characteristics

Sorting and grain sizes have been plotted in Figure 6.8. The results show that all of the samples are well to moderately well sorted and fine grained. Overall area increases in fine grained sands thus there is less pressure on individual contacts as compare to the coarse grained sands. The sorting and fine grain sizes are possibly important factors in preserving high intergranular volume for the sands in this study where none of the samples show less than 30% IGV (Table 6.1). It has already been experimentally shown that well sorted and fine

grained sands are compacted less compared to coarse grained and poorly sorted sands at any stress level (Chuhan et al. 2002).

Most of the samples in this study are sub-rounded to sub-angular. Although no correlation between grain shape and IGV have been observed. It seems that roundness of the grains helped in preserving the porosity (Appendix A). Angular grains show more compaction due to small grain to grain contact area (less contacts) resulting in more grain crushing (Fawad et al. 2011).

7.2.2 Impacts on reservoir quality

High IGV values and well preserved porosity indicates that mechanical compaction has not been very extensive for the cored interval. SEM analysis shows that microcrystalline quartz coating is present throughout the samples which could have delayed the quartz cementation and extended the mechanical compaction to deeper levels than in uncoated sandstones. But early carbonate cement, sorting and grain size possibly helped to reduce the mechanical compaction and preserved the intergranular volume (IGV) and porosity.

7.3 Chemical compaction

7.3.1 Carbonate cement

Three types of carbonate cement (calcite, dolomite and ankerite) have been observed in SEM analysis. Majority of the observed carbonate cement is calcite. Point count data (Table 6.1) shows that presence of carbonate cement varies throughout the sample interval. From point count data it has been observed an almost 1 meter (4339 – 4340 m RKB) carbonate cemented sand bed with more than 10% carbonate cement is present in the sampled interval.

Loosely packed sand grains in calcite cemented beds indicate the precipitation of calcite cement at shallow burial depth (Nedkvitne et al. 1993). Same kind of loosely packed sand grains have been observed in carbonate cemented interval (samples 4295, 4339, 4339.69) in this study (Appendix B). Less amount of quartz cement (point count) has been observed in samples with higher carbonate cement (samples 4295, 4339, 4339.69 m) suggesting that the carbonate cement was emplaced before the quartz cementation. Only small amounts of Ca-plagioclases have been observed throughout the samples indicating the biogenic origin of the calcite cement.

This early carbonate cementation hinders the quartz overgrowth and helped to reduce the mechanical compaction. However it also destroyed the reservoir quality by filling the pores. These carbonate cemented intervals act as a barrier to fluid flow during hydrocarbon production (Saigal & Bjørlykke 1987).

Figure 6.6 shows the cyclic increase in the carbonate cementation. From 4349.33 to 4339 m an increase in carbonate content is noticed. This is indicative of the fact that terrigenous input to the basin is reducing upwards. Increasing higher percentage of carbonates result from the reduced clastic input. This allows the enhanced deposition of carbonates moving upward in this zone until 4339 m depth. This depth (4339) m can be marked as a probable Maximum Flooding Surface (MFS) as it has the highest percentage of carbonates. Above the suggested MFS a sharp decrease in carbonate content can be interpreted as seaward movement of shoreline or lowering of sea-level. More clastic sediments are transported farther into the sea which dilutes and hinders the deposition of carbonates. From 4338m to 4295m a similar repetitive sequence has been observed.

7.3.2 Authigenic Illite

Among pore filling clays only authigenic illite has been observed in the samples. In most of the samples the amount of authigenic illite is more than 10%, indicating the moderate-high early meteoric water flushing of the sediments assuming a kaolinite precursor for the illite. Meteoric water has the ability to dissolve unstable minerals like feldspar and mica and precipitate kaolinite. In this study it is assumed that illite is formed by the conversion of kaolinite. The flow of meteoric water can extend beneath the seafloor into the sedimentary basins depending on the distribution of permeable sandstones layers and elevation of groundwater table (Bjorlykke and Jahren 2010).

The petrographic results of this study show that k-feldspar is still present in the sediments, while no kaolinite has been observed throughout the samples. Secondary porosity (Figure 6.29c) in feldspar grains has also been observed in most of the samples. These observations indicate that all of the kaolinite has been converted to the illite during deep burial of the sediments. The presence of k-feldspar justifies the conversion of kaolinite throughout the samples. This k-feldspar acted as the potassium source for the conversion of kaolinite to illite..

All of the samples in this study are buried below 4 Km (4272 – 4327 m SSTVD) and the bottom hole temperature for well 1/3-9S is 165°C. The geothermal gradient calculated from

the bottom hole temperature indicates that all of the samples have experienced more than 150 °C (at 4272 – 4327 m SSTVD). The high temperature, burial depth and presence of k-feldspar justify the absence of kaolinite and high concentration of illite throughout the samples. In the North Sea basin most of the authigenic illite is precipitated at temperatures between 130 to 140°C (Bjørlykke 1998) and the amount of authigenic illite found increase at depths close to 3.8 – 4.0 Km (Bjørlykke et al. 1986; Ehrenberg 1990).

7.3.2.1 Impacts on reservoir quality

Fibrous pore filling authigenic illite has been observed throughout the samples which in turn affects the reservoir quality by decreasing permeability. SEM analysis and point counting results indicate that amount of authigenic illite is higher in sequence B than the other sequences. This high concentration of authigenic illite reduces the permeability (Figure 6.26).

It is well known that thin hair or plate- like illite decreased the reservoir quality by reducing the permeability (Bjørlykke and Jahren 2010).

7.3.3 Quartz cement

The Point counting and SEM results shows that quartz cementation is the main porosity destroying agent for the cored interval. Two sub-populations of; 0-10% and 10-20% respectively, have been observed in samples of well 1/3-9S, with respect to their primary porosity (Table 6.1).

Petrographic data (point count) shows that 0-10% porosities are correlated with sequences B and C and 10-20% porosities are associated with sequences A1 and A2. The amount of authigenic quartz cement in all of the samples varies 2.30 – 15.30%. It has been observed (point counting) that samples with low porosity (sequence B); contain more quartz cement, as compared to the samples having high porosity (sequence A1, A2). Figure (6.4) demonstrating the quartz cementation is relatively higher in sequence B (low porosity) as compare to the sequences A1 and A2 (high porosity). Sequence C shows both low porosity and low quartz cement because of the higher percentages of carbonate cement. CL and backscattered images was used in combination to mark the authigenic quartz cement and detrital quartz grains (Figure 6.22).

The fact that sandstones in this study consist of fine grained samples, means that relatively large surface area was available for quartz cementation, potentially resulting in higher

amounts of quartz cement. The amount of quartz cementation is related to the area of the grain surfaces available for quartz cementation (Walderhaug 1994). But grain coating micro-quartz and illite is observed throughout the samples, blocking much of the area available for macro-quartz cement, which resulted in less quartz cementation in sequence A1, A2 and C. Samples with lower amount of grain coats show a higher amount of macro-quartz cementation as evident in sequence B (Table 6.1). These observations correlate very well with the porosity log. Figure (Appendix A), indicates that the high porosity zones (P2 and S2) are the result of the presence of grain coatings, capable of retarding the quartz precipitation.

Figure 6.13 shows a quartz grain coated with micro-quartz, inhibiting the both nucleation and growth of macro-quartz cement laterally across the detrital quartz grain. No considerable variation of IGVs has been observed in quartz cemented samples (zone B) compared to the high porosity samples (zone A1 and A2). Both high porosity zones and low porosity zones exhibit 33% IGV (average). These observations support that dissolution along stylolites is the possible source of quartz cement as compare to the intergranular pressure dissolution. Petrographic data of the Jurassic reservoirs in North Sea indicate that most of the quartz cement found in quartz rich sandstones is the product of dissolution of quartz at illite/mica rich stylolites (Oelkers et al. 1996).

Figures (6.16 and 6.20) show euhedral crystals of macro-quartz destroying the porosity where grain coats (micro-quartz and illite) are not present. Euhedral quartz overgrowths normally precipitate at low degree of supersaturation. When grains are coated with micro-quartz or clays, a higher degree of supersaturation is needed before quartz over-growth can occur (Ramm et al. 1997).

7.3.3.1Impacts on reservoir quality

SEM analysis and petrographic studies on all of the samples shows that sorting, grain size and grain shape are relatively uniform throughout the samples and has very little effect on the reservoir quality. Quartz cementation is the main factor related to the differences in the porosity of sampled interval. It is evident that porosity is well preserved in samples with extensive grain coating of micro-quartz and illite (sequence A1, A2) as compared to where little or no grain coating is found (sequence B).

7.4 Porosity preserving mechanisms

Relatively high IGV values have been observed in the studied samples, indicating that quartz cementation is the main porosity reducing process in the study area. Although the amount of quartz cementation is higher, sequence B of the sampled interval still has a high overall porosity considering the depth of the samples (> 4Km). Low quartz cementation and anomalously high porosity (10 – 20%) have been observed in sequences A1 and A2. Samples have been further investigated to identify the processes which preserved the porosity at such high burial depth. Micro-quartz and illite coating has been identified as the main porosity preserving agents.

7.4.1 Micro-quartz coating

All of the samples have been analyzed in the scanning electron microscope to investigate the extent of grain coating. A relative value of 0 – 3 have been assigned considering the coverage of micro-quartz coating (Table 6.4), where 0 = not present, 1 = little coverage, 2 = moderate coverage and 3 = good coverage. Results shown in Table 6.4 indicate that the sandstones of sequences A1 and A2 exhibits good coverage of micro-quartz grains, while sequences C and B has moderate and little coverage respectively.

As already discussed the A1 and A2 sequences have 15% average porosity compared to (6% average porosity) in sequence B. The SEM results make it clear that these high porosity values in sequences A1 and A2 are the result of higher amount of micro-quartz coating. This higher micro-quartz content inhibits the growth of macro-quartz cement in these samples (Figures 6.16 & 6.19). Although sequence C contains moderate coverage of micro-quartz coating which helps to stop some of the potential quartz cementation while initial higher content of early carbonate cement has already destroyed the porosity.

The SEM results (Table 6.4) indicate that the micro-quartz coverage on the detrital grains is significantly lower in sequence B compared to the A1 and A2 sequences. A possible reason for the lower micro-quartz content in sequence B could be little precursor material resulting in a lower supersaturation of silica in the pore water during micro-quartz formation. High percentage of macro-quartz cement (almost 15%) has been recorded in sequence B, indicating that the partial or little coverage of micro-quartz coating around the grains was unable to completely retards or stop the quartz overgrowth (Table 6.1), resulting in lower reservoir quality of sequence B compared to the sequences A1 and A2.

Anomalously high permeability and porosity (>20%) values have been recorded at depths greater than 4 Km, in Upper Jurassic sandstones of North Sea. It has been proposed that these high porosity values are the result of continuous micro-quartz coating on detrital quartz grains. These micro quartz coats in the North Sea occur because of the transformation of sponge spicules Rhaxella Perforata (Aase et al. 1996). These observations indicate that sediment age and depositional environments are important factors for the occurrence of micro-quartz coats.

The Ula formation was deposited in offshore shelf marine environment, consisting of fine to medium grained sandstones (Ramm et al. 1997). As Rhaxella sponge spicules have previously been reported in shallow marine environment (Aase et al. 1996), suggesting that the Ula formation is within the reworking paths of Rhaxella sponge spicules. In this study Sponge spicules of amorphous silica are considered as the source of micro-quartz crystals.

Precipitation of micro-quartz occurs at low temperature (60 - 65 ºC). At this temperature the pore water is highly supersaturated with respect to quartz because of the dissolution of Opal A and Opal CT (Bjørlykke and Jahren 2010). This high supersaturation could have been achieved by the transformation of siliceous sponge spicules.

7.4.1.1 Impacts on reservoir quality

The micro-quartz grain coating shows a good correlation with low and high reservoir quality zones of well 1/3-9S (Figure 7.1). The P2 and S2 zones are correlated with A1and A2 zones respectively. The high porosity values observed in P2 and S2 zones are perfectly justified by the distribution of micro quartz coating. While the lower reservoir quality of P4, P1 and S1 probably indicates the absence or little coverage of grain coating resulting in high quartz cementation.

7.4.2 Illite coating

Illite coating on detrital grains have been observed throughout the samples during the SEM analysis (Table 6.4). The amount of grain coating illite is not abundant in most of the samples as compared to the micro-quartz coating. Most of the coated grains are only partially covered with some illite coating. An attempt has been made to quantify the illite coating present in the samples (Table 6.4).

The SEM analysis shows that illite coating is present in combination with micro-quartz coating and helped to retard or stop the development of quartz overgrowth (Figure 6.17). Illite

coating is not present at the grain contacts indicating that the illite precursor was precipitated after deposition. It has been observed that illite coating is not present on the quartz overgrowths (Figure 6.18). These observations show that the coating developed prior to the quartz overgrowth.

In this study it has been assumed that illite coating originated from smectite. There could be two mechanisms to explain the presence of illite coating: 1) replacement of smectite 2) replacement of kaolinite (Storvoll et al. 2002). It has already been discussed that quartz cementation occur at 2.5 to 3km corresponding to 80 - 100 ºC. If illite coating originated from kaolinite at higher temperatures (120 - 140 ºC) then most of the porosity could have already been filled by the quartz cement, as quartz cementation starts at 70 – 90 ºC. While transformation of smectite to illite started at lower temperature prior to the quartz overgrowth. According to Ehrenberg (1990), in the North Sea precipitation of illite from kaolinite occurs at 3.5 – 4 km depths corresponding to (120 - 140 ºC). However precipitation of illite from smectite starts at 60 ºC (Storvoll et al. 2002).

The depositional environment of the Ula Formation is interpreted as a shallow marine environment. Storvoll et al. (2002) proposed that in shallow marine environments smectite precipitation may take place on the clastic grains because of the dissolution of volaco-clastic material during shallow burial.

Most of the illite coating observed in the SEM study of the samples represents honeycomb or cornflake morphology (Figure 6.16). Pollastro (1985) states that honey comb and cornflake morphology of illite supports that illite may have originated from smectite, as illite formed from kaolinite shows more sheet like morphology.

7.4.2.1 Impacts on reservoir quality

The effect of illite coating on porosity is difficult to estimate in this study, because of the extensive micro-quartz coating. Micro-quartz coats are present throughout the samples (except 4307 m, 4336.33 m), containing illite coating. The illite coats observed in this study are mostly thin and not covering the whole grain. Therefore their contribution to preserve the porosity is far less important compared to the micro-quartz coating.

8. CONCLUSION

- High IGV values (33 % average) show that mechanical compaction is not very significant. These high IGVs are possibly the result of early carbonate cementation, well sorting and fine grain size of the sandstone particles.
- Higher IGVs observed in samples with higher carbonate content indicates the emplacement of early carbonate cement which in turn stiffen the grain framework before the onset of chemical compaction.
- Grain-coating illite and micro-quartz has been observed in all of the samples. Coverage of micro-quartz coating is more extensive around the grains as compare to the illite coating (Table 6.4). Micro-quartz coating is considered as the main porosity preserving agent in this study.
- The point counting indicated a correlation between porosity and quartz cementation, indicating that quartz cementation is the main porosity destroying factor throughout the samples.
- Intervals with higher micro-quartz coating have significantly lower amount of quartz cement (A1, A2) since quartz cementation is inhibited because of the micro-quartz coating.
- Integration of petrophysical and petrographic data for well1/3-9S (Figure 7.1) shows that the high porosity zones (P2, S2) and low porosity zones (P4,P1 and S1) are well correlated with the higher and lower content of micro-quartz coating, respectively.

9. REFERENCES

AAGAARD, P., JAHREN, J. & EGEBERG, P. K. 1992. North Sea clastic diagenesis and formation water constraints. Water-rock interaction: Rotterdam, Balkema, 2, 1147-1152.

Aase, N., E., Bjorkum, P.A. and Nadeau, P.H. 1996. The effect of grain-coating microquartz on preservation of reservoir porosity. AAPG Bulletin 80, 1654-1673.

BADLEY, M., PRICE, J., DAHL, C. R. & AGDESTEIN, T. 1988. The structural evolution of the northern Viking Graben and its bearing upon extensional modes of basin formation. Journal of the Geological Society, 145, 455-472.

BARTHOLOMEW, I., PETERS, J. & POWELL, C. Regional structural evolution of the North Sea: oblique slip and the reactivation of basement lineaments. Geological Society, London, Petroleum Geology Conference series, 1993. Geological Society of London, 1109-1122.

BERGER, G., LACHARPAGNE, J.-C., VELDE, B., BEAUFORT, D. & LANSON, B. 1997. Kinetic constraints on illitization reactions and the effects of organic diagenesis in sandstone/shale sequences. Applied Geochemistry, 12, 23-35.

BERNER, R. A. 1980. Early diagenesis: A theoretical approach, Princeton University Press.

BJOLYKKE, K. 1998. Clay mineral diagenesis in sedimentary basins-a key to the prediction of rock properties. Examples from the North Sea Basin. Clay minerals, 33, 15-34.

BJØRLYKKE, K. 1980. Clastic diagenesis and basin evolution. Rev Instituto Invest Geol, 34, 21-24.

BJØRLYKKE, K. & AAGAARD, P. 1992. Clay minerals in North Sea sandstones. Origin, diagenesis, and petrophysics of clay minerals in sandstones, 47, 65-80.

BJØRLYKKE, K., AAGAARD, P., DYPVIK, H., HASTINGS, D. & HARPER, A. 1986. Diagenesis and reservoir properties of Jurassic sandstones from the Haltenbanken area, offshore mid-Norway. Habitat of hydrocarbons on the Norwegian continental shelf: London, Graham & Trotman, 275-286.

BJØRLYKKE, K., AAGAARD, P., EGEBERG, P. K. & SIMMONS, S. P. 1995. Geochemical constraints from formation water analyses from the North Sea and the Gulf Coast Basins on quartz, feldspar and illite precipitation in reservoir rocks. Geological Society, London, Special Publications, 86, 33-50.

BJØRLYKKE, K. & JAHREN, J. 2010. Sandstones and sandstone reservoirs. Petroleum Geoscience. Springer.

BLOCH, S., LANDER, R. H. & BONNELL, L. 2002. Anomalously high porosity and permeability in deeply buried sandstone reservoirs: Origin and predictability. AAPG bulletin, 86, 301-328.

BOLDY, S. & FRASER, S. Introduction and review. Geological Society, London, Petroleum Geology Conference series, 1999. Geological Society of London, 825-826.

BOLES, J. R. & FRANKS, S. G. 1979. Clay diagenesis in Wilcox sandstones of southwest Texas: implications of smectite diagenesis on sandstone cementation. Journal of Sedimentary Research, 49.

Chuhan, F.A., Kjeldstad, A., Bjorlykke, K. and Hoeg, K. 2002. Porosity loss in sand by grain crushing; experimental evidence and relevance to reservoir quality. Marine and Petroleum Geology 19, 39-53.

CORNFORD, C., GARDNER, P. & BURGESS, C. 1998. Geochemical truths in large data sets. I: Geochemical screening data. Organic Geochemistry, 29, 519-530.

DICKINSON, G. 1953. Geological aspects of abnormal reservoir pressures in Gulf Coast Louisiana. AAPG Bulletin, 37, 410-432.

EHRENBERG, S. 1990. Relationship Between Diagenesis and Reservoir Quality in Sandstones of the Garn Formation, Haltenbanken, Mid-Norwegian Continental Shelf (1). AAPG Bulletin, 74, 1538-1558.

ERRATT, D., THOMAS, G. & WALL, G. The evolution of the central North Sea Rift. Petroleum Geology of Northwest Europe: Proceedings of the 5th Conference. Geological Society, London, 1999. 63-82.

Fawad, M., Mondol, N.H., Jahren, J. and Bjørlykke, K. 2011. Mechanical compaction and ultrasonic velocity of sands with different texture and mineralogical composition. *Geophysical Prospecting*, no-no.

FOLK, R., ANDREWS, P. B. & LEWIS, D. 1970. Detrital sedimentary rock classification and nomenclature for use in New Zealand. New Zealand journal of geology and geophysics, 13, 937-968.

FOLK, R. L. 1951. Stages of textural maturity in sedimentary rocks. Journal of Sedimentary Research, 21, 127-130.

FORSBERG, A., GOWERS, M. & HOLTAR, E. 1993. Multi-disciplinary stratigraphic analysis of the Upper Jurassic strata of the Norwegian Central Trough. Generation, Accumulation and Production of Europe's Hydrocarbons III. Springer.

FRASER, S., ROBINSON, A., JOHNSON, H., UNDERHILL, J., KADOLSKY, D., CONNELL, R., JOHANNESSEN, P. & RAVNAS, R. 2003. Upper Jurassic. The Millennium Atlas: Petroleum Geology of the Central and Northern North Sea. Geological Society, London, 157-189.

FUCHTBAUER, H. 1983. Facies controls on sandstone diagenesis. Sediment Diagenesis. Springer.

FÆRSETH, R. 1996. Interaction of Permo-Triassic and Jurassic extensional fault-blocks during the development of the northern North Sea. Journal of the Geological Society, 153, 931-944.

GABRIELSEN, R., FÆRSETH, R., STEEL, R., IDIL, S. & KLØVJAN, O. 1990. Architectural styles of basin fill in the northern Viking Graben. Tectonic Evolution of the North Sea Rifts. Clarendon Press, Oxford, 158-179.

GILES, M., STEVENSON, S., MARTIN, S., CANNON, S., HAMILTON, P., MARSHALL, J. & SAMWAYS, G. 1992. The reservoir properties and diagenesis of the Brent Group: a regional perspective. Geological Society, London, Special Publications, 61, 289-327.

GLUYAS, J., LEONARD, A. & OXTOBY, N. Diagenesis and petroleum emplacement: the race for space-Ula Trend, North Sea. 13th International Sedimentological Congress. Abstracts, 1990. Utrecht: International Association of Sedimentologists.

GLUYAS, J., ROBINSON, A., EMERY, D., GRANT, S. & OXTOBY, N. The link between petroleum emplacement and sandstone cementation. Geological Society, London, Petroleum Geology Conference series, 1993. Geological Society of London, 1395-1402.

GLUYAS, J., SPIRO, B., RAISWELL, R., BERNER, R., LOWREY, C. J., COLEMAN, M., MASON, R., WHITAKER, J. M., SAIGAL, G. & CURTIS, C. 1985. Reduction and Prediction of Sandstone Reservoir Potential, Jurassic, North Sea [and Discussion]. Philosophical Transactions of the Royal Society of London. Series A, Mathematical and Physical Sciences, 315, 187-202.

HEALD, M. & LARESE, R. 1974. Influence of coatings on quartz cementation. Journal of Sedimentary Research, 44.

HEALD, M. & RENTON, J. 1966. Experimental study of sandstone cementation. Journal of Sedimentary Research, 36.

HOFFMAN, J. & HOWER, J. 1979. Clay mineral assemblages as low grade metamorphic geothermometers: application to the thrust faulted disturbed belt of Montana, USA.

Home, P. C. 1987. "The Ula oilfield block 7/12, Norway." Geology of the Norwegian oil and gas fields: Norwegian Petroleum Society, London, Graham & Trotman: 143-152.

JOHNSON, H. & FISHER, M. 1998. North Sea plays: geological controls on hydrocarbon distribution. Petroleum Geology of the North Sea: Basic Concepts and Recent Advances, Fourth Edition, 463-547.

KNOTT, S., BURCHELL, M., JOLLEY, E. & FRASER, A. Mesozoic to Cenozoic plate reconstructions of the North Atlantic and hydrocarbon plays of the Atlantic margins. Geological Society, London, Petroleum Geology Conference series, 1993. Geological Society of London, 953-974.

KRYNINE, P. D. 1948. The megascopic study and field classification of sedimentary rocks. The Journal of Geology, 56, 130-165.

KUSZNIR, N., MARSDEN, G. & EGAN, S. 1991. A flexural-cantilever simple-shear/pure-shear model of continental lithosphere extension: applications to the Jeanne d'Arc Basin,

Grand Banks and Viking Graben, North Sea. Geological Society, London, Special Publications, 56, 41-60.

MCBRIDE, E. F. 1989. Quartz cement in sandstones: a review. Earth-Science Reviews, 26, 69-112.

NEDKVITNE, T., KARLSEN, D. A., BJØRLYKKE, K. & LARTER, S. R. 1993. Relationship between reservoir diagenetic evolution and petroleum emplacement in the Ula Field, North Sea. Marine and Petroleum Geology, 10, 255-270.

OELKERS, E. H., BJORKUM, P. A. & MURPHY, W. M. 1996. A petrographic and computational investigation of quartz cementation and porosity reduction in North Sea sandstones. American Journal of Science, 296, 420-452.

OXTOBY, N. H., MITCHELL, A. W. & GLUYAS, J. G. 1995. The filling and emptying of the Ula Oilfield: fluid inclusion constraints. Geological Society, London, Special Publications, 86, 141-157.

PAXTON, S., SZABO, J., AJDUKIEWICZ, J. & KLIMENTIDIS, R. 2002. Construction of an intergranular volume compaction curve for evaluating and predicting compaction and porosity loss in rigid-grain sandstone reservoirs. AAPG bulletin, 86, 2047-2067.

PITTMAN, E. D., LARESE, R. E. & HEALD, M. T. 1992. Clay coats: Occurrence and relevance to preservation of porosity in sandstones. Pittman, eds., Origin, diagenesis, and petrophysics of clay minerals in sandstones: SEPM Special Publication, 47, 241-255.

POLLASTRO, R. M. 1985. Mineralogical and morphological evidence for the formation of illite at the expense of illite/smectite. Clays and Clay Minerals, 33, 265-274.

RAMM, M. 1992. Porosity-depth trends in reservoir sandstones: theoretical models related to Jurassic sandstones offshore Norway. Marine and Petroleum Geology, 9, 553-567.

RAMM, M., FORSBERG, A. W. & JAHREN, J. S. 1997. Porosity--Depth Trends in Deeply Buried Upper Jurassic Reservoirs in the Norwegian Central Graben: An Example of Porosity Preservation Beneath the Normal Economic Basement by Grain-Coating Microquartz.

RATTEY, R. & HAYWARD, A. Sequence stratigraphy of a failed rift system: the Middle Jurassic to Early Cretaceous basin evolution of the Central and Northern North Sea. Geological Society, London, Petroleum Geology Conference series, 1993. Geological Society of London, 215-249.

Ravnås, R., A. Nøttvedt, et al. 2000. "Syn-rift sedimentary architectures in the Northern North Sea: Dynamics of the Norwegian Margin." Geological Society of London, Special Publication 167: 133-177.

RITTENHOUSE, G. 1971. Mechanical compaction of sands containing different percentages of ductile grains: a theoretical approach. AAPG Bulletin, 55, 92-96.

ROBERTS, A., YIELDING, G. & BADLEY, M. 1990. A kinematic model for the orthogonal opening of the Late Jurassic North Sea rift system, Denmark-Mid Norway. Tectonic Evolution of the North Sea Rifts, 180-199.

ROBERTS, A., YIELDING, G., KUSZNIR, N., WALKER, I. & DORN-LOPEZ, D. 1995. Quantitative analysis of Triassic extension in the northern Viking Graben. Journal of the Geological Society, 152, 15-26.

ROBERTS, D., THOMPSON, M., MITCHENER, B., HOSSACK, J., CARMICHAEL, S. & BJØRNSETH, H.-M. Palaeozoic to Tertiary rift and basin dynamics: mid-Norway to the Bay of Biscay–a new context for hydrocarbon prospectivity in the deep water frontier. Geological Society, London, Petroleum Geology Conference series, 1999. Geological Society of London, 7-40.

ROTHWELL, N., SORENSEN, A., PEAK, J., BYSKOV, K. & MCKEAN, T. 1993. GYDA: Recovery of Difficult Reserves by Flexible Development and Conventional Reservoir Management. Offshore Europe.

Saigal, G.C., Morad, S., Bjorlykke, K., Egeberg, P.K. and Aagaard, P. 1988. Diagenetic albitization of detrital K-feldspar in Jurassic, Lower Cretaceous, and Tertiary clastic reservoir rocks from offshore Norway; I, Textures and origin. Journal of Sedimentary Petrology 58, 1003-1013.

SCOTCHMAN, I., JOHNES, L. & MILLER, R. 1989. Clay diagenesis and oil migration in Brent Group sandstones of NW Hutton Field, UK North Sea. Clay Minerals, 24, 339-374.

SELLEY, R. 1978. Porosity gradients in North Sea oil-bearing sandstones. Journal of the Geological Society, 135, 119-132.

SMITH, G. Geology of the deep Tuscaloosa (Upper Cretaceous) gas trend in Louisiana. Habitat of Oil and Gas in the Gulf Coast: Proc. of the Fourth Annual Research Conf., Gulf Coast Section Society of Economic Paleontologists and Mineralogists Foundation, 1985. 153-190.

SPENCER, A., HOLTER, E., CAMPBELL, C., HANSLIEN, S., NELSON, P., NYSÆTHER, E. & ORMAASEN, E. 1987. Geology of the Norwegian oil and gas fields: London. Graham and Trotman.

Storvoll, V., Bjorlykke, K., Karlsen, D. and Saigal, G. 2002a. Porosity preservation in reservoir sandstones due to grain-coating illite; a study of the Jurassic Garn Formation from the Kristin and Lavrans fields, offshore mid-Norway. Marine and Petroleum Geology 19, 767-781.

Swarbrick, R. E. 1999. "Diagenesis in North Sea HPHT clastic reservoirs—Consequences for porosity and overpressure prediction." Marine and Petroleum Geology 16(4): 337-353.

THOMAS, M. 1986. Diagenetic sequences and K/Ar dating in Jurassic sandstones, Central Viking Graben: effects on reservoir properties. Clay Minerals, 21, 695-710.

THOMSON, A. 1959. Pressure solution and porosity. Silica in sediments: SEPM Special Publication, 7, 92-110.

THOMSON, A. 1979. Preservation of porosity in the deep Woodbine/Tuscaloosa trend, Louisiana.

THYBERG, B., JAHREN, J., WINJE, T., BJØRLYKKE, K., FALEIDE, J. I. & MARCUSSEN, Ø. 2010. Quartz cementation in Late Cretaceous mudstones, northern North Sea: changes in rock properties due to dissolution of smectite and precipitation of micro-quartz crystals. Marine and Petroleum Geology, 27, 1752-1764.

WALDERHAUG, O. 1994. Precipitation rates for quartz cement in sandstones determined by fluid-inclusion microthermometry and temperature-history modeling. Journal of Sedimentary Research, 64.

WALDERHAUG, O. 1994. Temperatures of quartz cementation in Jurassic sandstones from the Norwegian continental shelf--evidence from fluid inclusions. Journal of Sedimentary Research, 64.

WALDERHAUG, O. 1996. Kinetic modeling of quartz cementation and porosity loss in deeply buried sandstone reservoirs. AAPG bulletin, 80, 731-745.

WILLIAMS, L. A., PARKS, G. A. & CRERAR, D. A. 1985. Silica diagenesis, I. Solubility controls. Journal of Sedimentary Research, 55.

WORDEN, R. & MORAD, S. 2000. Quartz cementation in oil field sandstones: a review of the key controversies. Quartz cementation in sandstones, Special publications of international association of sedimentologists, 29, 1-20.

ZANELLA, E. & COWARD, M. 2003. Structural framework. The Millennium Atlas: Petroleum Geology of the Central and Northern North Sea, 45-59.

ZIEGLER, P. 1975. Geologic evolution of North Sea and its tectonic framework. AAPG Bulletin, 59, 1073-1097.

http://factpages.npd.no/factpages/Default.aspx?culture=en. Last accessed 30th May, 2013.

APPENDIX

Appendix A : Grain textural data

Sample No.	Depth (m)	Grain Size (mm)	Sorting	Grain shape	IGV
1	4295,66	0,2052	moderately sorted	sub-rounded	37,8
2	4298,00	0,2092	moderately sorted	sub-rounded	33,5
3	4299,00	0,2317	moderately sorted	sub-angular	30,2
4	4300,33	0,222	moderately sorted	sub-angular	31,5
5	4302,33	0,1827	moderately sorted	sub-angular	32,2
6	4305,66	0,197	moderately sorted	sub-angular	31,9
7	4307,33	0,189	moderately sorted	sub-angular	34
8	4333,33	0,2264	moderately sorted	sub-angular	31,8
9	4336,33	0,218	moderately sorted	sub-angular	34,4
10	4337,33	0,211	moderately sorted	sub-angular	33,1
11	4338,33	0,2022	moderately sorted	sub-rounded	33,9
12	4339,00	0,1898	moderately sorted	sub-angular	38,1
13	4339,69	0,2066	moderately sorted	sub-angular	35,2
14	4340,33	0,2061	moderately sorted	sub-rounded	32,1
15	4341,33	0,2068	moderately sorted	sub-rounded	31,8
16	4342,33	0,1962	moderately sorted	sub-angular	30,2
17	4343,33	0,2068	moderately sorted	sub-angular	33,8
18	4344,00	0,1952	moderately sorted	sub-rounded	34,1
19	4347,33	0,1896	moderately sorted	sub-angular	32,8
20	4349,33	0,20	moderately sorted	sub-angular	37,5

Appendix B: Thin sections

B1: loosely packed grains in sample 43669.66 m

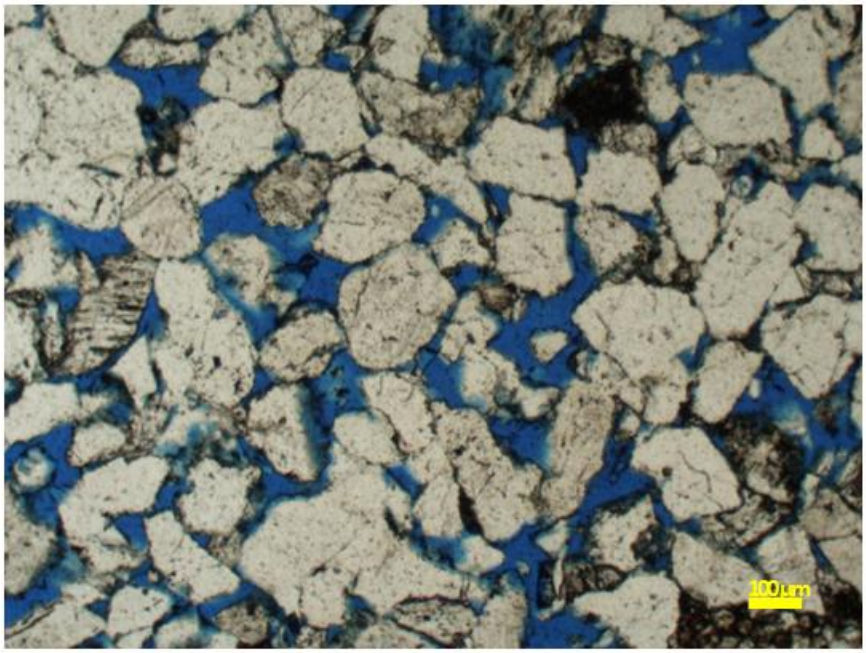

B2: loosely packed grains in sample 4339 m